CHARLES UNIVERSITY IN PRAGUE
FACULTY OF SCIENCE

Study program:
Biology

Branch of study:
Cellular and Developmental Biology

Bc. Aneta Gandalovičová

The plasticity of melanoma cell invasiveness
Plasticita invazivity melanomových buněk

Master´s thesis

Supervisor: doc. RNDr. Jan Brábek, Ph.D.

Prague, 2016

Declaration:

I declare that I completed this master thesis independently and that all sources used are properly acknowledged and cited. Neither this thesis nor any part of it was used to obtain another or similar academic degree.

Prague, 1 May, 2016 Bc. Aneta Gandalovičová

Acknowledgments:

I thank my supervisor doc. RNDr. Jan Brábek, Ph.D. for his time and helpful advice during writing, but also for providing me the opportunity to be a member of the Laboratory of cancer cell invasion. I would also like to thank all other members for technical assistance, help with experiments and for moral support. Special thanks belongs to my closest colleagues, Mgr. Ladislav Merta, for being a great teammate, and Mgr. Vladimír Čermák, Ph.D. to whom I am especially grateful for all discussions, valuable advice and mentorship that he has provided me during my studies.

I would further like to express my endless gratitude for support from my partner and family.

Contents

List of abbreviations:

AMT	Amoeboid-to-mesenchymal transition
aPKC	Atypical protein kinase C
ARHGAP22	Rho GTPase-activating protein 22
ARHGAP24	Rho GTPase-activating protein 24
Arp 2/3	Actin-related proteins 2/3 complex
C1R	Complement component 1, r subcomponent
C1S	Complement component 1, s subcomponent
C3a1	Complement component 3a receptor 1
ca	Constitutively active
Cdc42	Cell division control protein 42
cDNA	complementary DNA
CEMIP	Cell migration-inducing and hyaluronan-binding protein
CITED1	Cbp/p300-interacting transactivator 1
CMV	Human cytomegalovirus
CRISPR	Clustered Regularly Interspaced Short Palindromic Repeats
CSC	Cancer stem cell
c-Src	Rous sarcoma oncogene cellular homolog
DAS	Dasatinib
dd	Double-distilled
DIAPH3	Diaphanous-related formin 3
DMSO	Dimethyl sulfoxide
dNTPs	deoxynucleotides
DOCK10	Dedicator of cytokinesis 10
DOCK3	Dedicator of cytokinesis 3
DOX	Doxycycline
ECM	Extracellular matrix
EGFP	Enhanced green fluorescent protein
EMT	Epithelial-to-mesenchymal transition
ERM	Ezrin-radixin-moesin
FA	Focal adhesion
FACS	Fluorescence activated cell sorting
FAK	Focal adhesion kinase
FMNL2	Formin-like protein 2
GAP	GTPase-activating protein
GAS	Gamma IFN activated site
GDI	GDP Dissociation Inhibitor
GEF	Guanine nucleotide exchange factor
GILZ	Glucocorticoid-Induced Leucine Zipper
GOI	Gene of interest
Gp130	Glycoprotein 130
HMC	Hoffman modulation contrast
IFI35	Interferon-induced protein 35
IFI44L	Interferon-induced protein 44-like
IFI6	Interferon-alpha-inducible protein 6
IFIH1	Interferon-induced with helicase C domain 1
IFIT1	Interferon-induced protein with tetratricopeptide repeats 1
IFIT2	Interferon-induced protein with tetratricopeptide repeats 2

IFIT3	Interferon-induced protein with tetratricopeptide repeats 3
IFITM1	Interferon induced transmembrane protein 1
IFITM3	Interferon induced transmembrane protein 3
IFN-α	Interferon alpha
IFN-β	Interferon beta
IFN-γ	Interferon gamma
IFN-ε	Interferon epsilon
IKK-α	IκB kinase alpha
IKK-β	IκB kinase beta
IKK-γ	IκB kinase gamma
IL-1β	Interleukin 1 beta
IL-6	Interleukin 6
IL-11	Interleukin 11
IL-24	Interleukin 24
IRES	internal ribosome entry site
ISRE	IFN stimulated response element
IκB	Inhibitor of NF-κB
Jak1	Janus-family tyrosine kinase 1
Jak2	Janus-family tyrosine kinase 2
Jak3	Janus-family tyrosine kinase 2
LIF	leukemia inhibitory factor
MAPK	Mitogen-activated protein kinase
MAT	Mesenchymal-to-amoeboid transition
mDia1	Diaphanous-related formin-1
MLC	Myosin light chain
MLCK	Myosin light chain kinase
MLCP	Myosin light chain phosphatase
MMP	Matrix metalloproteinase
MRCK	Myotonic dystrophy kinase-related Cdc42-binding kinase
MT1-MMP	Membrane type 1 matrix metalloprotease
MX1	MX dynamin-like GTPase 1
MX2	MX dynamin-like GTPase 2
NEDD9	Neural precursor cell expressed, developmentally down-regulated 9
Nemo	NF-kappa-B essential modulator
NF-kB	Nuclear factor κ B
NG2	Neural/glial antigen 2
OAS1	2'-5'-oligoadenylate synthetase 1
OAS2	2'-5'-oligoadenylate synthetase 2
Oct-4	octamer-binding transcription factor 4
PAK1	P21-activated kinase 1
PAK2	P21-activated kinase 2
Par3	Partioning defective homolog 3
Par6	Partioning defective homolog 6
PCR	Polymerase chain reaction
PEI	Polyethylenimine
PI3K	Phosphatidylinositol-4,5-bisphosphate 3-kinase
PIP3	Phosphatidylinositol(3,4,5)triphosphate
Rac1	Ras-related protein Rac1
RE	restriction enzyme
RhoA	Ras homolog gene family, member A
RhoC	Ras homolog gene family, member C
ROCK	Rho-associated, coiled-coil containing protein kinase 1
RRAD	Ras-Related Associated With Diabetes

RSAD2	Radical S-adenosyl methionine domain containing 2
RT	Room temperature
SAA1	Serum amyloid A1
SAA2	Serum amyloid A2
SigP	Signal peptide
siRNA	Small interfering RNA
Smurf1	SMAD specific E3 ubiquitin protein ligase 1
SOCS	Suppressor of cytokine signalling
Stat1	Signal transducer and activator of transcription 1
Stat2	Signal transducer and activator of transcription 2
Stat3	Signal transducer and activator of transcription 3
SV40	Simian vacuolating virus 40
TGFβ	Transforming growth factor beta-1
Tiam1	T-lymphoma invasion and metastasis-inducing protein 1
TNFα	Tumor necrosis factor alpha
Tyk2	Tyrosine Kinase 2
USP18	Ubiquitin specific peptidase 18
WASP	Wiskott-Aldrich syndrome protein
WAVE	WASP family protein member
ZEB1	Zinc finger E-box-binding homeobox 1
ZIPK	Zipper-interacting protein kinase
βPIX	PAK-interacting exchange factor β

Abstract and keywords:

During metastasis, cancer cells can invade the extracellular matrix using various strategies. When invading individually, they employ either the amoeboid invasion mode, during which the cell body dynamically deforms by enhanced contractility to squeeze through pores within the matrix, or protease dependent mesenchymal migration that takes advantage of the possibility to digest the surrounding matrix. Cells migrating in one mode can actively switch to the other by mesenchymal-amoeboid (MAT) or amoeboid-mesenchymal transitions (AMT). This enables escape mechanisms and considerably complicates anti-metastatic treatment. It is well known that Rho GTPases are master regulators of cytoskeleton re-arrangements and thus, unsurprisingly, play a major role in both invasion modes and can directly drive the transitions. However, upstream activation of these pathways is still largely unclear. This thesis aimed to optimize 3D conditions suitable for studying plasticity of cell invasion *in vitro,* establish AMT and MAT in melanoma cells based on manipulation of Rho GTPases and verify novel candidates regulating cell invasion plasticity based on previous RNA sequencing of cells before and after MAT. Last, by synthesis of published data, results from sequencing and new findings presented in this thesis, we propose that the amoeboid phenotype is established as a consequence of autocrine/paracrine signaling loops maintained by production of cytokines driven by RhoA-mediated inflammatory pathways- Jak/Stat and NFκB, which themselves converge on RhoA. Moreover, the relation to cancer stem cells and possible connection to *in vivo* amoeboid migration is discussed.

Key words: invasiveness, amoeboid, Rho GTPases, Jak/Stat, NFκB, MAT, AMT

Abstrakt a klíčová slova:

Během metastazování mohou rakovinové buňky využívat různé strategie pro invazi skrz extracelulární matrix. Při individuální invazi využívají buď améboidní migrační mód, během kterého buňka dynamicky mění tvar díky zvýšené kontraktilitě tak, aby mohla prolézat póry v extracelulárním prostředí, nebo mesenchymální migraci, která je závislá na proteolytickém štěpení a využívá možnosti degradace okolní tkáně. Buňky migrující v daném módu mohou aktivně přecházet do druhého módu v procesu mesenchymálně-améboidního přechodu (MAT) nebo améboidně-mesenchymálního přechodu (AMT). To jim nabízí únikové cesty, což značně komplikuje léčbu metastatické rakoviny. Je známo, že Rho GTPázy jsou hlavními regulátory přestavby cytoskeletu a není tedy překvapením, že hrají důležitou roli v obou migračních modech a mohou přímo řídit přechody mezi nimi. Nicméně, aktivace těchto drah je stále poměrně nejasná. Tato práce si kladla za cíl optimalizovat 3D podmínky vhodné pro studium plasticity invazivních módů *in vitro*, poté na bázi manipulace s Rho GTPázami ustanovit modely pro studium AMT a MAT v melanomových buňkách a ověřit nové kandidáty regulující plasticitu buněčné invazivity dle předchozích dat získaných sekvenováním RNA z buněk před a po MAT. Nakonec, pomocí syntézy publikovaných dat, výsledků ze sekvenování a nových poznatků prezentovaných v této práci, bylo navrženo, že améboidní fenotyp je výsledkem autokrinní/parakrinní signalizace zajištěné pomocí produkce cytokinů, což je zprostředkováno RhoA řízenými zánětlivými drahami- Jak/Stat a NFκB, jejichž signalizace se navíc na RhoA sbíhá. Navíc, vztah k rakovinovým kmenovým buňkám a potencionální vazba na *in vivo* améboidní migraci jsou diskutovány.

Klíčová slova: invazivita, améboidní, Rho GTPázy, Jak/Stat, NFκB, MAT, AMT

1. Introduction

Cancer is a group of diseases that arise as a result of abnormal behavior of cells within the organism, which leads to pathological states such as uncontrolled proliferation, disintegration of tissues or loss of homeostasis. The development of cancer is a gradual process based on genomic mutations and altered environment, which both stand out as a general cause of cell transformation. Cancer progression can be identified by the acquisition of 8 characteristics, often considered cancer hallmarks, which include: sustaining proliferative signaling, evading growth suppressors, resisting cell death, enabling replicative immortality, inducing angiogenesis, activating invasion and metastasis, reprogramming energy metabolism and evading immune destruction (reviewed in Hanahan and Weinberg, 2011). Out of these, only activation of invasion and metastasis is restricted to malignant cancer (not shared by benign tumors) and as such, it can be considered the only true hallmark of cancer (Lazebnik, 2010). The fact that the majority of cancer-associated deaths are not caused by the primary tumor, but by secondary tumors (Sleeman and Steeg, 2010; Sporn, 1996), implies the necessity to target cancer cell invasion for successful cancer treatment.

Invading cells can employ various invasion modes that differ in their dependency on intercellular contact, cell-ECM (extracellular matrix) contact and in force generation. Collective migration and mesenchymal migration are both dependent on protrusive forces and digestion of the adjacent extracellular matrix (Friedl and Wolf, 2008), whereas amoeboid migration is based on enhanced actomyosin contractility (reviewed in Charras and Paluch, 2008). Moreover, cancer cells migrating in one mode can actively switch to another mode (reviewed in Friedl, 2004), which is a major obstacle for anti-metastatic treatment

Since transitions among individual invasion modes comprise considerable changes in cell shape, it is not surprising that major players during conversion from one invasion mode to another are Rho GTPases, which are key regulators of cytoskeleton rearrangement (summarized in Parri and Chiarugi, 2010). However, it seems that Rho GTPases are the main executors of the invasion modes, while the inducers remain largely undefined. There is increasing evidence for the role of signaling pathways involved in the inflammatory response, such as the Jak/Stat, NFκB or MAPK signaling pathways (reviewed in Fan et al., 2013; Yeh et al., 2013). In addition, there is apparent influence of the extracellular matrix conditions. Altogether, precise characterization of factors decisive for each migration mode is necessary for efficient cancer treatment.

2. Aims of this thesis

The overall aim of this thesis was to establish efficient model systems of the amoeboid-mesenchymal transition (AMT) and, conversely, mesenchymal-amoeboid transition (MAT) for proteomic and transcriptomic analysis with the goal of identifying factors responsible for each invasion mode.

The thesis encompasses several minor goals:

1) To optimize 3D matrices and conditions suitable for
    a. Morphology assays
    b. Live cell imaging
2) To establish AMT and MAT systems based on manipulating Rho GTPase activity in melanoma cell lines
    a. Prepare stable cell lines with inducible constitutively active RhoA
    b. Test inhibitors of pathways known to be important for amoeboid/mesenchymal migration
    c. Clone potential inducers of transitions and test their effect *in vitro*
3) To verify novel candidates for regulators of AMT and MAT based on results from RNA sequencing
    a. Test inhibitors of candidate targets
    b. Clone candidate genes for further evaluation of their role in AMT/MAT

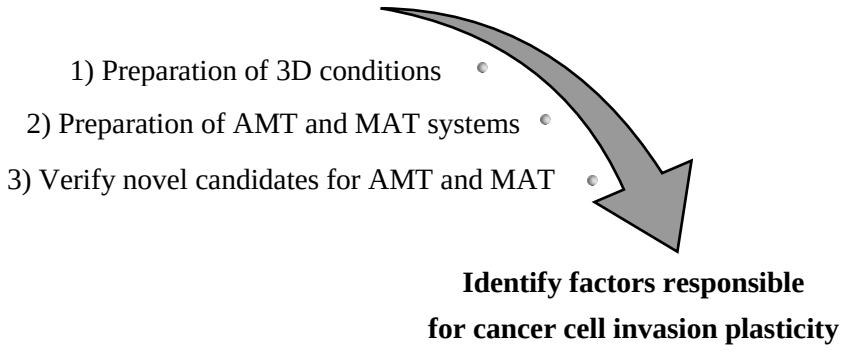

Fig. 1: Overview of individual goals

3. Literature Review

3.1. The origin of cancer cell invasion

Cancer cell invasion can be defined as the ability of cancer cells to migrate through the extracellular matrix and invade the surrounding tissue. It requires the gain of a migratory phenotype, which is enabled by establishing front-rear polarity, loosening cell-cell contact and activating pro-migratory signaling pathways (Friedl and Wolf, 2009; Geiger and Peeper, 2009; Macara and McCaffrey, 2013; Nelson, 2009). These processes are typical of the epithelial-mesenchymal transition (EMT), which is often considered the initial step of cancer cell invasion (reviewed in Thiery et al., 2009). In case of epithelial cells, which are the origin of cancer in most cases (summarized by McCaffrey and Macara, 2011), EMT is described as the transition from a non-migratory state with apico-basal polarity and intercellular junctions to a migratory phenotype with defined front-rear polarity (summarized in Halaoui and McCaffrey, 2014) (Fig. 2). The most common triggers of EMT include the transforming growth factor β (TGFβ) signaling pathway and various oncogenes e.g. Ras, PI3K and Src. The EMT program is accompanied by transcriptional changes such as the activation of pro-mesenchymal factors Snail, Twist or ZEB, which leads to the downregulation of epithelial genes and, simultaneously, upregulation of pro-migratory genes such as N-cadherin, vimentin and integrins (reviewed in Lamouille et al., 2014).

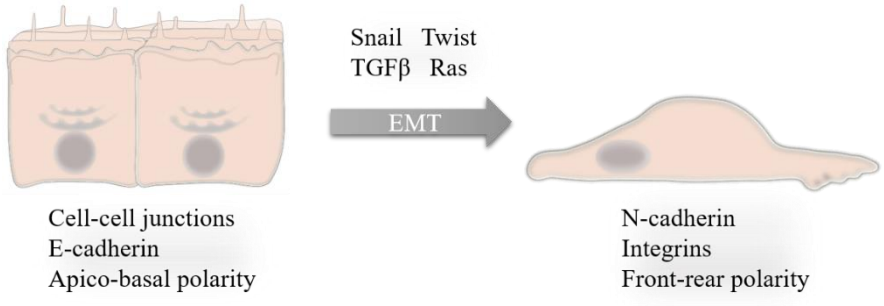

Fig. 2: The loss of apico-basal polarity and transition to front rear polarity during EMT

3.2. Invasion modes

The net result of EMT are individually invading cells of mesenchymal phenotype (Fig. 2). However, many partial-EMT phenotypes can be observed, since activation of the migratory phenotype is often customized and differs in individual cells according to heterogeneous response to signaling pathways, extracellular conditions and cell origin (Friedl and Wolf, 2010). This gives rise to many intermediate phenotypes and invasion modes.

The generally accepted classification distinguishes among collective cell migration and two modes of individual migration- amoeboid and mesenchymal. Unlike individual migration, during which all cell-cell contacts are abolished, collective cell migration maintains contact within the migrating cell cohort (Nabeshima et al., 1999). Only the cells in the front, often referred to as leading cells, resemble cells after EMT (Khalil and Friedl, 2010). These cells promote invasion by digesting the surrounding extracellular matrix and by exerting pulling forces on the cell cohort (Nabeshima et al., 2000). Concurrently, the cell cohort exhibits pushing forces by cell proliferation. Collective cell migration has become of central interest recently as documented by the number of reviews published, and the recent finding that it is the prevalent invasion mode used for detachment from primary tumors has only validated this trend (Bronsert et al., 2014). However, this thesis is restricted to single cell invasion plasticity, and for this reason collective cell migration will not be further discussed.

Individual migration is generally independent of intercellular contacts. Single migrating cells can employ either the amoeboid or mesenchymal migration mode, which differ mainly in their strategy of maneuvering through the ECM and consequently, the nature of force generation (see Fig. 6 and Table 1).

Mesenchymal cells rely on the generation of traction forces enabled by cell-ECM contact (reviewed in Huttenlocher and Horwitz, 2011). The cells form protrusions that adhere to surrounding fibers through focal adhesions (FA), multiprotein adhesive complexes composed of integrins and adaptor proteins such as talin or paxillin (Nagano et al., 2012; Parsons et al., 2010). The adhesions generate traction forces for forward movement, while the rear of the cells retracts by disrupting previous adhesions and through enhanced contraction (Friedl and Wolf, 2009). This is enabled by spatial distribution of signaling proteins, most notably Rho GTPases RhoA, Rac1 and Cdc42 (summarized in Murali and Rajalingam, 2014) (Fig. 3). At the leading edge, Rac1 and Cdc42 drive the formation of

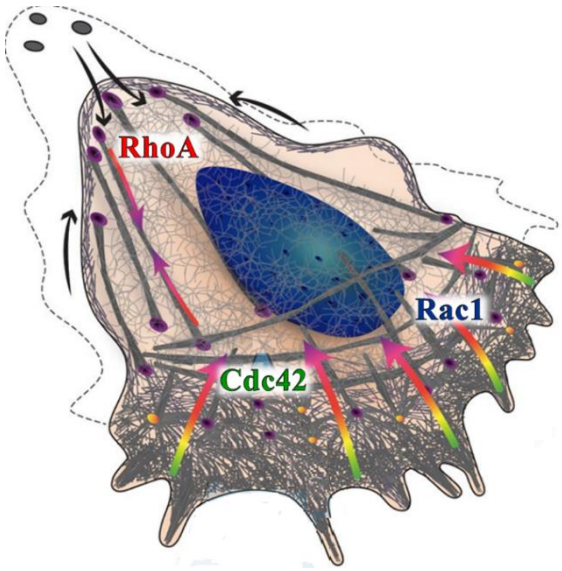

Fig. 3: Mesenchymal migration- distribution of Rho GTPases. RhoA drives contraction of the rear, while Cdc42 and Rac1 activate actin polymerization at the leading edge. Purple dots- focal adhesions, rainbow arrows- actin turnover. Adapted from (Blanchoin et al., 2014).

protrusions such as lamellipodia and filopodia through signaling to proteins of the WASP/-SCAR/WAVE family that activate Arp2/3 (Actin-related proteins 2/3 complex) mediated actin polymerization (Eden et al., 2002; Rohatgi et al., 1999).

Underlying mesenchymal migration is the proteolytic digestion of the surrounding ECM, which is necessary for generating space for the cell body. The digestion itself is localized 5-20 µm from the leading edge, which enables protrusions to maintain cell-ECM adhesion necessary for force generation, but enables the mass of the cell body to progress forward (Wolf et al., 2007). In fact, the digestion is clearly visible as "microtracks" cut through the ECM (Friedl and Wolf, 2008) (Fig. 4).

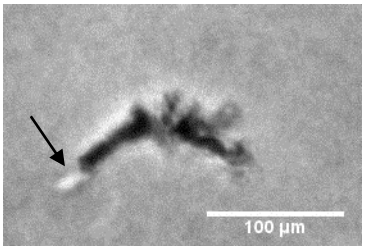

Fig. 4: Microtrack in collagen digested by mesenchymally migrating macrophage.

Responsible for the digestion of the ECM components are proteolytically active enzymes, such as serine proteinases, cathepsin proteinases and, most commonly, MMPs (matrix metalloproteinases). These enzymes can be either membrane bound (e.g. MT-MMP1) or secreted in vesicles (e.g. MMP-2, MMP-9) (Artym et al., 2006; Kobayashi et al., 2003; Tester et al., 1993). The MMPs localize to specialized invasion structures formed by mesenchymally migrating cells- to invadopodia and podosomes (collectively termed invadosomes). Invadosomes are composed of an actin core and surrounding actin-regulatory proteins such as Arp 2/3, cortactin or WASP (Albiges-Rizo et al., 2009; Tolde et al., 2010). They form at the cell-ECM interface and degrade the surrounding ECM due to the presence of MMPs (summarized in Gimona et al., 2008; Linder et al., 2011).

Altogether, the formation of cell-ECM contacts and proteolysis of ECM enables an elongated cell morphology with a distinct leading and retracting edge (Fig. 6). A different strategy is utilized by amoeboid cells that generate energy for motility by up-regulating actomyosin contractility (Kosla et al., 2013; Rösel et al., 2008; Terry et al., 2012), which results in accumulation of hydrostatic pressure. The pressure is key for the formation of membrane blebs that enable directional forward movement by forming transient adhesions and pulling in the contracting body (Charras and Paluch, 2008; Lämmermann and Sixt, 2009; Lämmermann et al., 2008). Moreover, spatial distribution of blebs dictates directionality of invasion (Lorentzen et al., 2011).

The event mediating enhanced actomyosin contraction is the phosphorylation of MLC (myosin light chain), which promotes its interaction with actomyosin filaments. Underlying MLC phosphorylation are signaling pathways mediated by RhoA- activated ROCK kinase (Rho-associated, coiled-coil containing protein kinase), and in part by Cdc42- activated MRCK (myotonic dystrophy kinase-related Cdc42-binding kinase). ROCK phosphorylates MLC directly (Amano et al., 1996) and also indirectly by interaction with MLCP (myosin light chain phosphatase) and ZIPK (zipper-interacting protein kinase). When active, MLCP dephosphorylates MLC, and this phosphatase activity is inhibited by ROCK phosphorylation (Kimura et al., 1996). ROCK also activates ZIPK, which acts upstream of MLCK (myosin light chain kinase) (Hagerty et al., 2007). MRCK increases phosphorylated MLC through the inhibition of MLCP (Wilkinson et al., 2005). In summary, phosphorylation of MLC, MLCK and MLCP all results in increased levels of phosphorylated MLC, which promotes myosin ATPase activity resulting in enhanced actomyosin contractility (Fig. 5).

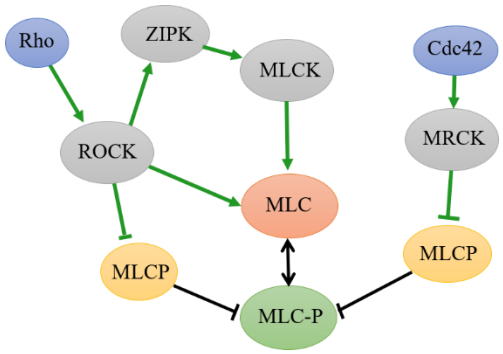

Fig. 5: Scheme of signaling pathways involved in regulation of cell contractility.

The high cell deformability enables cells to squeeze through pores in the ECM without the need to digest the surrounding matrix (Wolf et al., 2003; Wyckoff et al., 2006). Thus, amoeboid migration was thought to be independent of MMPs production, however this was recently challenged by Orgaz et al., who demonstrated that amoeboid melanoma cells produce and utilize various MMPs such as MMP-9 or MMP-13 (Orgaz et al., 2014a). Notably, the bleb-driven migration does not require integrin- mediated cell-ECM adhesion and instead forms transient adhesions, supposedly mediated by various glycoproteins (reviewed in Schmidt and Friedl, 2010). Important proteins in amoeboid migration are ezrin, moesin and radixin (ERM proteins), which function as linking proteins between the actin cortex and the plasma membrane. Particularly, ezrin localizes to the cell rear, where it limits bleb formation and thus promotes directional invasion (Lorentzen et al., 2011).

Overall, amoeboid cells exhibit over one magnitude faster invasion when compared to mesenchymal cells as they do not form strong cell-ECM adhesions (Sahai and Marshall, 2003). In fact, amoeboid cancer cells have been shown to migrate up to 15 µm/min (Pinner and Sahai, 2008) and in case of lymphocytes that naturally adopt this invasion mode, velocities of up to 25 µm/min have been documented (Friedl et al., 1994). The rate limiting step during

amoeboid migration is deformation of the nucleus. While the deformability of the cell body can be pushed up to the limit of 1 μm2 in diameter, the cell nucleus is not able to deform in such extent and thus can halt invasion completely (Wolf et al., 2013). On the other hand, the velocity of mesenchymal migration is limited by digestion of the ECM and by focal adhesion turnover, which results in notably slower invasion of approx. 0.1-1 μm/min (Zijl et al., 2011). Thus, the resulting invasion mode represents a negotiation between fast, but physically limited migration and slow, but persistent migration (Krause and Wolf, 2015).

	Mesenchymal	Amoeboid
Morphology	Elongated with protrusions at the leading edge	Rounded with membrane blebs
Adhesion to the ECM	strong, numerous FA	weak, integrin independent
Force generation	Cell-ECM adhesion and protrusive activity at the leading edge	Enhanced cell contractility due to actomyosin cortex
Speed	0.1 -1 μm/min	up to 15 μm/min
Rate limiting step	Proteolysis of the ECM FA turnover	Nucleus deformation
Predominant GTPase	Rac1, Cdc42	RhoA

Table 1: Comparison of characteristic features of amoeboid and mesenchymal migration

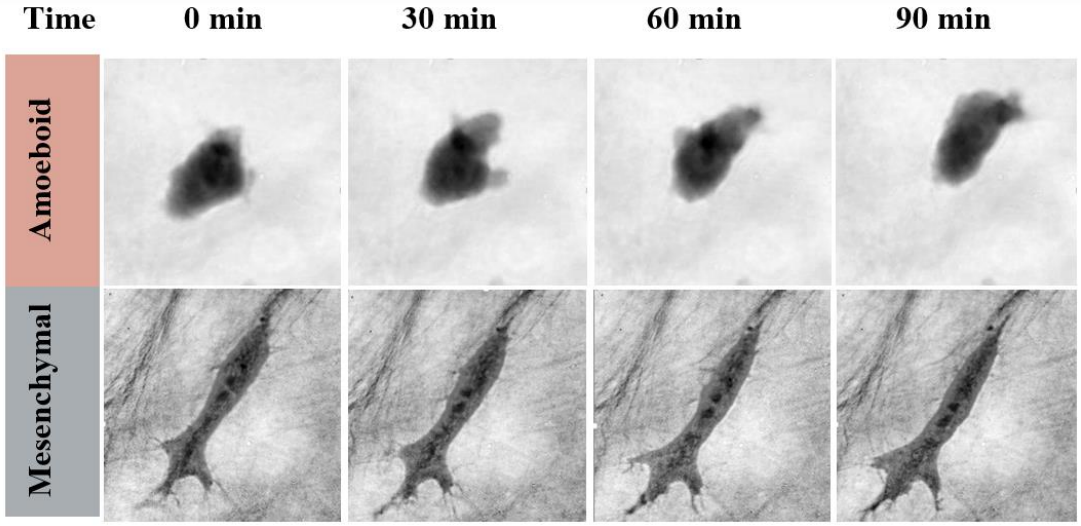

Fig. 6: Example of amoeboid and mesenchymally invading cells. Typical characteristics are visible- blebs forming at the leading edge and cell body deformability in case of amoeboid invasion (upper panel) and elongated cell body in case of mesenchymal cells (lower panel). Images were obtained thanks to RNDr. Ondřej Tolde, PhD by live-cell imaging using digital holographic microscopy.

3.3. Rho GTPases as master regulators of cytoskeleton arrangement

The invasion modes are largely the result of cytoskeleton organization. The main regulators underlying the re-arrangements are small Rho GTPases (Nobes and Hall, 1999). Through signaling to downstream proteins, Rho GTPases control actin polymerization, cell polarity, contractility and mediate ECM sensing (summarized by Sadok and Marshall, 2014). The activation of individual Rho GTPases is controlled by regulatory proteins. A main role is attributed to GAPs (GTPase activating proteins), GEFs (guanine exchange factors) and GDIs (guanine nucleotide dissociation factors). Rho GTPases are active when bound to GTP, therefore GEFs, which exchange GDP for GTP have an activating role (Schmidt and Hall, 2002), while GAPs decrease the activity by promoting GTP hydrolysis (Tcherkezian and Lamarche-Vane, 2007). Rho GDIs act as inhibitory factors as they sequester the non-active proteins (Dovas and Couchman, 2005).

The three prominent representatives of Rho GTPases are RhoA, Cdc42 and Rac1. They represent a main signaling hub for cell contraction, polarity and actin nucleation, respectively.

As mentioned earlier, RhoA drives cell contractility by activating ROCK, a serine-threonine kinase. ROCK is activated by binding RhoA at its coiled coil domain (Amano et al., 2010). When activated, ROCK phosphorylates MLC and its regulatory protein MLCP, resulting increased levels of phosphorylated MLC. This stimulates actomyosin contraction, which is necessary not only for amoeboid migration, but also rear retraction of mesenchymally migrating cells (Mitchison and Cramer, 1996). Correspondingly, in mesenchymal cells, RhoA localizes predominantly to the rear (Pertz et al., 2006), whereas in in amoeboid cells it is broadly activated at the cell membrane and contributes to bleb formation (Charras et al., 2006). RhoA also further promotes actin nucleation by binding and activating formin mDia1(Watanabe et al., 1999).

Apart from RhoA, other isoforms have been shown to contribute to cell invasion (Ridley, 2013). RhoB promotes invasion by promoting the activity of urokinase-type plasminogen activator (Alfano et al., 2012), a protease involved in both mesenchymal and amoeboid migration (Margheri et al., 2014). Furthermore, RhoB contributes to directional migration by contributing to stabilization of integrins at the leading edge (Vega et al., 2012). The role of RhoC is mainly in protrusion formation. It has been shown to regulate cofilin, an actin severing protein, at the site of invadopodia and lamellipodia, and through this

mechanism influence directionality of migrating cells (Bravo-Cordero et al., 2011, 2013). While this imposes a role for RhoC in mesenchymal cells, it also contributes to amoeboid migration by interacting with formin FMNL2 (formin-like protein 2), an actin nucleation protein (Kitzing et al., 2010).

In addition to RhoA, Cdc42 also contributes to cell contractility by activating MRCK, which inhibits the activity of myosin phosphatase MLCP (Wilkinson et al., 2005). It also drives the formation of filopodia that enhance cell migration and invasion by promoting adhesion (Gao et al., 2013; Yang et al., 2006). However, its main role lies in regulating cell polarity (Etienne-Manneville, 2004; Srinivasan et al., 2003). By interaction with polarity proteins, Cdc42 drive the establishment of the nuclear-centrosomal polarity axis (Etienne-Manneville and Hall, 2003). Unsurprisingly, Cdc42 has shown to promote directional migration (Etienne-Manneville et al., 2005; Li et al., 2003).

The dominantly pro-mesenchymal GTPase is Rac1. It localizes to the leading edge where it regulates protrusion formation and membrane ruffling (Kraynov et al., 2000). To a large extent, it activity is regulated by second messengers and polarity proteins. One such pathway involves Rac1 activation in response to integrin signaling at the leading edge. Integrins that accumulate at focal adhesions activate PI3K, which produces the second messenger PIP3 leading to activation of Tiam1, a GEF for Rac1 (Fleming et al., 2000). Importantly, by promoting actin polymerization through Arp2/3, Rac1 drives the formation of lamellipodia (Ten Klooster et al., 2006).

Quite surprisingly, mutations of the Rho GTPases are not common in human cancers, although some mutations have been recently identified (Alan and Lundquist, 2013). Rather, these proteins modulate cell behavior by their overexpression or downregulation (Orgaz et al., 2014b) The pathway is further deregulated on the level of regulatory proteins, such as GEFs, GDIs and GAPs, which have been consequently proposed as potential targets for treatment (Cho et al., 2010; Kusama et al., 2006; Lazer and Katzav, 2011).

Nevertheless, activating and dominant negative mutations have been identified and serve as a valuable tool in studying the role of Rho GTPases in cell behavior. These variants were determined by point mutation with reference to earlier described mutations in the Ras oncogene, mostly due to precise work of Alan Hall and coworkers (Nobes and Hall, 1999). The identified dominant negative mutations (for example RhoAN19, Rac1N17 and Cdc42N17) lead to preferential binding of GDP opposed to GTP. On the other hand, activating mutations

result in loss of intrinsic GTPase activity. For example RhoA with mutated glycine for valine at position 14 (Fig. 7), leads to significantly decreased GTPase activity, which prolongs the lifetime of RhoA in its active (GTP-bound) state (Diekmann et al., 1995; Ihara et al., 1998).

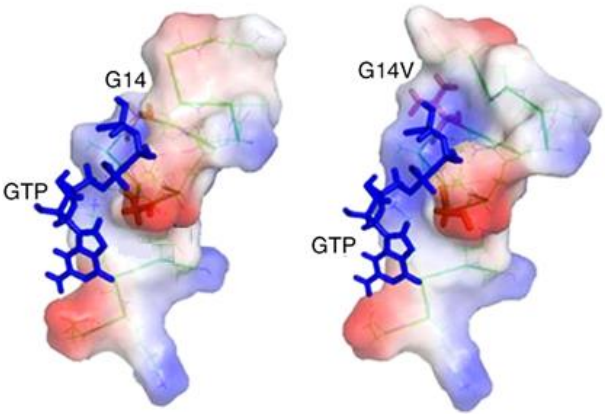

Fig. 7: Schematic image of RhoA with loaded GTP. Left, wild-type RhoA with glycine at position 14, right RhoA with valine at position 14. Structural differences of binding sites is most prominent around mutated site. Adapted from (Yoo et al., 2014)

Another possible approach to modify the function of Rho GTPases is by affecting their prenylation, which is necessary for their correct membrane targeting. Non-prenylated Rho GTPases do not show any change in GTP hydrolysis, nevertheless their interaction with GAPs was impaired (Molnar et al., 2001). Moreover, prenylation of GTPases was studied as a potential anti-metastatic target, however it did not prove very efficient in therapy (Holstein and Hohl, 2012).

Inhibiting RhoA signaling is further possible by C3 exotransferase, an enzymatically active toxin produced by *Clostridium botulinum* bacteria. C3 exotransferase ADP-ribosylates RhoA at the site of asparagine 41, which is in close proximity of the GTP binding site (Sekine et al., 1989). The binding of ADP impairs loading of GTP to the active site by preventing the association between RhoA and its GEFs (Fig. 8).

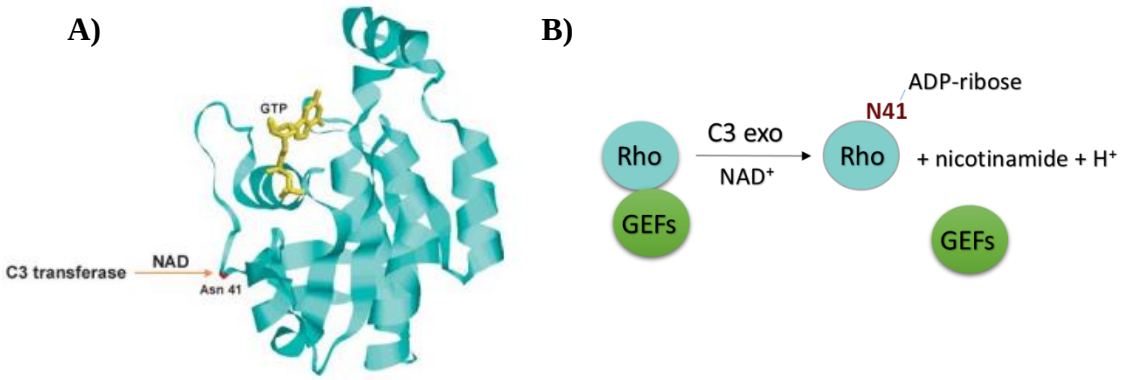

Fig. 8: C3 exotransferase mediated inhibition of RhoA signaling. A) Structure of RhoA with bound GTP, the site of ADP-ribosylation is highlighted Adapted from (Aktories et al., 2004). B) Schematic summary of ADP-ribosylation catalyzed by C3 transferase.

3.4. Plasticity of invasion

The invasion mode is not definite. Rather, it represents the most advantageous strategy in the given conditions with respect to the cell's signaling pathways settings (reviewed in Krause and Wolf, 2015). Due to this interchangeability, cancer cells can escape drug intervention, which represents a major obstacle for anti-metastatic treatments. For example, drugs against MMPs did halt mesenchymal invasion by disabling proteolytic digestion of the ECM, but the affected cells were able to switch to the proteolytically independent amoeboid migration (Wolf et al., 2003). This is referred to as mesenchymal-amoeboid transition (MAT). Correspondingly, amoeboid cells can switch to mesenchymal invasion in a process called amoeboid- mesenchymal transition (AMT) (Fig. 9).

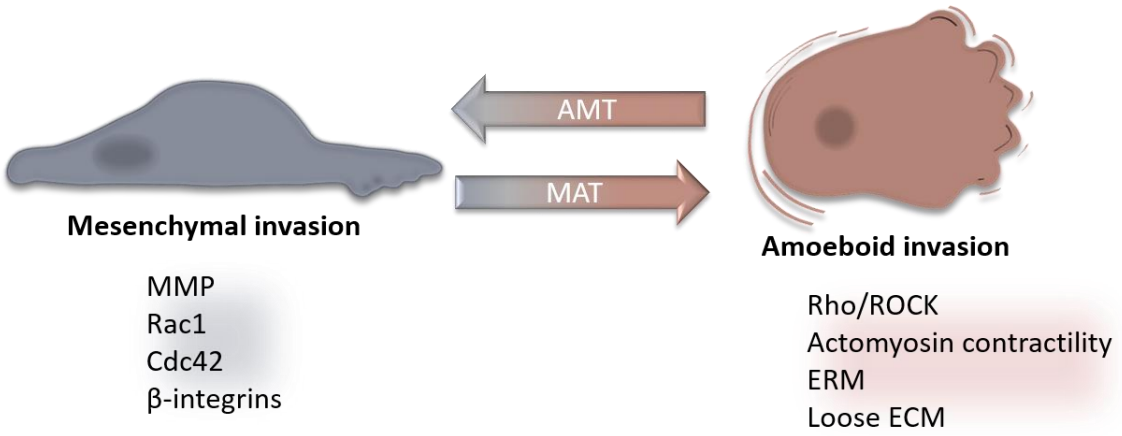

Fig. 9: The schematic illustration of AMT and MAT and key factors for each migration mode.

It is not surprising that Rho GTPases stand out as key players and the balance between Rac1 driven actin polymerization and RhoA mediated cell contractility largely dictates the choice of the invasion strategy.

Of note, Rac1 and RhoA naturally regulate their signaling pathways in mutual manner (summarized in Guilluy et al., 2011). Rac1 is known to activate p21-activated protein kinase 1 (PAK1), which inhibits MLCK resulting in downregulated cell contractility (Sanders et al., 1999). PAK1 itself can also reduce RhoA activation by phosphorylating and inactivating p115-RhoGEF (Rosenfeldt et al., 2006). On the other hand, RhoA abates Rac1 signaling through activation of Rac-GAP proteins ArhGAP22 and ArhGAP24 (Ohta et al., 2006; Sanz-Moreno et al., 2008).

Cdc42 upholds its ambiguous role as it activates PAK1, but also PAK2 which, opposingly to PAK1, enhances cell contractility (Coniglio et al., 2008). The identified mechanism of PAK2 activation involves DOCK10, a GEF for Cdc42 (Gadea et al., 2008).

By modulating these signaling pathways, AMT and MAT can be induced. Silencing ArhGAP22 led to AMT, while knockdown of a Rac GEF, DOCK3 and its associated protein NEDD9, resulted in MLC phosphorylation, which is typical of amoeboid motility (Sanz-Moreno et al., 2008). Enhancing the Rho/ROCK pathway by expression of constitutively active RhoA (caRhoA) activates the amoeboid phenotype (Sahai and Marshall, 2003). MAT can further be induced by downregulating Smurf1, which is able to target RhoA for degradation (Sahai et al., 2007). Opposingly, silencing NG2 glycoprotein impaired RhoA signaling resulting in AMT (Paňková et al., 2012). Silencing of DOCK10 also induced the mesenchymal phenotype by impairing the DOCK10-PAK2-Cdc42 signaling pathway (Gadea et al., 2008).

In addition, the use of inhibitors that block a critical component of the certain invasion mode also results in invasion transition. Inhibitors of MMPs prevent proteolytical digestion of the ECM, which results in transition to the protease-independent, e.g. amoeboid, invasion mode (Wolf et al., 2003). On the other hand, inhibition of cell contractility by ROCK inhibitors can result in AMT (Sahai and Marshall, 2003; Vaskovicova et al., 2015). Moreover, dasatinib, which is a c-Src/Abl inhibitor causes MAT (Ahn et al., 2012). It binds Src at the ATP site, and inhibits its kinase activity (Lombardo et al., 2004).

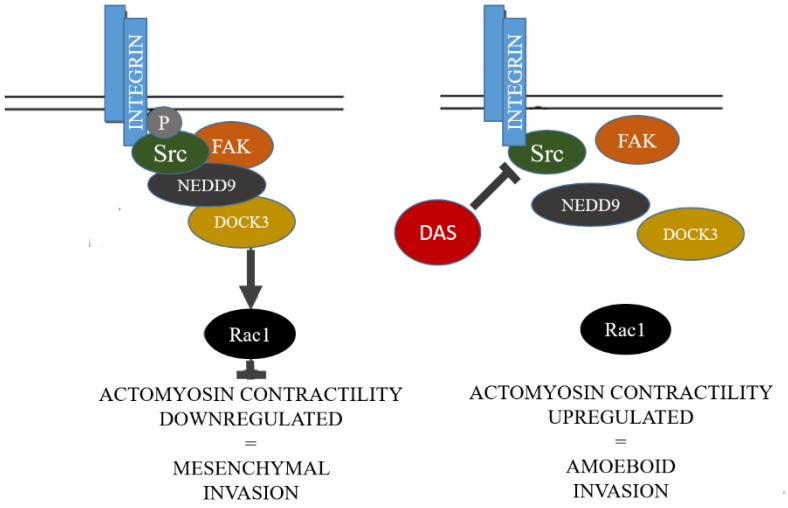

Fig. 10: Schematic illustration of the effect of dasatinib on Rac1 activation and down-stream signaling.
Created according to (Ahn et al., 2012).

Inhibition of Src by dasatinib disrupts the activation of Rac1 mediated by DOCK3-NEDD9 complex, which leads to the gain of the amoeboid phenotype (Ahn et al., 2012) (Fig. 10). Dasatinib also blocks mesenchymal migration and invasion by impairing focal adhesion formation as it reduces Src-mediated FAK phosphorylation (Shor et al., 2007). In addition, Abl kinase, which is also targeted by dasatinib, also signals through Rac (Bassermann et al., 2002; Skorski et al., 1998). Thus, dasatinib blocks mesenchymal migration by both Src and Abl kinase inhibition.

Overall, this lead to the assessment of Rac1-RhoA antagonism as the underlying principle of cell invasion plasticity. This theory has been supported also by mathematical modeling of cell invasive behavior (Byrne et al., 2016; Huang et al., 2014).

However, various cell lines have distinct pre-requisite requirements for signaling. Moreover, cells can often compensate for the inactivation of a certain protein. For example, inactivation of RhoA does not inhibit invasion, which suggests the cells are able to activate other substitute pathways, such as RhoC- or Cdc42- mediated cell contractility to compensate for RhoA inactivation (Monypenny et al., 2009; Simpson et al., 2004).

Hence, the resulting invasion mode is always determined as a complex decision which encompasses ECM conditions, signaling and intrinsic signaling requirements.

3.5. Influence of the extracellular matrix on cell invasion

The behavior of invading cells is to a large extent dictated by the experimental conditions. In the field of cell migration, conditions ranging from 1D migration to 3D migration are used. Conditions that study cell migration in defined narrow fibers are considered 1D (Doyle et al., 2009). These conditions copy the *in vivo* situation up to some extent, since cancer cells often migrate along "tracks" provided by large vessels. 1D conditions are suitable for studying chemotaxis, but do not provide enough complexity to be suitable for studying amoeboid and mesenchymal invasion, since they do not encompass the divergence offered by second and third dimensions. Studying cell migration in 2D conditions, exemplified by migration assays on plastic or coated surfaces, provided valuable information on cell motility, but cannot fully mimic *in vivo* conditions (reviewed in Kramer et al., 2013; Shamir and Ewald, 2014). This emphasizes the necessity to study cell invasion in 3D conditions that best resemble metastasis *in vivo*.

There are various conditions available for the preparation of 3D matrices. One of the commonly used 3D matrixes is Matrigel, which is composed mainly of proteins of the basal lamina and is therefore most suitable for experiments with epithelial cells or for studying EMT (Kleinman and Martin, 2005). Other commonly utilized 3D matrices are constituted of collagen, which is the most abundant extracellular protein. Collagen matrices therefore represent an appropriate 3D matrix.

Natural collagen is a network of covalently cross-linked fibers (Fig. 11). It can be prepared from tissues rich in collagen either by pepsin extraction (Fujimoto, 1968, as cited in Cliche et al., 2003), which leads to disruption of telopeptides that link N- a C- terminal ends of native collagen, or by acidic extraction, which leaves the telopeptides intact (Bornstein, 1958, as cited in Garcia-Gareta, 2014). Sabeh et al. dispute that collagen matrixes prepared from pepsin extracted- collagen might lead to conditions considerably different than those obtained by gelation of collagen after acidic extraction (Sabeh et al., 2009). While doubts concerning substitutability of collagen prepared by pepsin extraction are legitimate, since lack of telopeptides was shown to promote breast cancer invasion (Demou et al., 2005), concerns that amoeboid migration is limited to collagen derived by pepsin extraction have not shown to be justified, as demonstrated by published results (Geraldo et al., 2012; Wyckoff et al., 2006) as well as data presented in this thesis.

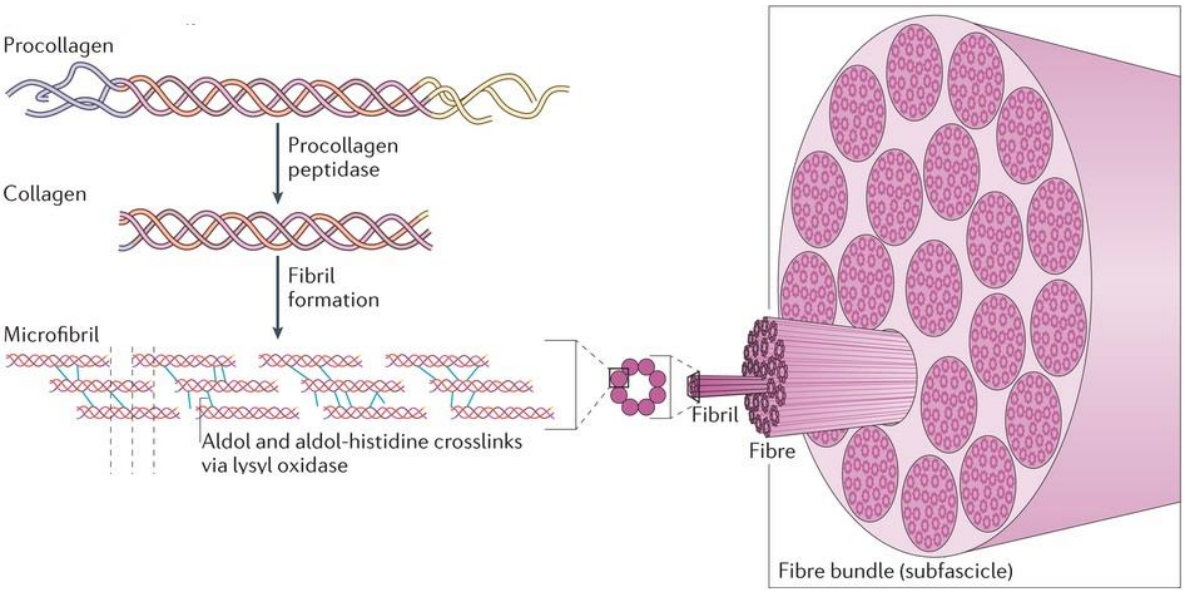

Fig. 11: The structural organization of collagen. Collagen fibers consist of fibrils composed of crosslinked microfibrils. Adapted from (Mouw et al., 2014)

Nevertheless, it has been demonstrated that the ECM characteristics can influence the choice of the invasion mode (Friedl and Alexander, 2011; Van Goethem et al., 2010; Gu et al., 2014; Taddei et al., 2013). Amoeboid migration is based on cellular contractility, during which translocation of the nucleus, which has limited deformability, remains the limiting factor (Davidson et al., 2014; Harada et al., 2014; Wolf et al., 2013). For this reason, amoeboid migration is possible only in conditions of less rigid extracellular matrix. On the other hand, mesenchymal migration is preferable in dense conditions, since mesenchymally migrating cells possess the ability to digest the surrounding matrix (Friedl and Wolf, 2008, 2009; Poincloux et al., 2009).

The influence of the extracellular matrix is best exemplified on the case of human macrophages, which naturally adopt their invasion mode according to the extracellular conditions. In conditions of concentrated collagen, they activate the mesenchymal invasion strategy, whereas in less dense environment, they adopt the amoeboid phenotype (Van Goethem et al., 2010).

3.6. Unconventional signaling pathways involved in individual cancer cell invasion

Recently, research has focused on revealing upstream signaling pathways regulating the choice of the certain invasion mode.

Multiple evidence has now proved the role of polarity proteins in the plasticity of cancer cell invasion (summarized in Gandalovičová et al., 2016). Particularly, polarity protein signaling regulates the activity of Rho GTPases and promotes their spatio-temporal regulation in invading cells. For example, polarity protein Scribble promotes activity of β-PIX, a RhoGEF known to activate Cdc42 and Rac1 (Audebert et al., 2004), but also, via srGAP1, inhibits RhoA (Kutys and Yamada, 2014). Moreover, another polarity protein, Par3, can activate Rac1 through its GEF protein Tiam1, which promotes formation of the leading edge (Pegtel et al., 2007). At the leading edge, Cdc42 activates Par6, which recruits Smurf1, a RhoA-degrading protein (Sahai et al., 2007). On the other hand, RhoA/ROCK can phosphorylate Par3, which impairs Tiam1- mediated Rac1 activation (Nakayama et al., 2008).

Interestingly, various transcriptional changes have also been associated with regulation of either invasion mode.

Stem cell pluripotency transcription factors Nanog and Oct4 were shown to drive the expression of pro-amoeboid genes and downregulate mesenchymal genes (Borrull et al., 2012). Accordingly, it was recently demonstrated that MAT is associated with the gain of stem cell-like features, including the activation of pluripotency genes (Taddei et al., 2014)

Another pathway proposed to regulate cancer cell invasion plasticity is TGF-β. Recently its signaling via Smad2-CITED1 was identified as an important pro-amoeboid pathway in melanoma cells (Cantelli et al., 2015). However, other studies have described a role of TGF-β signaling in mesenchymal migration (Sun et al., 2011) by upregulating fascin, a pro- mesenchymal protein involved in formation of invadopodia (Li et al., 2010).

Moreover, there is increasing evidence for the involvement of inflammatory signaling pathways in cancer (summarized in Coussens and Werb, 2002; Solinas et al., 2010). The two main signaling pathways that mediate inflammation include the Jak/Stat and NFκB pathway. Since these pathways are of importance in context of data presented in this thesis, they are described in more detail.

3.6.1. The Jak/Stat pathway

The Jak/Stat signaling drives many biological processes ranging from differentiation, development to cell proliferation or apoptosis. This is enabled by a range of pleiotropic cytokines that drive autocrine and paracrine cell communication. Ligand binding to receptors induces their oligomerization. However, they lack intrinsic tyrosine kinase activity and instead, transduce signals by activating Jaks (Janus family kinases) that further transmit signal by phosphorylating Stats (Signal transducers and activators of transcription). Phosphorylated Stats can dimerize and translocate to the nucleus, where they drive transcription of various inflammatory-associated genes.

Ligands activating Jak/Stat signaling include interferons (IFNs), growth factors and various cytokines. Each ligand preferentially activates certain Jaks and Stats. Stat3 mediates signaling of cytokines of the IL-6 family, such as IL-6 or LIF, that signal through the common receptor subunit gp130 (Murakami et al., 1993). On the other hand, Stat1 is mainly associated with IFN signaling. While Stat1 is proposed to have tumor suppressor activity, as it reduces cell proliferation, Stat3 is considered as an oncogene by driving cancer-associated inflammation and cell proliferation (reviewed by Regis et al., 2008).

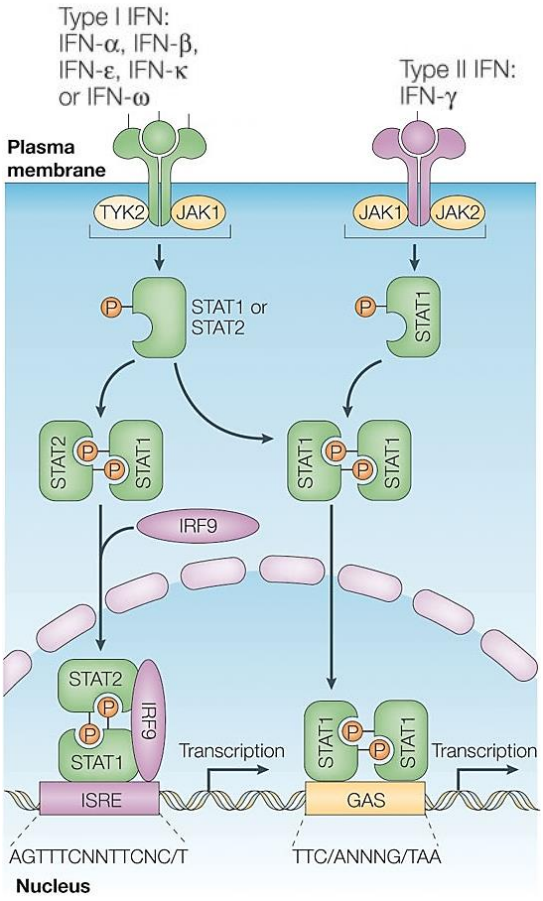

Fig. 12: Schematic overview of the IFN-response mediated by Jak/Stat signaling. Adapted from (Platanias, 2005).

IFNs can be divided into two types- type I IFNs (IFNα and IFNβ) and type II (IFNγ). Type I and II IFNs respond to distinct stimulation and differ in downstream signaling. Type I response is mediated by Jak1 and Tyk2, which act upon heterodimers composed of Stat1 and Stat2 or Stat3 that bind to ISRE (IFN Stimulated Response Element) motifs. On the other hand, IFNγ signals through Jak1 and Jak2 to activate Stat1 homodimers, which bind to GAS sequences (Gamma IFN activated site) and regulate proteins of the innate immune response (Schindler and Plumlee, 2008).

3.6.2. The NFκB pathway

NFκB signaling is also implicated in inflammatory pathways. It is activated in response to reactive oxygen species, lipopolysaccharides and cytokines such as sTNFα and IL-1β. Its main purpose is to regulate cytokine expression, as such, it plays role in development, immunity but also cancer (Dolcet et al., 2005).

NFκB comprises of 5 transcription factors, e.g. p50, p52, RelA, c-Rel and RelB, out of which only RelA, RelB and c-Rel possess transcriptional activity. As such, p50 and p52 operate in complex with either Rel protein.

The activity of NFκB is regulated by cytoplasmic inhibitory proteins- IκBs, (inhibitor of kappa B) that are phosphorylated and degraded upon NFκB activation. The canonical pathway involves the degradation of IκB by IKK complex, composed of IKKα, IKKβ and adaptor protein NEMO (also known as IKKγ). The non-canonical pathway is executed by proteolysis of precursor protein p100 to an active p52 unit that forms an active complex with RelB (summarized in Sun, 2011).

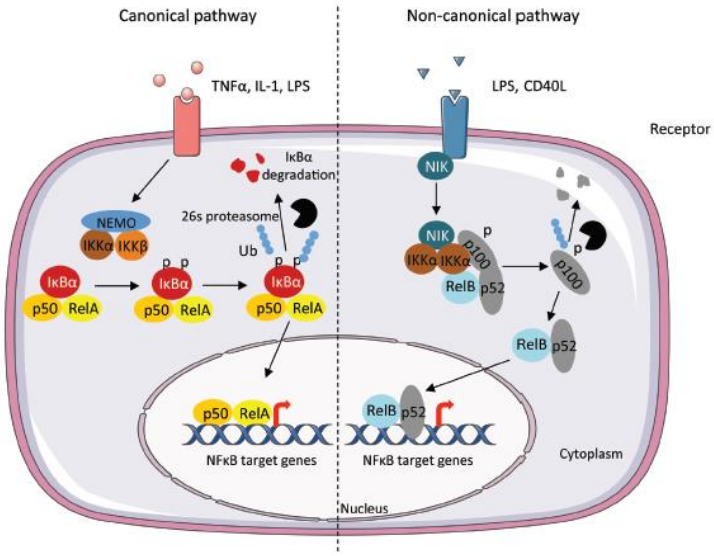

Fig. 13: Illustration of the canonical and non-canonical pathway in NFκB activation. Adapted from (Viennois et al., 2012)

Both Jak/Stat and NFκB pathways are often deregulated in cancers (summarized in Fan et al., 2013). However, current knowledge on their role in cancer cell plasticity is limited. There is direct evidence for the role of the IL-6-Stat3 pathway in actomyosin contractility and in enhancement of the amoeboid phenotype (Sanz-Moreno et al., 2011). On the other hand, NFκB can stimulate protease dependent cell invasion by promoting the secretion of MMPs (Bond et al., 2001).

Novel possible links between these pathways and individual cell invasion plasticity are presented in this thesis.

4. Material and methods

4.1. Cell culture methods

4.1.1. Organisms

HT1080: fibrosarcoma, established July 1997
A375m2: malignant melanoma, derived metastatic line from A375 in 2004
BLM: malignant melanoma, derived from BRO cells
WM3629: malignant melanoma, established from lymph node metastasis

4.1.2. Solutions

Cell culture medium:

All cell lines were cultured in Dulbecco's Modified Eagle's Medium (DMEM; Sigma, D6429) supplemented with 10% fetal bovine serum (FBS; Sigma, F7524) and gentamicin (Sigma, G1272).

Trypsin for splitting cells:

Trypsin-EDTA solution 0.25 % (Sigma, T4049)

Cell culture freezing medium:

90 % FBS
10 % dimethyl sulfoxide (DMSO, Sigma, D2650)

10x PBS (Sigma, D1408)

FACS medium:

1x PBS supplemented with 2% v/v FBS and 20mM glucose (Sigma, G 7021).

Inducer of expression:

Doxycycline (Sigma, D9891), working concentration 250 nM

Transfection reagent:

Polyethylenimine (PEI) (Polysciences, Inc., 23966)

Inhibitors

Dasatinib (LC Laboratories, D3307), working concentration 1 μM

PS-1145 (Santa Cruz Biotechnology, sc-301621), working concentration 10 μM

Ruxolitinib (LC Laboratories, R-6600), working concentration 10 μM

Antibiotics:

Puromycin (Sigma, P7255)

Blasticidin (Sigma, 15205)

G418 (Sigma, A1720)

4.1.3. Culturing cells

All cells were cultured under standard conditions in 37˚C and humidified atmosphere with 5% CO_2. According to need, cells were cultivated in dishes or in wells (for surface size, volume of medium and average cell number for each dish/well see Table 2). Cells were regularly examined under a light microscope (Nikon-Eclipse TES100) to determine cell confluence and checked for potential contamination. Cells were regularly splitted to avoid overgrown cultures.

Type of cultivation plate	Surface (cm^2)	Volume of culture medium (ml)	Average n. of cells at 100 % confluence
10 cm dish	55	10	8.8×10^6
6 cm dish	21	4	3.2×10^6
3,5 cm dish	9	2	1.2×10^6
6- wells plate	9	2	1.2×10^6
12- wells plate	4	1.5	0.4×10^6
24- wells plate	2	0.5	0.2×10^6

Table 2: Information for various sizes of cell culture dishes.

4.1.4. Splitting cells

Cells were splitted according to need every 2-4 days to achieve a confluence between 30-90 %.

1. Prepare trypsin solution and leave at RT (room temperature) to adjust temperature, pre-heat medium to 37°C
2. Aspirate medium from cells by vacuum pump
3. Wash cells with PBS (1/10 of original medium volume)
4. Add trypsin (1/10 of original medium volume) and spread over whole plate surface by rocking plate back and forth
5. Leave trypsin on cells until detachment (2-5 min)
6. Add medium (same volume as trypsin) to halt effect of trypsin
7. Re-suspend cell suspension
8. Remove given volume (according to splitting ratio)
9. Add medium to reach proper volume to remaining cells

4.1.5. Stock cells

Cells, when not in culture are stored in liquid nitrogen (-196 °C) for long term storage or in deep freezers (-80°C) for short term storage.
Stock cells are prepared from cell culture of confluence 70-90 %.

Preparation of cell stocks:

1. Prepare freezing medium (1 ml per aliquot) and one 15 ml tube with 4 ml of medium per cell line
2. Prepare trypsin solution and leave at RT (room temperature) to adjust temperature, pre-heat medium to 37°C
3. Aspirate medium from cells by vacuum pump
4. Wash cells with PBS (1/10 of original medium volume)
5. Add trypsin (1/10 of original medium volume) and spread over whole plate surface by rocking plate back and forth
6. Leave trypsin on cells until detachment (2-5 min)
7. Add medium (same volume as trypsin) to halt effect of trypsin
8. Re-suspend cell suspension and transfer to 15 ml tube
9. Spin cells, 180 g for 4 min (Eppendorf Centrifuge 5804R)

10. Resuspend cell pellet in corresponding amount of freezing medium
11. Add 1 ml of cell suspension to each cryotube
12. Place cryotubes in a freezing container
13. Place container in -80°C
14. For long term storage, move cryotubes to liquid nitrogen within 2-3 days

Thawing frozen cells:

1. Pre-heat medium to 37°C
2. Prepare one 15 ml tube with 4 ml of medium for each cell line to be thawed
3. Transfer cryotube with given cells from freezer/liquid nitrogen on ice
4. Thaw cells in water bath
5. Transfer cell suspension to 15 ml tube
6. Spin cells, 180 g for 4 min (Eppendorf Centrifuge 5804R)
7. Aspirate medium
8. Resuspend cell pellet in fresh medium
9. Transfer cell suspension to new dish/plate and add medium to reach given volume according to dish/plate size
10. Next day, check cell viability, eventually transfer to larger dish

4.1.6. Cell transfection

For cell transfection, polyethylenimine (PEI) was used. PEI is a stable cationic polymer that forms complexes with DNA (Boussif et al., 1995), The complexes can bind the cell membrane and, subsequently, undergo endocytosis. The amount of DNA, PEI and diluent (medium without FBS) is dependent on the amount of cells to be transfected, see Table 3.

Type of cultivation plate	Diluent volume (µl)	DNA (µg)	PEI (µl)
10 cm dish	1000 –x*	14	42
6 cm dish	500-x	5	15
6- wells plate	200-x	1.5	4.5
12- wells plate	100-x	1	3
24- wells plate	50-x	0.5	1.5

*X= DNA volume + PEI volume

Table 3: Information for various sizes of cell culture dishes

1. Prepare one 1.5 ml tube for each construct to be transfected
2. Add diluent, DNA and PEI in given order
3. Mix on vortex for 10 s, briefly spin down
4. Leave at RT for 15-30 min
5. Drop-wise, add to cells
6. Rock gently back and forth to ensure even distribution
7. Change medium after 18-24 hours

4.1.7. Preparation of cell suspension of given concentration

1. Prepare one 15 ml tube per cell line to be counted
2. Prepare trypsin solution and leave at RT to adjust temperature, pre-heat medium to 37°C
3. Aspirate medium from cells by vacuum pump
4. Wash cells with PBS (1/10 of original medium volume)
5. Add trypsin (1/10 of original medium volume) and spread over whole plate surface by rocking plate back and forth
6. Leave trypsin on cells until detachment (2-5 min)
7. Add medium (same volume as trypsin) to halt effect of trypsin
8. Re-suspend cell suspension and transfer cells to 15 ml tube
9. Count number of cells in 1 ml of suspension
    i. Add 15 µl of cell suspension to Bürker chamber
    ii. Count average number of cells per square
    iii. Determine number of cells in 1 ml
10. Spin down, 4 min 180 g and aspirate medium
11. Resuspend in calculated volume to achieve desired cell concentration

4.1.8. Preparation of stable cell lines

Stable cell lines are generated for sustained expression of gene of interest (GOI), most commonly by culturing transfected cells with a selection antibiotic.

For the generation of stable cell lines, two methods were used:

a) Linearization of plasmid DNA and cultivation with antibiotics, see chapter 4.1.8.1
b) Lentiviral transduction of cells and cultivation with antibiotics, see chapter 4.1.8.2

4.1.8.1. Stable cell lines with constitutive gene expression

1. Linearize plasmid containing GOI (choose an unique enzyme with a digestion site outside of any coding or promoter sequence; see chapter 4.3.9)
2. Purify linearized DNA using magnetic beads (see chapter 4.3.8.1)
3. Transfect cells (see chapter 4.1.6)
4. After 48 hours, add selection antibiotics
5. Culture cells in the presence of antibiotic for 10-21 days
6. If GOI is fluorescently tagged, check for positive cells regularly
7. To ensure high percentage of positive cells, sort cells by flow cytometry (refer to 4.1.9)

4.1.8.2. Stable cell lines with inducible gene expression

For inducible expression, we used lentiviral based gene transfer of Tet-On Advanced Gene expression system from Clontech. This system enables to adjust the level of expression of GOI by using different concentrations of the inducer-doxycycline. Fig. 14 summarizes the procedure.

First, stable cell lines with the regulator vector TOB (Tet-On Advanced with blasticidin resistance, obtained as a gift from dr. Anděra) were prepared. Subsequently, second transfection with responsive vector was performed.

1. Perform transfection according to chapter 4.1.6

   DNA overall amount is the same, each plasmid 1/3 amount

   (psPAX2: pMD2.G: regulator or responsive vector ratio 1:1:1)
2. After 12-24 hours, change medium
3. After 12-24 hours, collect medium in 15 ml tube, centrifuge 15 min, 180 g
4. Carefully transfer medium onto host cells
5. Repeat transfer 3-5x times every 12-24 hours
6. Add selection antibiotics and culture cells in its presence for 10-21 days
7. If GOI is fluorescently tagged, check for positive cells by inducing expression with doxycycline
8. To ensure high percentage of positive cells, sort cells by flow cytometry (refer to 4.1.9)

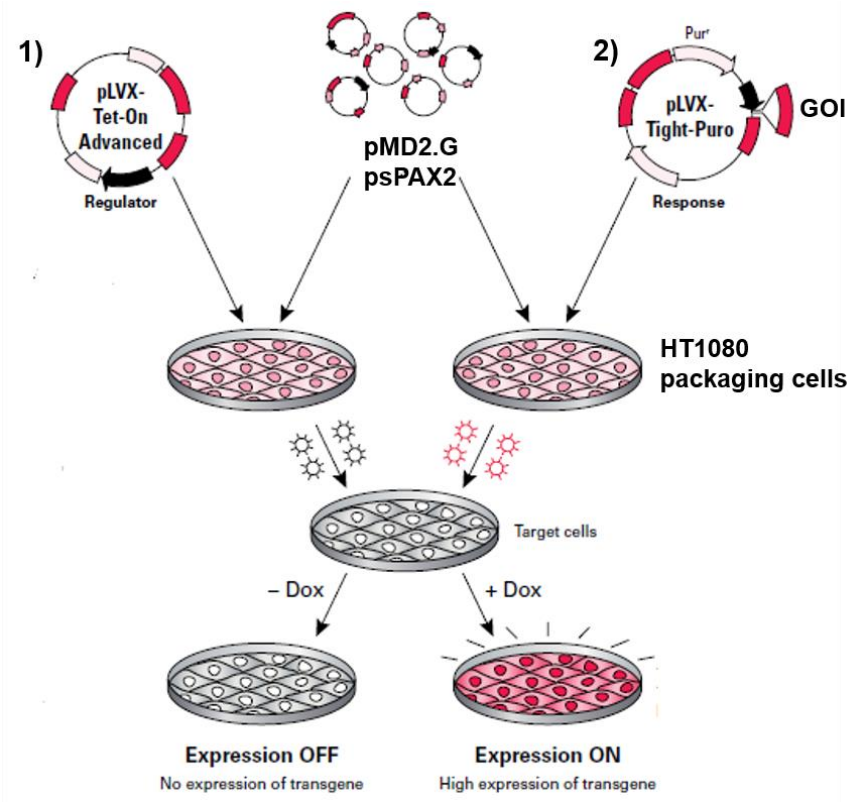

Fig. 14: Schematic illustration of lentiviral transduction of host cells. Packing cells were transfected with packaging vectors and regulatory or responsive vectors in the first and second round of transfection, respectively. Adapted from Lenti-X™ Tet-On® Advanced Inducible Expression System User Manual[1].

[1] A*vailable online:* http://www.clontech.com/xxclt_ibcGetAttachment.jsp?cItemId=17567&embedded=true

4.1.9. Flow cytometry and Fluorescence activated cell sorting

Flow cytometry was used to assess the results of stable cell line preparation. If percentage of positive cells was lower than 80%, cells were sorted for fluorescent signal using fluorescence activated cell sorting (FACS). It was not necessary to stain cells since our protein of interest is fluorescently tagged.

1. The day before, induce expression of fluorescently-tagged GOI
2. Prepare one 15 ml tube per cell line to be measured (always measure control cells as well)
3. Trypsinize cells
4. After detachment, transfer cells to 15 ml tube
5. Count number of cells in 1 ml of suspension (see chapter 4.1.7)
6. Spin down, 4 min 180 g and wash with 5 ml of flow cytometry medium
7. Spin down, 4 min 180 g and aspirate medium
8. Resuspend in such volume of flow cytometry medium to obtain a concentration of 5-10^6 cells per 1 ml
9. Place tubes with cells on ice
10. Measure on flow cytometer according to standard procedure
    i. Start LSRII and perform start-up steps
    ii. Start DIVA software
    iii. Mix cells by pipetting and transfer to measuring tubes
    iv. Set parameters (forward scatter, side scatter, fluorescence)
    v. Acquire control cells
    vi. Adjust forward and side scatter
    vii. Set gate for viable cells and eliminate cell doublets
    viii. Measure (10 000-50 000 events)
    ix. Change tube and acquire cells expressing fluorescent protein
    x. Set gate for positive and negative cells
    xi. Measure (10 000-50 000 events)
    xii. Determine percentage of positive cells within measured population

If determined percentage of positive cells is below 80%, sort cells. Cell sorting was performed at FACS facility at IMG, ASCR with the assistance of Zdeněk Cimburek.

After cell sort, cells were re-examined by flow cytometry.

4.2. Preparation of 3D matrices

4.2.1. Solutions and reagents

Matrigel (Corning, 356237)

Collagen:

Collagen R (Serva, 47256.01)

Collagen G (Biochrom, L7213)

Nutragen (AdvancedBioMatrix, 5010)

Fibricol (AdvancedBioMatrix, 5133)

DMEM 10x (Sigma, D2429)

$NaHCO_3$ 7.5% (Sigma, S8761)

NaOH (Sigma, 59223C)

HEPES (Sigma, H4034)

Gentamicin (Sigma, G1272).

Folic acid (FA) (Sigma, F8758)

Agarose (Thermo Scientific, 16500500)

4.2.2. General information

When preparing 3D matrices following conditions were maintained, unless stated otherwise.

1. All handling of stock solutions of 3D matrices was done on ice
2. Cells were prepared as a suspension of concentration $4*10^6$ cells/ml
3. DMEM with 1% FBS was used as covering medium
4. If inhibitors or other drugs were added, they were present in the same concentration in both matrix and covering medium.
5. Volume of cell suspension is 1/10 of total 3D matrix volume, summarized in Table 4

Type of cultivation plate	Volume of 3D matrix (µl)	Volume of covering medium (µl)
3 cm dish	1500	2000
12- wells plate	1000	1500
24-wells plate	500	1000
48- wells plate	250	500
96- wells plate	150	200

Table 4: Volumes of matrix and media used for various cell culture dishes.

4.2.3. Preparation of Matrigel

1. Let Matrigel thaw on ice
2. Pre-cool pipette tips in freezer
3. Prepare cell suspension of concentration $4*10^6$ cells/ml
   Refer to chapter 4.1.7
4. Add cell suspension to Matrigel
5. Carefully mix by pipetting (use pre-cooled pipette tip)
6. Transfer to well
7. Place in incubator for 30 min
8. Cover with given volume of 1% FBS in DMEM

4.2.4. Preparation of collagen matrixes

A pre-mix for rat tail collagen was prepared. The pre-mix was mixed with collagen and cells, and water was added to adjust to final concentration of either 1 mg/ml or 0.5 mg/ml collagen matrix.

Pre-mix for collagen preparation:

DMEM 10x	4.5 ml
$NaHCO_3$	2.5 ml
NaOH 1M	0.424 ml
HEPES 750mM	1 ml
Gentamicin	0.25 ml
FA 1mM	0.05 ml
H_2O	17.526 ml
Total volume	26.25 ml

1. Prepare cell suspension of concentration $4*10^6$ cells/ml
   Refer to chapter 4.1.7
2. Prepare collagen solution by mixing pre-mix, water, collagen and cells in ratio 5.25:1.25:2.5:1, respectively, to achieve a final concentration of collagen 1mg/ml
   or 5.25:2.5:1.25:1 to achieve a final collagen concentration of 0.5 mg/ml
3. Carefully mix by pipetting
4. Optional: add inhibitor/drug
5. Transfer given volume of collagen mix to wells (see Table 4)
6. Place in incubator for 30 min
7. Cover with DMEM with 1%FBS (see Table 4)

For preparation of higher concentration collagen, the individual components were mixed directly before use. The amount of water was adjusted for desired collagen concentration.

4.2.5. Live cell imaging

1. Prepare 0.5 mg/ml collagen matrix with embedded cells (see 4.2.4)
2. Place in the incubator for at least 3 hours before imaging to let cells adjust to the 3D conditions.

For live cell imaging using Nikon-Eclipse TE2000-S

3a. Exchange cover media for media supplemented with 7.5mM HEPES to buffer the pH without the presence of 5% CO_2 atmosphere
4a. Place dish/plate in chamber pre-heated to 37°C.
5a. Set automatic image acquisition to 1 image in 60 or 120 seconds Process acquired image sequence in ImageJ software.

For live cell imaging using JULI Fl+Br station

3b. Place dish/plate on JULI microscope in the incubator
4b. Set automatic image acquisition to 1 image in 60 or 120 seconds
5b. Process acquired image sequence in ImageJ software.

4.2.6. Morphology analysis

1. Prepare 1 mg/ml collagen matrix with embedded cells (see 4.2.4)
2. Place in incubator
3. After 48 hours, acquire 10-15 images per well using 10x objective and Hoffman modulation contrast (HMC)
4. Analyze cell morphology by counting round and elongated cells using CellCounter plug-in in ImageJ software
    i. Open image stack in ImageJ
    ii. Open CellCounter
    iii. Initialize
    iv. Choose cell type (Type I, Type II etc.)
    v. Count cells for each type
    vi. Round cells have a width-length ratio smaller than <1.5 , elongated cells have a ratio >1.5

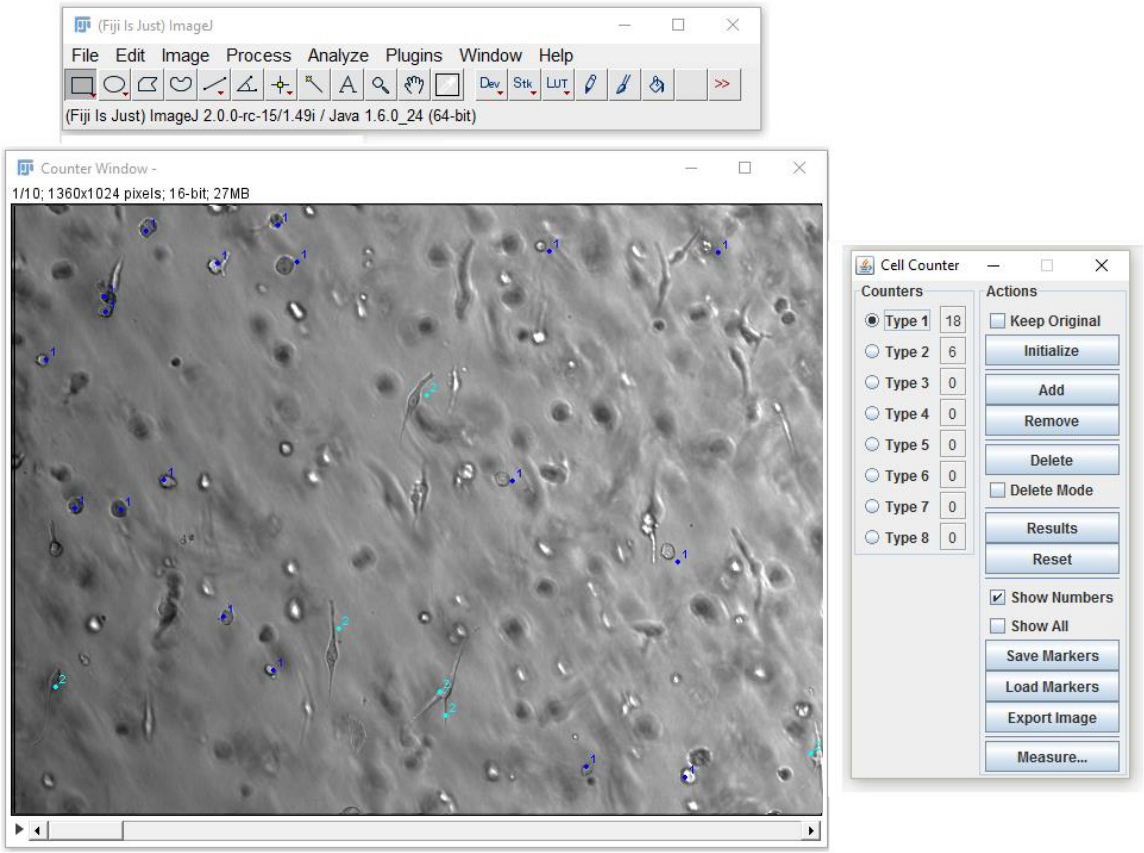

Fig. 15: Morphology analysis using Cell Counter in ImageJ

4.2.7. Spheroid invasion assays

Spheroid formation:

1. Prepare agarose forms:
    i. Prepare 50 ml of 1 mg/ml agarose in PBS in 100 ml bottle
    ii. Sterilize in autoclave at 121°C for 20 min
    iii. Leave agarose to cool down, meanwhile prepare given amount of micro-molds (Fig. 16) (MicroTissues® 3D Petri Dish® micro-mold spheroids; Sigma)
    iv. Pipette 500 µl of agarose onto the molds equally to all sides, avoid adding bubbles
    v. Leave agarose to solidify
    vi. Prepare 12-wells dish with 2 ml of medium per well (1 well for each mold)
    vii. Detach agarose from mold, place into the well containing medium
    viii. To saturate agarose with medium, leave 15 minutes in the incubator
    ix. Aspirate medium and add fresh medium, repeat step viii.
2. Prepare cell solutions of concentration $3.25*10^6$ cells/ml
    Cell concentration can be adjusted according to desired spheroid size
3. Pipette 190 µl of cell suspension drop-wise to mold
4. Leave 15 min in incubator to let cells sediment
5. Carefully cover with 2 ml medium
6. Leave 48-72 hours in incubator for spheroid formation

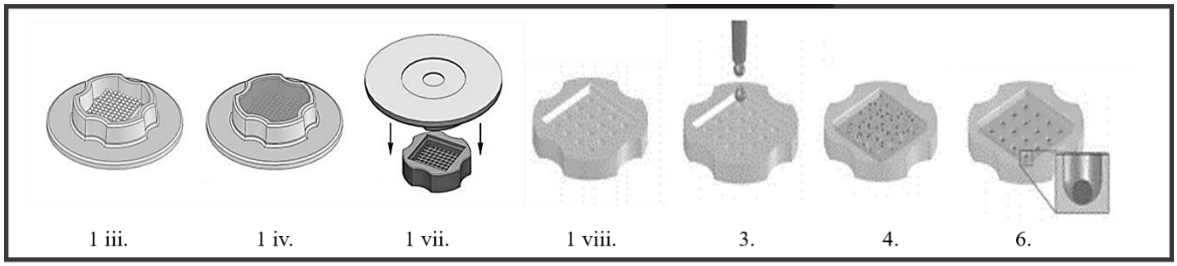

Fig. 16: **Schematic summary of the main steps of spheroid formation.**
Image composed from (Napolitano et al., 2007) and image available at producers website (http://www.microtissues.com/).

Spheroid embedding in 3D collagen:

7. Prepare collagen matrix 1 mg/ml (see chapter 4.2.4)
8. Pipette ½ of given collagen volume (according to well size- ideally 48- or 96-well plates, see Table 4) to each well and place in incubator
9. Transfer spheroids from mold to dish with medium
10. After collagen solidifies, carefully add 1 spheroid per well by transferring it in small amount of medium (50 µl)
11. Carefully cover spheroid with remaining collagen
12. Place in incubator, after 30 minutes, add covering medium
13. After 1 hour, visualize cells before invasion using 4x objective
14. After 48-72 hours of incubation, visualize cell invasion

Spheroid invasion assay analysis:

The invasion of cells was measured as a ratio of cell area before invasion (e.g. the size of the spheroid) and the total area invaded by cells after 72 h.

4.3. Molecular biology

4.3.1. Organisms:

Escherichia coli: DH5α: dlacZ Delta M15 Delta (lacZYA-argF) U169 recA1 endA1 hsdR17(rK-mK+) supE44 thi-1 gyrA96 relA1

Bacteria were cultivated under standard conditions in 37°C either in KB medium or on agar plates with given selection antibiotics.

4.3.2. Chemicals and reagents:

Universal pepton (Merck, 1070431000)
Yeast extract (Amresco, J850)
Sodium dodecyl sulfate (SDS) (Sigma, L3771)
Bromophenol blue (P-lab, R 15121)
Tris- EDTA (TE) (Sigma, T9285)
Boric acid (Sigma, B0394)
Sodium acetate trihydrate (NaAc) (Sigma, S9513)
NaOH (Penta, 11002006)
Lithium chloride (LiCl) (Sigma, 203637)
Ammonium acetate (NH_4Ac) (P-lab, 01101)
Disodium hydrogenphosphate dodecahydrate (Na_2HPO_4) (Penta, 10039324)
Sodium dihydrogenphosphate (KH_2PO_4) (Penta, 7778770)
Phenol (Sigma, P1037)
Chloroform ($CHCl_3$) (Lach:ner, 20034-AT1)
Ethanol 96% (EtOH) (Lach:ner, 20025-A96)
Isopropanol (Lach:ner, 20037-AT0)
Glycerol (AppliChem, A1123)
NaCl (Sigma, S3014)
dNTPs 10mM (New England BioLabs, N04475)
Glycogen (Thermo Scientific, R0561)
Agarose (Thermo Scientific, 16500500)

Antibiotics

Ampicillin (Biotika), working concentration: 100 µg/µl

Magnetic beads for DNA purification:

Agencourt AMPure XP (Beckman Coulter, A63881)

4.3.3. Solutions

TEG: 50 mM glucose, 25mM Tris-HCl, 10 mM EDTA, pH 8.0

Lysis solution: 8.8 ml H20, 200 µl 10M NaOH, 1 ml 10% SDS

Neutralizing solution: 10M NH_4Ac

High glucose medium: SOC Medium (New England BioLabs, B9020S)

RNAse solution: RNAse A (Thermo Scientific, EN0531) diluted in TE

Phosphates solution: 1.6M Na_2HPO_4, 0.4M NaH_2PO_4, pH 7.2

Phenol-chloroform: phenol-Tris with $CHCl_3$ 1:1 v/v

6x loading dye (60 % glycerol, 0.06 % bromophenol blue, 60mM EDTA)

GeneRuler 1 kb DNA Ladder (Thermo Scientific, SM0311)

DNA Stain G (Serva, 3980301)

20x TBE:
1 g NaOH
216 g Tris
110 g boric acid
14.8 g of EDTA
Add water to 1 l

KB medium:
10 g Universal pepton
10 g Yeast extract
Add water up to 1 l
Sterilize in autoclave at 121°C for 20 min
After medium cools to RT, add glucose 0.5% w/v
and phosphates solution (100mM final concentration)

Bacteriological agar for plates:
5 g agar
2.5 g Universal pepton
1.25 g Yeast extract
1.25 g NaCl
Add water up to 250 ml
Sterilize at 121°C, 20 min
After cooling to approx. 50°C, add antibiotics for selection

4.3.4. Enzymes

Klenow fragment (2000 U/ml) (Thermo Scientific, EP0054)

T4 DNA ligase (5000 U/ml) (Thermo Scientific, EL0011)

Taq DNA polymerase (5000U/ml) (New England BioLabs, M0273L)

Q5 DNA polymerase (2000 U/ml) (New England BioLabs, M0491L)

RNAse A (Thermo Scientific, EN0531)

Buffers for enzymatic reactions:

T4 DNA ligase buffer 10x (Thermo Scientific, B69)

Taq polymerase buffer 10x (New England BioLabs, M0273L)

Q5 polymerase buffer 5x (New England BioLabs, B9027S)

CutSmart buffer 10x (New England BioLabs, B7204S)

Restriction enzyme buffer 3.1 10x (New England BioLabs, B7203S)

Restriction enzymes:

All utilized restriction enzymes (RE) are summarized in Table 5. All enzymes were provided by New England Biolabs. Buffers were used according to manufacturer recommendation.

Enzyme	Restriction site	Catalogue n.
BamHI-HF*	G/GATCC	R3136S
BglII	A/GATCT	R0144S
EcoRI-HF	G/AATTC	R3101S
HindIII-HF	A/AGCTT	R3104S
KpnI-HF	GGTAC/C	R3142S
MluI	A/CGCGT	R0198S
NdeI	CA/TATG	R0111S
NheI-HF	G/CTAGC	R3131S
PstI-HF	CTGCA/G	R3140S
Sac1-HF	GAGCT/C	R3156S
SmaI	CCC/GGG	R0141S
XbaI	T/CTAGA	R0145S

Table 5: List of restriction enzymes. *HF= high fidelity

4.3.5. Vectors

For vector maps see 11.5 in Attachment.

4.3.6. Inserts

Inserts were amplified by PCR from cDNA obtained by reverse transcription of mRNA of either human macrophages, primary fibroblasts or HT1080 cells. Primer design for amplification and cloning is the merit of Mgr. Vladimír Čermák, Ph.D. For sequences see 11.4 in Attachment.

4.3.7. Polymerase chain reaction (PCR)

PCR for amplification of insert from cDNA

Reaction volumes are 20 µl or 100 µl for small and large reactions, respectively.

1. Prepare reaction mix on ice
2. 1x Q5 mix for 1 small reaction:

   4.0 µl 5x buffer
   0.4 µl 10mM dNTPs
   0.4 µl Q5 polymerase (2U/µl)
   Add ddH_20 to 20 µl
3. Add primers (dilute 200x for final concentration 250 nm)
4. Mix on vortex
5. Add template DNA (cDNA- 1µl, linearized plasmids- 0.2-0.5 µl)
6. Run PCR

i.	95°C	1 min	
ii.	95°C	20 s	
iii.	X °C	20s	
iv.	72°C	1-3 min	
v.	95°C	10 s	Repeat v.-vii. 29x
vi.	Y°C	20 s	
vii.	72 °C	1-3 min (for each kb 1 min)	
viii.	72°C	5 min	
ix.	4°C	unlimited	

7. Run 5 µl of reaction on agarose gel and visualize DNA

X- Annealing temperature of primers without non-complementary overhangs

Y- Annealing temperature of primers including non-complementary overhangs

Colony PCR:

1. Prepare reaction mix (1xTaq mix)

   1xTaq mix:

   100 µl 10x buffer

   10 µl dNTPs 10mM

   30 µl DMSO

   4 µl Taq polymerase (5U/µl)

   Add ddH_20 to 1 ml

   Taq mix can be stored in freezer for future use

2. Transfer given volume of 1xTaq mix to tube - 10 µl per reaction
3. Add primers (dilute 200x for final concentration 250 nm)
4. Mix on vortex
5. Pipette 10 µl of reaction mix with primers to each tube (8-strip tubes)
6. Prepare new agar plate
7. Using a 200 µl tip, replicate bacterial colony to new agar plate
8. Add bacteria to reaction mix by pipetting up and down
9. Run PCR

i.	95°C	3 min	
ii.	95°C	20 s	Repeat
iii.	X°C	20 s	ii.-iv. 30x
iv.	68°C	1-3 min (for each kb 1 min)	
v.	68°C	5 min	
vi.	4°C	unlimited	

10. Add 6x DNA dye to reaction, load gel
11. Run agarose gel to visualize DNA

4.3.8. DNA purification

4.3.8.1. Magnetic beads

1. Let beads adjust to RT
2. Mix magnetic beads by gently swirling
3. Add beads (1.8x volume of DNA v/v) to DNA solution
4. Mix by pipetting 10 times
5. Leave at RT for 10 min
6. Transfer tubes to magnetic holder and leave at RT for 5 min
7. Carefully aspirate solution, leave beads intact
8. Add 500 µl 70% EtOH
9. After 1 min, remove EtOH by pipetting
10. Repeat steps 8.-9. twice
11. Carefully aspirate all EtOH by vacuum pump
12. Leave at RT to dry (do not over-dry)
13. Add 30-50 µl H_20 (according to presumed DNA concentration)
14. Mix on vortex
15. Place on magnetic holder
16. Transfer solution to new tube without disrupting beads

4.3.8.2. Phenol-chloroform extraction

1. Add TE to obtain final volume of 360 µl
2. Add 40 µl 5M NaAc
3. Add 250 µl phenol-chloroform
4. Mix by turning upside down and vortex vigorously
5. Centrifugation, 5 min 16 000 g
6. Carefully, transfer upper phase to new tube
7. Add 1 µl glycogen
8. Add 1100 µl 96% EtOH and mix by turning upside down
9. Incubate at RT for 10 min
10. Centrifugation, 15 min, 16 000 g
11. Carefully, pour EtOH into the sink
12. Wash pellet with 500 µl 80% EtOH
13. Carefully aspirate EtOH by vacuum pump

14. Dry the pellet at RT
15. Add 10-50 µl of H_2O to dissolve DNA

4.3.8.3. DNA isolation from agarose gels

1. Cut fragment from gel and transfer to 1,5 ml tube
2. Add 400 µl phenol-Tris
3. Place into thermoblock set to 72°C
4. Leave 10-20 minutes until agarose is completely dissolved
5. Add 300 µl TE
6. Add 25 µl 10 LiCl
7. Vortex and centrifuge, 10 min 16 000 g
8. Carefully transfer upper phase to new tubes
9. Add 100 µl 10 LiCl
10. Add 300 µl of phenol-chloroform solution
11. Mix by turning upside down, vortex, centrifuge, remove upper phase
12. Add 1 µl glycogen
13. Add isopropanol- 0.7x volume transferred
14. Mix by turning upside down, incubate at RT for 10 min
15. Centrifugation 15 min, 16 000 g
16. Carefully, discard isopropanol
17. Wash pellet with 500 µl 80% EtOH
18. Carefully aspirate EtOH by vacuum pump
19. Dry the pellet at RT
20. Add 10 µl of H_2O to dissolve DNA

4.3.9. Restriction enzyme digestion

1. Prepare reactions in 1.5 ml tube. Adjust final volume according to amount of DNA (for each µg of DNA approx. 10 µl of total reaction volume)
2. Add:

   DNA: 0.5-5 µg

   10x reaction buffer

   Restriction enzyme: 2-5 U of enzyme per 1µg of DNA

   H_2O to final volume
3. Incubate in 37°C for estimated time
4. Verify on agarose gel

4.3.9. Ligation

1. Prepare one 1.5 ml tube for each reaction (total volume 15 µl)
2. For each reaction, add:

20-50 ng	vector DNA cut with RE	Plasmid: insert molar ratio is 1:4-10
50-500 ng	insert DNA cut with RE	
1.5 µl	10x ligation buffer	
0.3 µl	T4 DNA ligase (5U/µl)	

   Add H_2O to final volume
3. Leave at RT for 12 hours
4. Transfer to freezer for storage

4.3.10. Generation of blunt DNA ends

1. Prepare reaction by adding

1 µg	DNA
1 µl	10x ligase buffer
0.1µl	10mM dNTPs
0.1µl	Klenow fragment of DNA polymerase I (2U/µl)
2. Leave at RT for 20 min
3. Purify modified DNA directly or store in freezer

4.3.11. Transformation of chemically competent bacteria

1. Transfer bacteria from deep-freezer on ice

   50 µl of bacterial suspension per transformation
2. Add 10-30% of ligation mixture (maximum added volume should not exceed 10% v/v of bacterial suspension)
3. Mix gently by shaking
4. Incubate on ice for 30 min
5. Meanwhile, pre-heat thermoblock for 42°C
6. Place in 42°C for 1 min to exert heat shock
7. Immediately place on ice and add 50 µl high glucose medium
8. Spread on pre-warmed ampicillin selection agar plates
9. Incubate plate in 37°C for 12-16 hours

4.3.12. DNA isolation by phenol-chloroform mini-preps:

1. The day before, inoculate bacteria colonies each in 2 ml of KB medium
2. Incubate in 37°C for 12-16 hours
3. Transfer 1 ml of bacterial culture to 1.5 ml tubes
4. Centrifuge 1 min, 16 000 g
5. Remove medium with a vacuum pump
6. Add 100 µl TEG
7. Re-suspend bacterial pellet by mixing on vortex or pipetting
8. Prepare fresh lysis solution in a 15 ml tube
9. Add 280 µl of lysis solution while mixing on vortex for 2 s
10. Add 420 µl of neutralizing solution while mixing on vortex for 5 s
11. Add 280 µl of phenol-chloroform solution
12. Vortex vigorously for 10 s
13. Centrifuge 16 000 g for 5 minutes
14. Prepare and label new 1.5 ml tubes
15. Carefully transfer the upper phase into the new tube
16. Add isopropanol (0.7x volume transferred)
17. Mix well
18. Incubate 15 min at RT
19. Centrifuge, 15 min 16 000 g

20. Decant isopropanol, be careful not to spill out the pellets
21. Add 500 µl 80% EtOH and mix by turning upside down, pellets should float
22. Centrifuge 16 000 g for 1 min
23. Carefully aspirate EtOH using vacuum pump
24. Leave at RT to dry pellet
25. Add 20 µl of RNase solution and place in 37°C for 1 h
26. Transfer to freezer to for storage

4.3.13. Gel electrophoresis

Preparation of agarose gels:

1. Prepare agarose gel by dissolving agarose in 100 ml 0.5% TBE buffer in Erlenmeyer flask
   For fragments 1-10 kbps prepare 1% w/v agarose gel
   For fragments smaller than 1 kbps prepare 2% w/v agarose gel
2. Melt agarose by heating in microwave
3. Prepare a gel tray with combs
4. Let agarose cool down to 40-50°C
5. Add DNA stain (1% v/v)
6. Pour agarose gel into the gel tray, adjust combs in place
7. Leave to solidify at RT
8. Run gel directly or place in the fridge for short term storage

Running agarose gels:

1. Place gel in apparatus
2. If necessary, fill apparatus with 0.5% TBE (change buffer every week)
3. Load 4 µl of 1 kb DNA marker
4. Load 0.2-1 µg of DNA mixed with 6x loading dye
5. Run gel at 150 V until the dye reaches 75% of gel length
6. Transfer to UV trans-illuminator an visualize fragments

4.3.14. Measuring DNA concentration

1. Dilute DNA 100x in Tris (pH 7.4)
2. Measure absorbance at wavelengths 230, 260, 280
    a) Absorbance of blank (Tris, pH 7.4) on UV-spectrophotometer
    b) Absorbance of DNA in Tris, (pH 7.4) on UV-spectrophotometer
3. Calculate DNA concentration and purity

4.4. Equipment

NanoEntek JULI Fl+Br station microscope

Nikon-Eclipse TE2000-S

Nikon-Eclipse TS100

Flow cytometer BD LSR II

Heated chamber Ibidi Heating system, Universal Fit

Eppendorf Centrifuge 5415 D

Eppendorf Centrifuge 5417 R

Eppendorf Centrifuge 5804 R

Thermocycler BIOER-Gene Pro

Trans illuminator Syngene InGenius3

Source Lifetechnologies Inc, BRL Model 500 high current

Thermoblock Major Science Dry Bath Incubator

Biosan Environmental Shaker Incubator ES-20

Spectrophotometer Shimadzu UV-1650PC

5. Results

5.1. Optimization of 3D conditions

Initially, suitable conditions for studying cell invasion in 3D environment were tested. It was necessary to optimize conditions for morphology assays and live cell imaging. Conditions for live cell imaging should enable cell invasion of both amoeboid and mesenchymal cells to verify that the phenotypic changes observed are not an artifact of prevented motility. However, these conditions are not very suitable for evaluating primary morphology, since migrating cells, particularly amoeboid cells, often employ various shapes when invading through the ECM, which complicates the evaluation of primary phenotypes based on static cell shape.

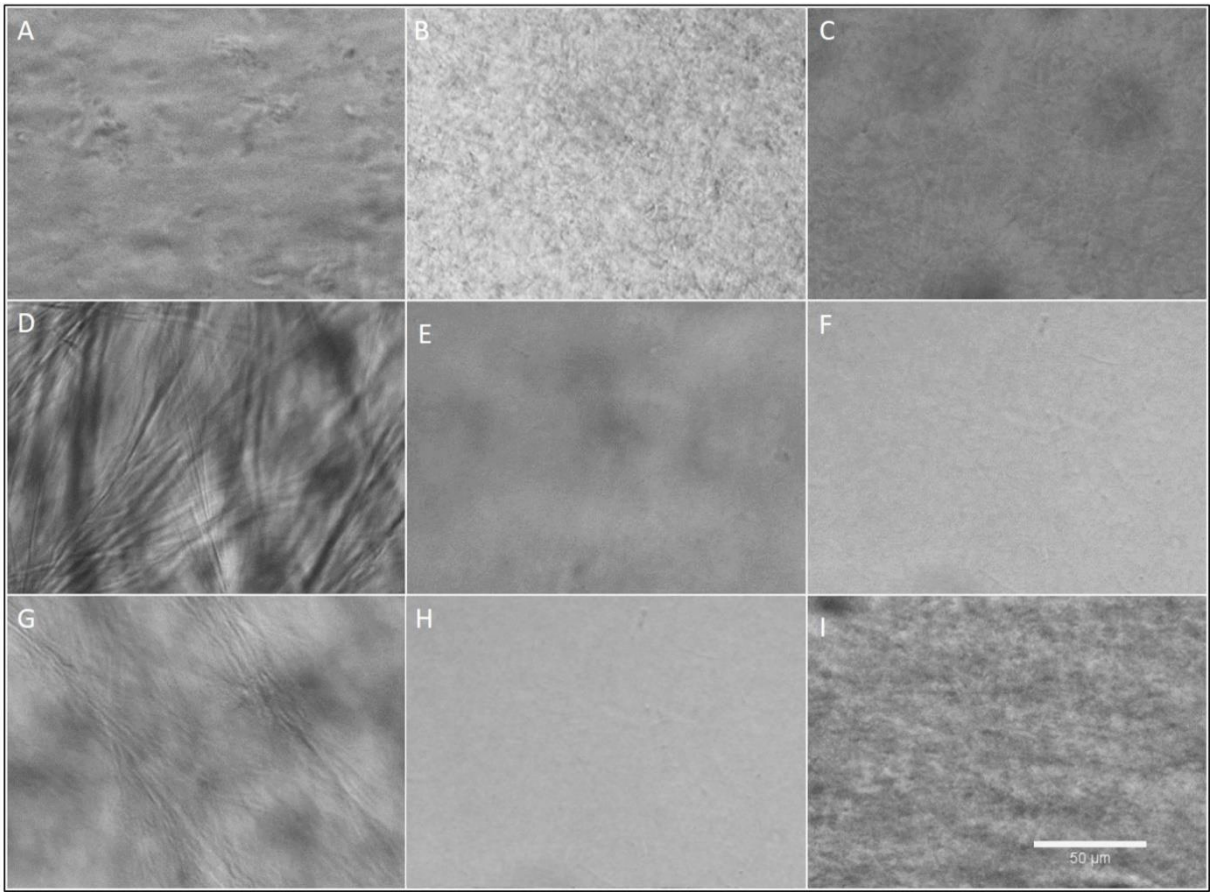

Fig. 17: Example of available 3D conditions. A: Matrigel 8 mg/ml; B: Fibricol 8mg/ml; C: Nutragen 2 mg/ml; D: Collagen G with 1M NaOH; E: Collagen R 0.5 mg/ml; F: Collagen R 1.5 mg/ml; G: Collagen G with 200mM NaOH; H: Collagen R 1 mg/ml; I: Nutragen 4.8 mg/ml.

Overall, the effect of the matrix concentration and stiffness on cell behavior is well documented (Brábek et al., 2010; Tozluoğlu et al., 2013; Wolf et al., 2013). Therefore, we observed melanoma cells in various 3D conditions to test the effect of prepared matrixes on cell morphologies. Available 3D conditions are summarized in Fig. 17.

For standard morphology assays, we decided to use rat tail collagen of concentration 1mg/ml for following reasons- rat tail collagen is not devoid of cross-links and should thus be more similar to *in vivo* conditions (Sabeh et al., 2009). Second, it showed to be suitable for morphology analysis as all cells exhibited expected morphology, e.g. amoeboid in case of A375m2, mixed in case of WM3629 and mesenchymal in case of BLM cells.

Next, we focused on determining the best conditions available for live cell imaging of amoeboid and mesenchymal invasion. Recently, various studies have confirmed that pore size is a limiting factor for amoeboid migration due to limited nuclear deformability (Davidson et al., 2014; McGregor et al., 2016; Wolf et al., 2013). The study by Wolf et al. reported that only pore sizes larger than 7 μm^2 are sufficient for cell invasion. To obtain rat tail collagen with pores larger than 7 $\mu m^{2,}$ it is necessary to decrease collagen concentration to 0.3-0.5 mg/ml or decrease polymerization temperature to 9°C. Therefore, we tested both approaches. Although decreasing polymerization temperature turned out to be unsuitable due to long polymerization times, during which most cells sedimented to the bottom, decreasing collagen concentration to 0.5 mg/ml was feasible. Moreover, it proved to be suitable for both migration modes as demonstrated by live cell imaging (see Fig. 19, Fig. 30).

5.2. Testing dense collagen as a potential inducer of AMT

It has been documented that in case of human macrophages the conditions of the ECM itself can induce morphological changes (Van Goethem et al., 2010). Thus, we were interested whether the concentration of collagen could be itself enough to induce morphological changes in melanoma cell lines. First, to test whether our prepared collagen matrices are suitable for testing morphological changes, we conducted control experiments with human macrophages according to Van Goethem et al. Accordingly to the published results, we observed amoeboid morphology of macrophages in porous collagen (Nutragen, 2 mg/ml) and mesenchymal morphology in dense collagen (Nutragen, 4.8 mg/ml) (data not shown). These control experiments confirmed that our prepared 3D matrices are suitable for testing morphological changes caused by rigid collagen. Therefore we proceeded with testing melanoma cell lines in these conditions. We seeded A375m2 cells in bovine collagen of high concentration (Nutragen, 4.8 mg/ml). In these conditions, A375m2 cells remained round. Thus, we further tested these cells in bovine collagen of concentration 8 mg/ml. Even in these conditions cells maintained round morphology (Fig. 18). However, the cells were constricted of any movement and died within 72 hours. Since the same effect was observed in other cell lines as well (data not shown), we did not continue with these experiments, owing to which statistical analysis is not provided for these results.

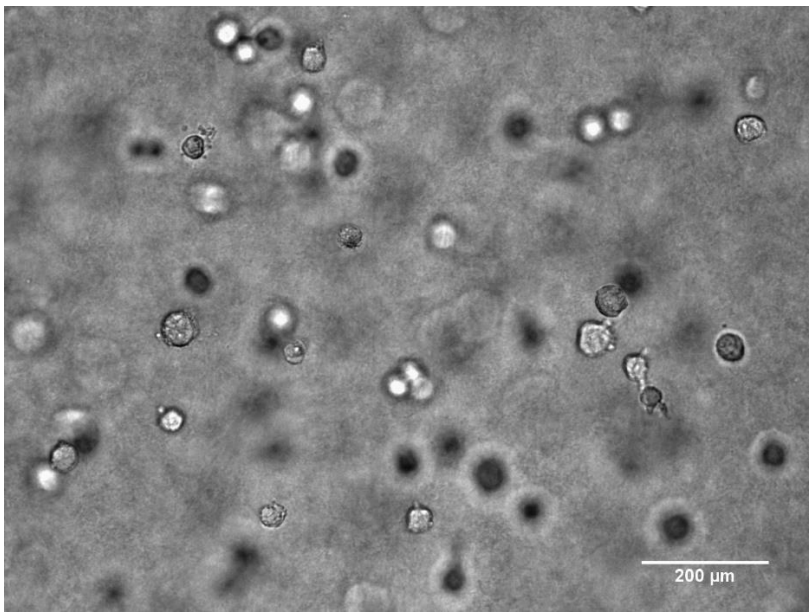

Fig. 18: Morphology of A375m2 cells in dense collagen.

Cells after 24 hours, imaged using 10x obj, HMC, Nikon-Eclipse TE2000-S. Representative photo is shown.

5.3. Manipulating Rho GTPase pathways

5.3.1. Expression of caRhoA induces MAT in melanoma cells

We have previously established a system for inducing MAT based on the inducible expression of caRhoA tagged with EGFP in HT1080 sarcoma cells (V. Čermák et al., manuscript in preparation). HT1080 cells, which are primarily mesenchymal in standard 3D conditions, switch to the amoeboid phenotype within 12-16 hours upon induction of EGFP-caRhoA as demonstrated by live cell imaging (Fig. 19). To visualize MAT in HT1080 cells, cells were embedded in collagen without doxycycline and left to adjust to the 3D conditions for a few hours. Just before imaging, medium without doxycycline was carefully aspirated and exchanged for medium with doxycycline.

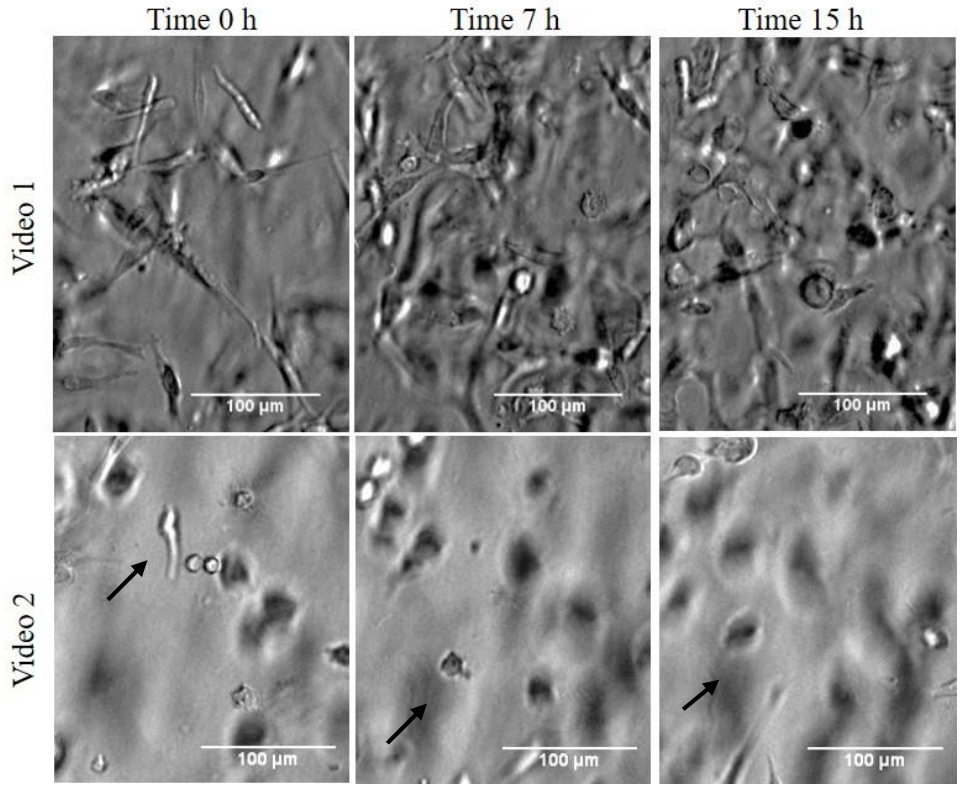

Fig. 19: Mesenchymal-amoeboid transition of HT1080 cell after caRhoA expression. Cells were imaged every 1 minute for 15 hours using 10x obj, HMC, Nikon-Eclipse TE2000-S. Representative photos from two videos show cells in time 0, 7 and 15 hours. For Video 2, black arrows depict the position of the same cell.

To further extend the Rho-inducible MAT analysis, we decided to establish melanoma stable cell lines expressing EGFP-caRhoA. As model cell lines we chose BLM cells, which are primarily mesenchymal, and WM3629 cells that naturally employ both invasion modes.

We favored the generation of stable cell lines over transient transfection, because stable cell lines are more convenient for long-term experiments and high-throughput analyses as DNA is incorporated into the genome during the process, unlike transient transfection, during which protein expression is diluted in time (Kim and Eberwine, 2010). Moreover, stable cell lines are less prone to exhibit artifacts due to high overexpression, uneven levels of gene expression within the cell population or temporary phenotypes when compared to transient transfection.

We used lentiviral transduction for the generation of stable cell lines. Initially, we established BLM-TOB (TOB: Tet-On Advanced with blasticidin resistance) and WM3629-TOB stable cell lines, which incorporated the regulatory sequences necessary for doxycycline regulated induction in their genome. The regulatory vector, pLVX-TOB carries the tetracycline-controlled transactivator (rTA Advanced), which is a mutated tet-operator that binds to the tet-sequence in presence of doxycycline or tetracycline, opposite to its original function. BLM-TOB and WM3629-TOB lines were established by selection with blasticidin for 2 weeks.

Subsequently, these cell lines were transduced with the responsive vector, pLVX-Tight-Puro-EGFP-RhoA-G14V. This vector contains the inducible promoter, which comprises the tet-responsive elements fused to a modified CMV promoter, after which the gene of interest is located. Upon doxycycline induction, the transactivator binds to the responsive elements and promotes transcription from the CMV promoter (Fig. 20).

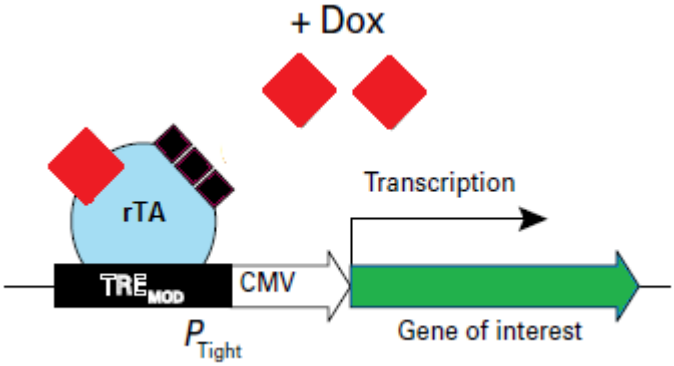

Fig. 20: Schematic illustration of doxycycline induced expression of GOI. In the presence of doxycycline, rTA, coded by the regulatory vector, activates transcription from the CMV promoter and GOI is transcribed. Adapted from Lenti-X™ Tet-On® Advanced Inducible Expression System User Manual[2].

.

[2] A*vailable online:* http://www.clontech.com/xxclt_ibcGetAttachment.jsp?cItemId=17567&embedded=true

The vector further encodes puromycin resistance and, importantly, RhoA with mutated glycine for valine at position 14 and EGFP cDNA at 5'-terminus. The G14V mutation causes the protein to be constitutively active by reducing its GTPase activity, which prolongs the active RhoA-GTP state (Diekmann et al., 1995; Ihara et al., 1998).

To select for positive clones, we treated cells with puromycin, an antibiotic suitable for selection of mammalian cells. However, while the use of antibiotics can greatly enhance the population of positive cells, it rarely results in positive-only populations, as cells can selectively incorporate only the gene for antibiotic resistance, or become resistant during the selection process (Lanza et al., 2013).

For this reason, we sorted cells for EGFP (after brief induction with doxycycline), a marker of RhoA expression due to the fusion. After the first round of sorting, the cell population still showed more than 20 % percent of negative cells, as determined by flow cytometry. This can be attributed to the limited accuracy of cell sorting and also genomic instability of cancer cells. Nevertheless, the second round of sorting resulted in the vast majority of positive cells. The percentage of positive cells was 97 % for BLM-TOB-EGFP-RhoA-G14V and 95 % for WM3629-TOB- EGFP-RhoA-G14V stable cell lines (Fig. 21).

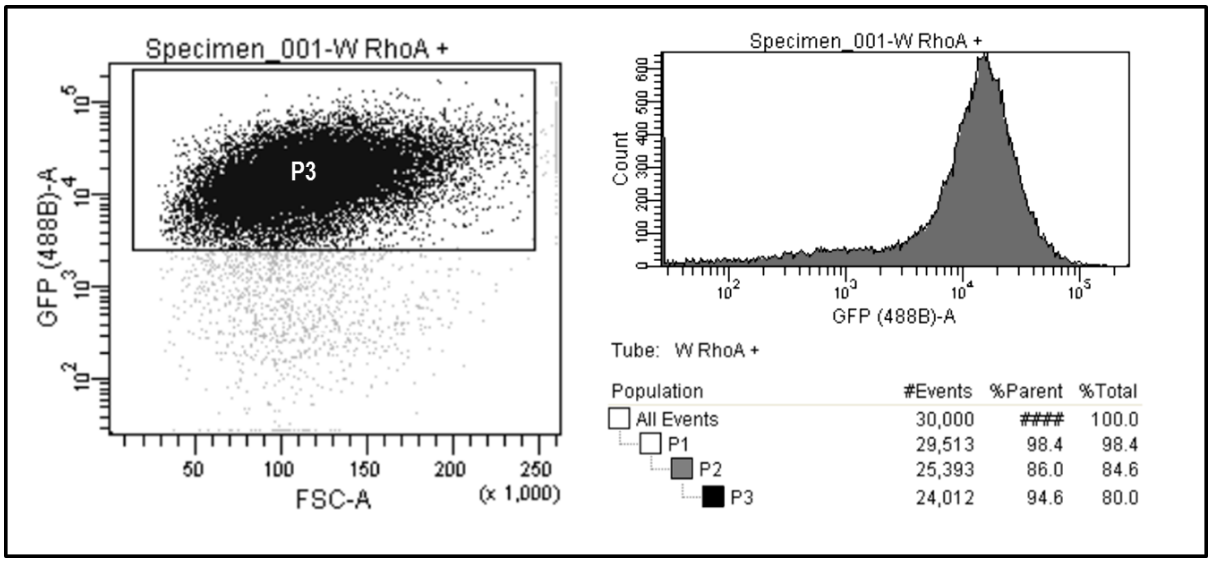

Fig. 21: Results of flow cytometry analysis of WM3629 with induced caRhoA

Left, dot plot showing EGFP positive population (P3). Upper right, histogram depicting distribution of EGFP intensities. Lower right, percentages of individual population. P3 population represents 94.6% of parental population (P2, all viable cells).

Next, we analyzed the morphology of cells with and without induced caRhoA expression. Cells were embedded in 1mg/ml collagen for 48 hours in the presence of the inducer of expression, e.g. doxycycline (+DOX), in case of treated cells and without doxycycline (-DOX) in case of control cells. The experiments were repeated three times to obtain biological replicates. For each repetition, approx. 350 cells were counted to ensure that at least 1000 cells for each condition were analyzed. Cell morphology was analyzed according to cell length:width ratio. Cells were considered amoeboid if their length:width ratio was smaller than <1.5, and mesenchymal if they showed elongated morphology and ratio >1.5. These indexes have been applied in our previous studies (Vaskovicova et al., 2015). However, in this case we did not consider a third, intermediate, group of cells since cells exhibited clear amoeboid or mesenchymal morphologies.

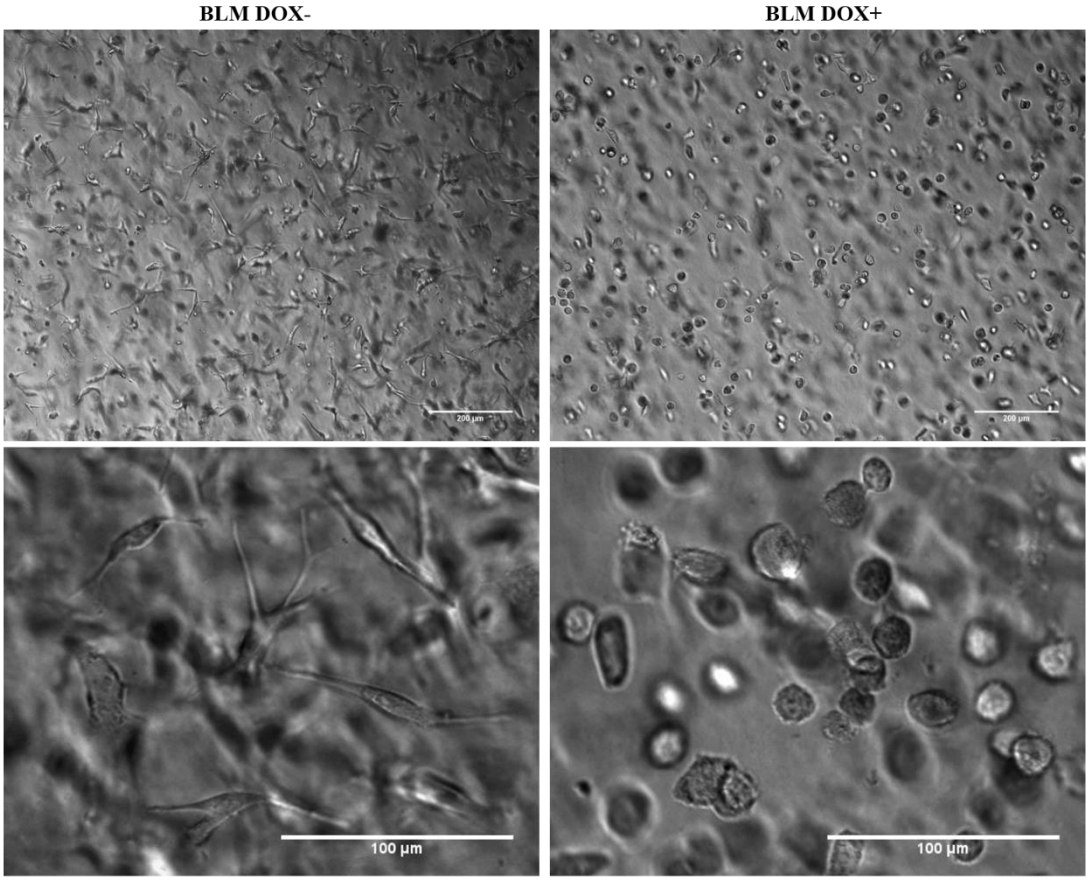

Fig. 22: Morphology of BLM cells without or with induced caRhoA. Representative images are shown. Cells were imaged after 48 hours using Nikon-Eclipse TE2000-S, HMC with 10x obj or 20 x obj shown in upper and lower row, respectively. Scale bar in upper row 200 µm, lower row 100 µm.

.

The first cell line analyzed were BLM melanoma cells, which primarily exhibit mesenchymal morphology. After induction of caRhoA, the vast majority of cells were rounded with visible membrane blebs (Fig. 22). The quantification of cell morphologies is summarized in Fig. 23.

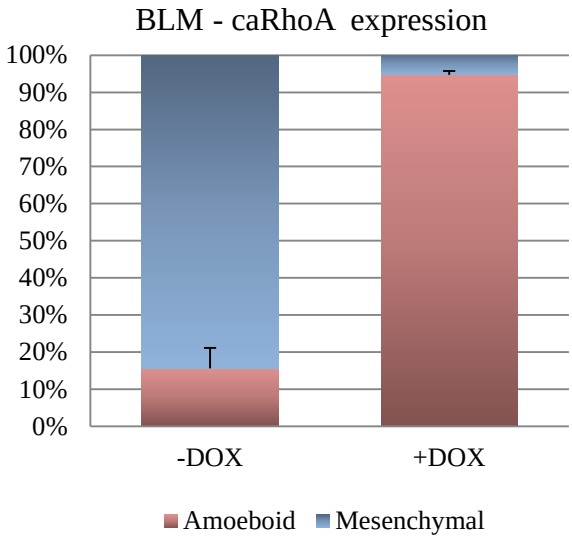

Fig. 23: Quantification of morphology of BLM cells without or with induced caRhoA.
The results of three independent experiments are shown. Error bars represent standard deviations.

We further repeated these experiments on WM3629 cells that primarily comprise both amoeboid and mesenchymal cells. After induction of caRhoA expression in these cells, almost all cells exhibited the amoeboid phenotype (Fig. 25), in agreement to BLM cells. The quantification is summarized in Fig. 24.

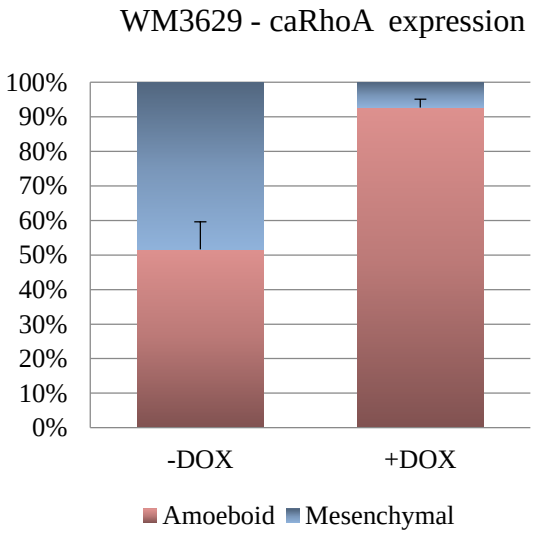

Fig. 24: Quantification of morphology of WM3629 cells without or with induced caRhoA.
The results of three independent experiments are shown. Error bars represent standard deviations.

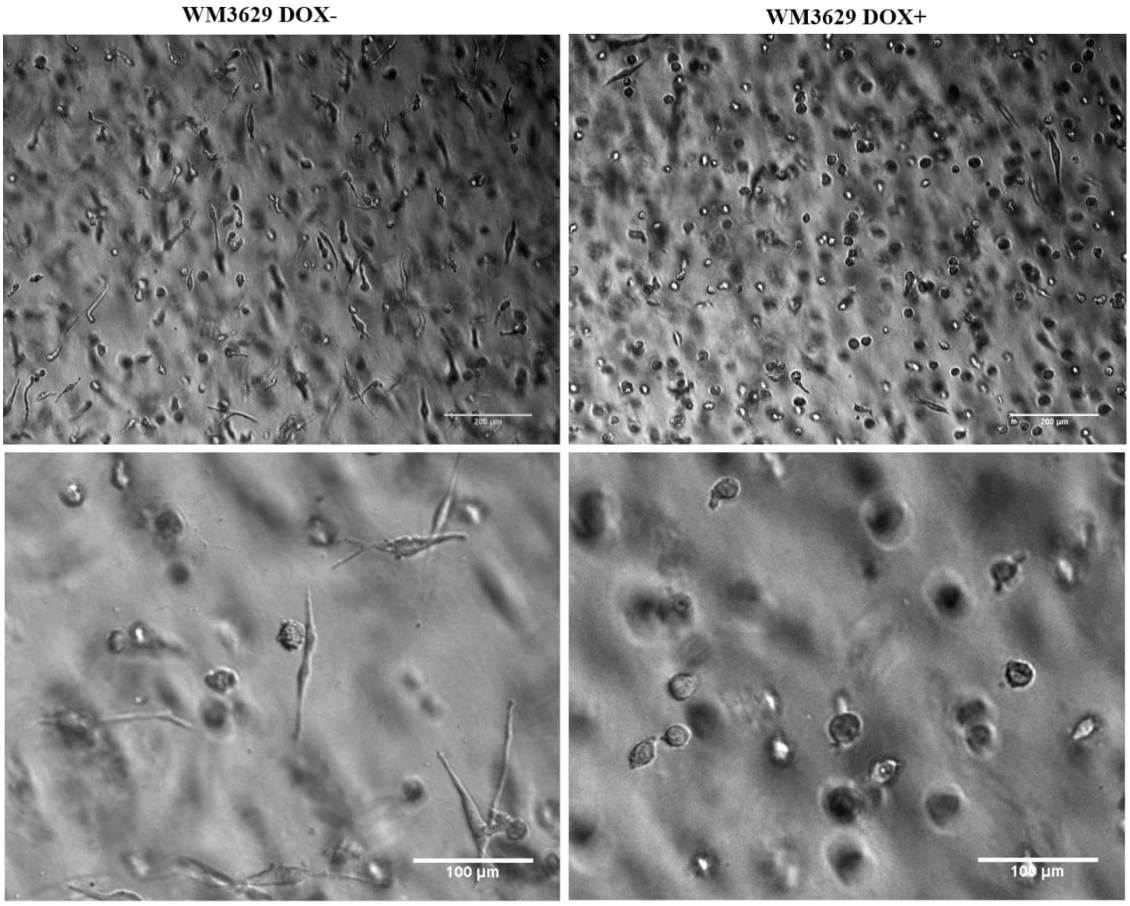

Fig. 25: Morphology of WM3629 cells without or with induced caRhoA. Representative images are shown. Cells were imaged after 48 hours using Nikon-Eclipse TE2000-S, HMC, 10x obj. Upper row, full field, scale bar 200 µm. Lower row, detailed view, scale bar 100 µm.

5.3.2. Morphology of melanoma cells after dasatinib treatment

An alternative approach to induce MAT in melanoma cells is treatment with dasatinib, which inhibits Src and Abl kinases, key factors for mesenchymal migration (Buettner et al., 2008; Courtemanche et al., 2015; Peacock et al., 2007). The use of dasatinib for induction of MAT has been reported previously (Ahn et al., 2012). We embeded cells in 3D collagen in the presence of 0.1% DMSO as a control and 1µM dasatinib (DAS) in DMSO (final DMSO concentration 0.1%), and analyzed cell morphology after 48 h (as described in 5.3.1). Morphology analysis confirmed that dasatinib is a potent inducer of MAT since melanoma BLM and WM3629 cells treated with dasatinib almost invariantly employed the amoeboid invasion mode (Fig. 26 and Fig. 28). For BLM cells, dasatinib treatment resulted in a morphological switch, as the percentage of amoeboid cells before MAT was around 15%, which is comparable to that of mesenchymal cells after MAT (Fig. 27). WM3629 that primarily exhibit a mixed phenotype gained the round morphology in over 95 % (Fig. 29).

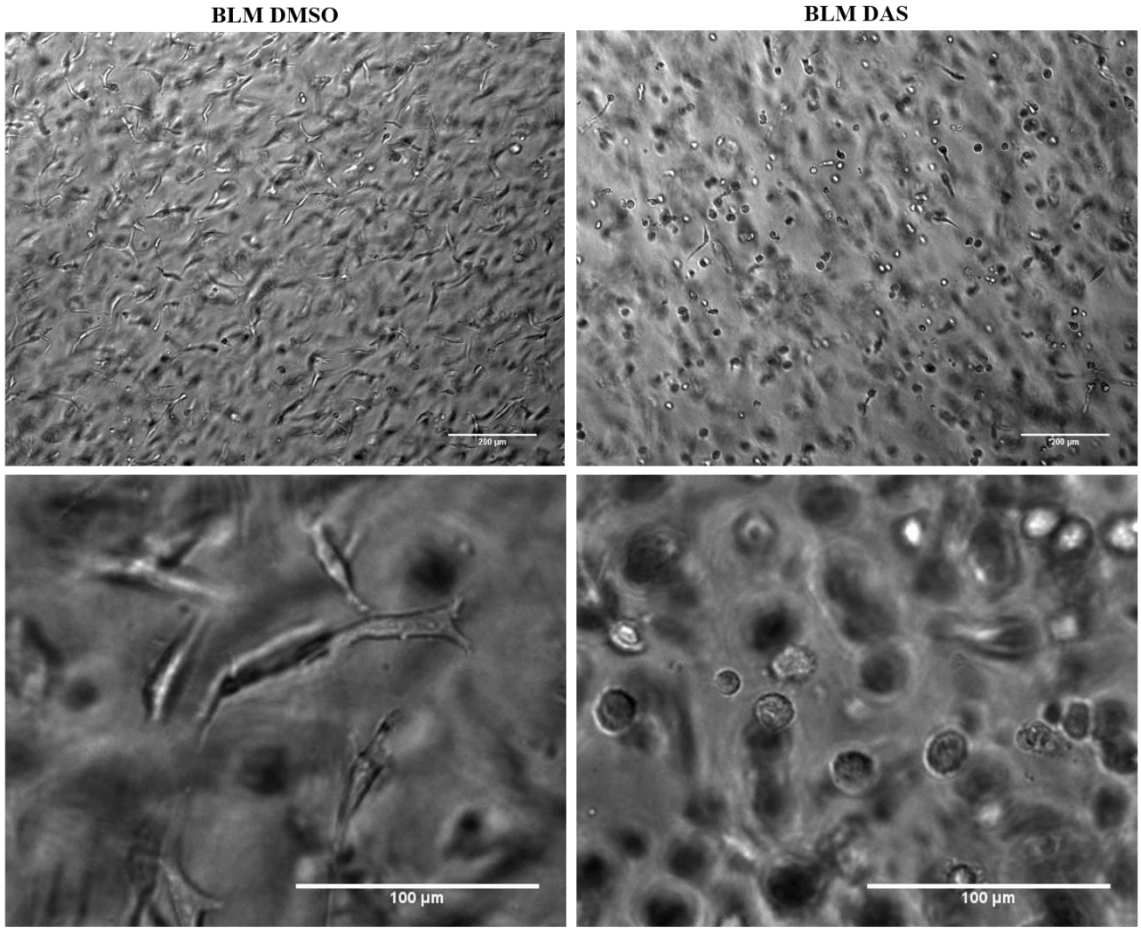

Fig. 26: Morphology of BLM cells without or with DAS. Representative images are shown. Cells were imaged after 48 hours using Nikon-Eclipse TE2000-S, HMC with 10x obj or 20 x obj shown in upper and lower row, respectively. Scale bar in upper row 200 µm, lower row 100 µm.

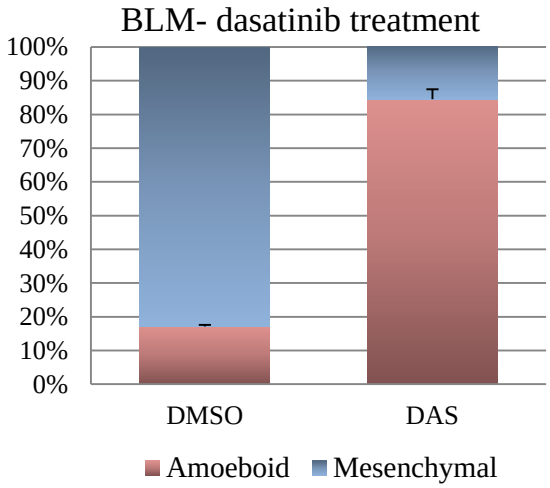

Fig. 27: Quantification of morphology of BLM cells without or with DAS

The results of three independent experiments are shown. Error bars represent standard deviations.

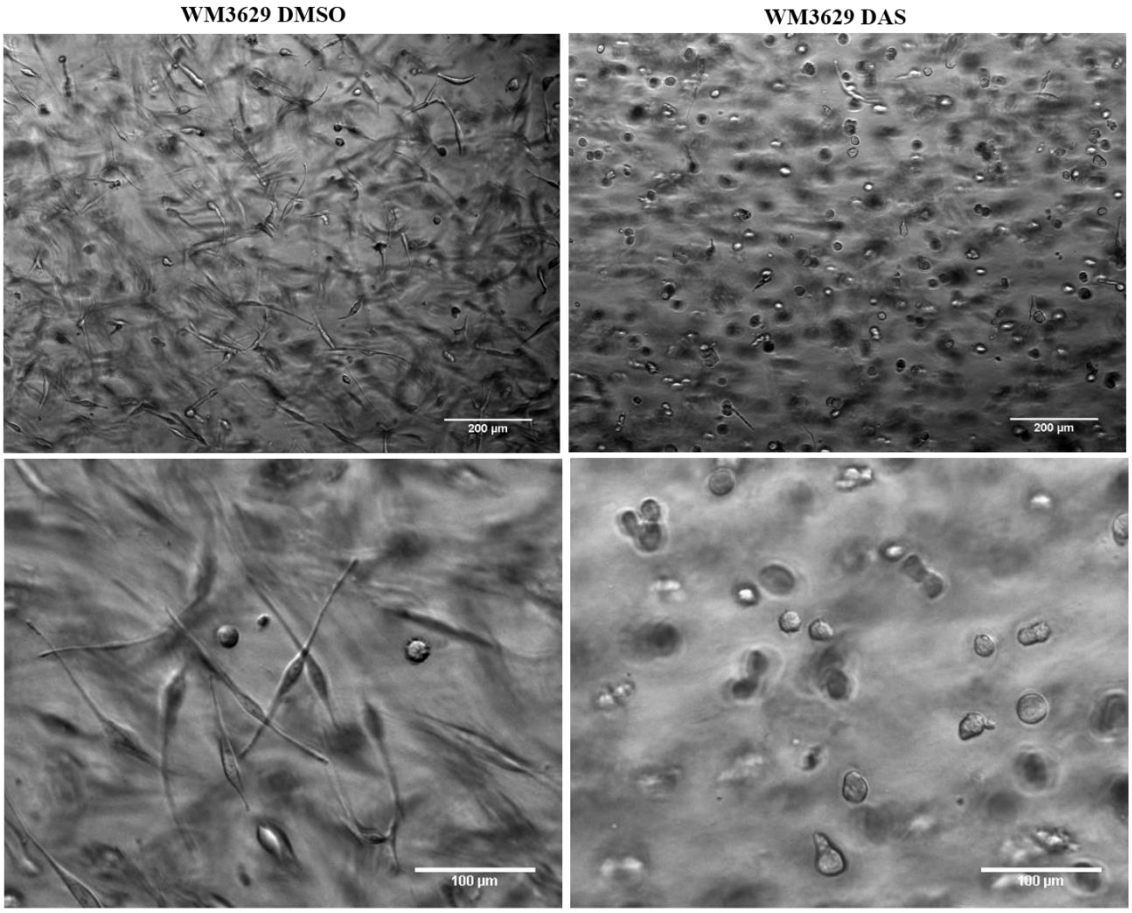

Fig. 28: Morphology of WM3629 cells without or with induced DAS. Representative images are shown. Cells were imaged after 48 hours using Nikon-Eclipse TE2000-S, HMC, 10x obj. Upper row, full field, scale bar 200 µm. Lower row, detailed view, scale bar 100 µm.

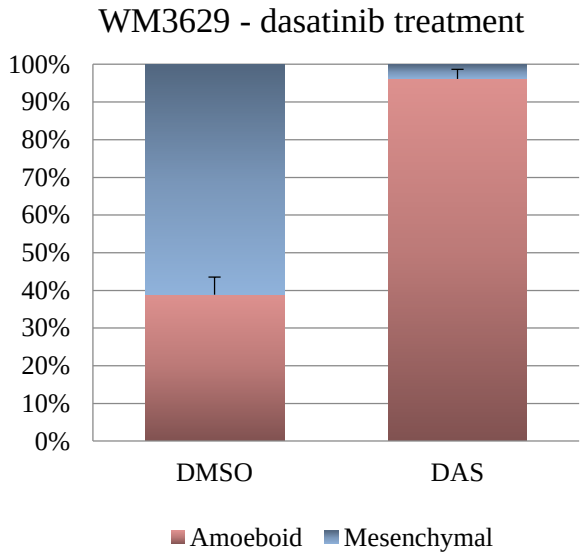

Fig. 29: Quantification of morphology of WM3629 cells without or with DAS. The results of three independent experiments are shown. Error bars represent standard deviations.

We also used live cell imaging to observe invasion of individual cells with and without dasatinib treatement. Instead of forming prostrusions, clearly visible in control cells, dasatinib treated cells exhibited enhanced cell body deformability and formed numerous membrane blebs during migration through collagen matrix (Fig. 30), which is typical of amoeboid cells.

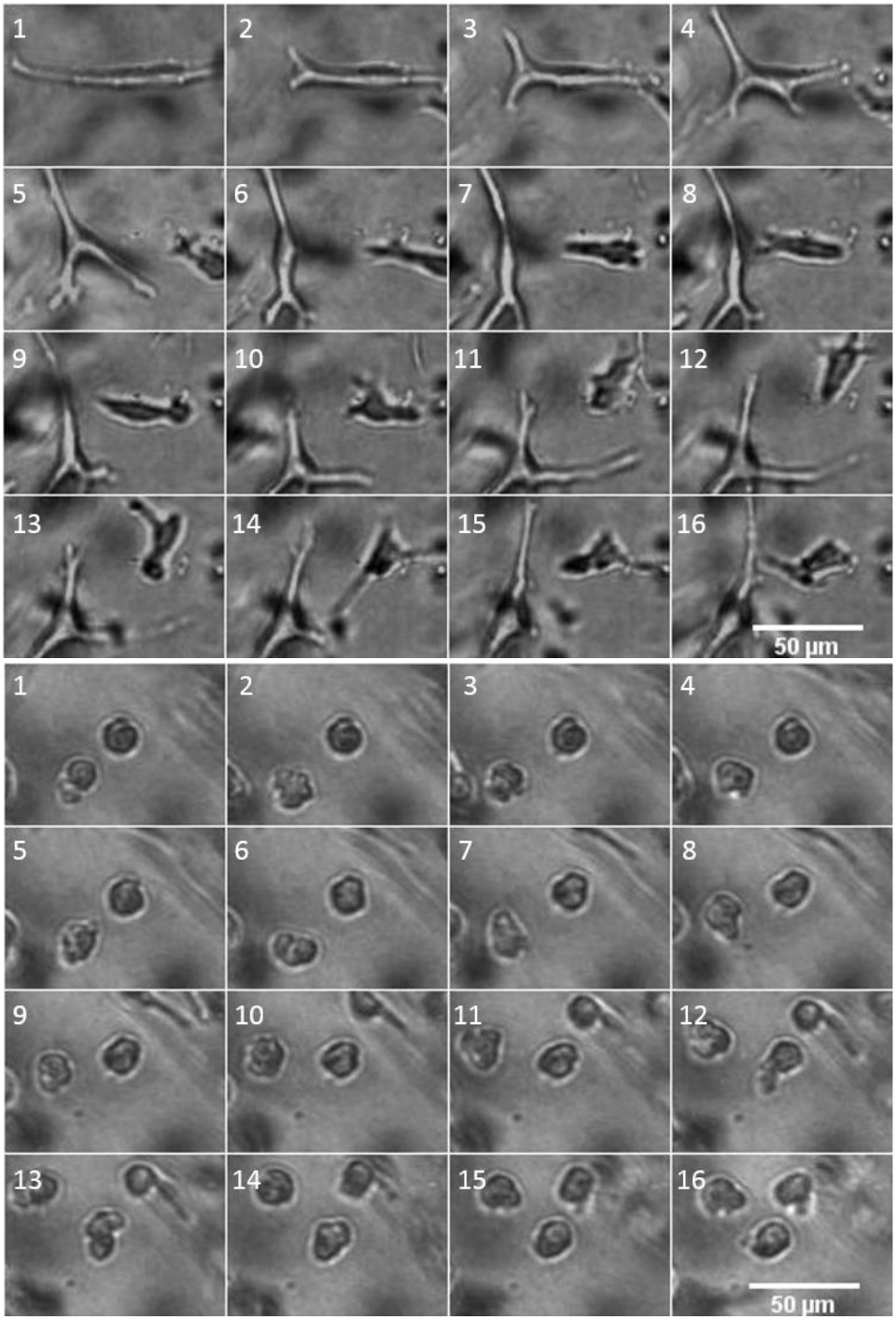

Fig. 30: Image sequences of BLM mesenchymal and amoeboid invasion derived from live-cell imaging videos. Upper sequence shows mesenchymal invasion of control BLM cells, lower sequence amoeboid invasion of BLM cells after dasatinib treatment. Time interval between individual photos is 20 minutes. Images were obtained using JULI Fl+Br. Scale bar represents 50 µm.

5.3.3. Invasion of melanoma cells after MAT treatment

We also assessed the invasion of melanoma cells after MAT induced by both dasatinib and caRhoA expression. For invasion assays, BLM cells were used. These cells are predominantly mesenchymal and thus are appropriate to test whether the invasion potential of cells after MAT, induced by both caRhoA and dasatinib, is affected.

To measure invasion of mesenchymal cells, spheroids of BLM cells were prepared. Spheroids were formed without the presence of any treatment so as not to affect spheroid formation by treatment. After 72 hours, spheroids were embedded in collagen 1 mg/ml either with or without dasatinib or doxycycline. Just after gelation of collagen, the spheroids were imaged using Nikon-Eclipse TE2000-S, 4x obj. Within the next 72 h, cells disseminated from the spheroid and invaded the surrounding collagen. Subsequently, images of invaded cells were obtained by Nikon-Eclipse TE2000-S, 4x obj.

The invasion of cells was measured as a ratio of cell area before invasion (e.g. size of the spheroid) and the total area invaded by cells after 72 h. Data analysis was performed using ImageJ. The invasion ratio was normalized to invasion of control cells and is summarized in Fig. 31 Fig. **32**. Overall, cells after MAT clearly employed the amoeboid invasion mode when disseminating from the spheroid. Their invasion capabilities were reduced 2.5x and 1.3x in case of caRhoA expression and dasatinib treatment, respectively. Both the decrease observed after caRhoA expression and dasatinib treatment proved to be statistically significant (chapter 6).

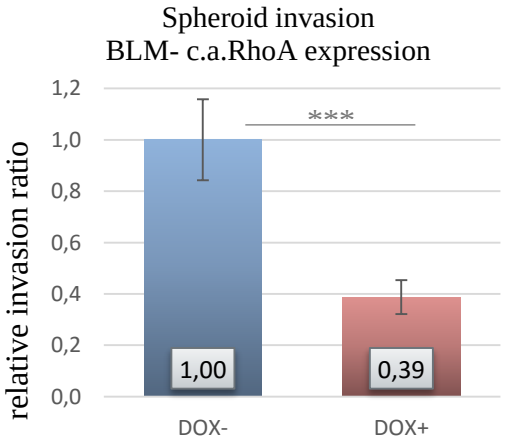

Fig. 31: Quantification of spheroid invasion of BLM cells without or with caRhoA expression. The results of three independent experiments are shown. Error bars represent standard deviations. P value <<< 0.5.

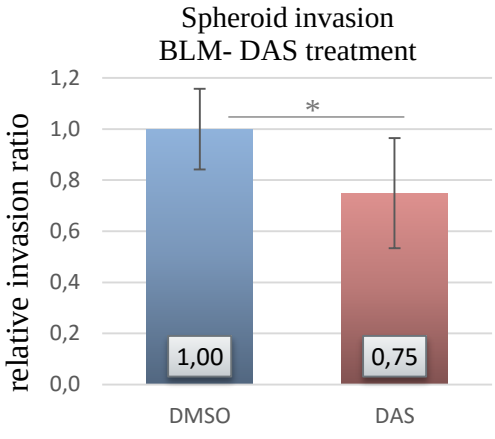

Fig. 32: Quantification of spheroid invasion of BLM cells without or with DAS. The results of three independent experiments are shown. Error bars represent standard deviations. P value < 0.5.

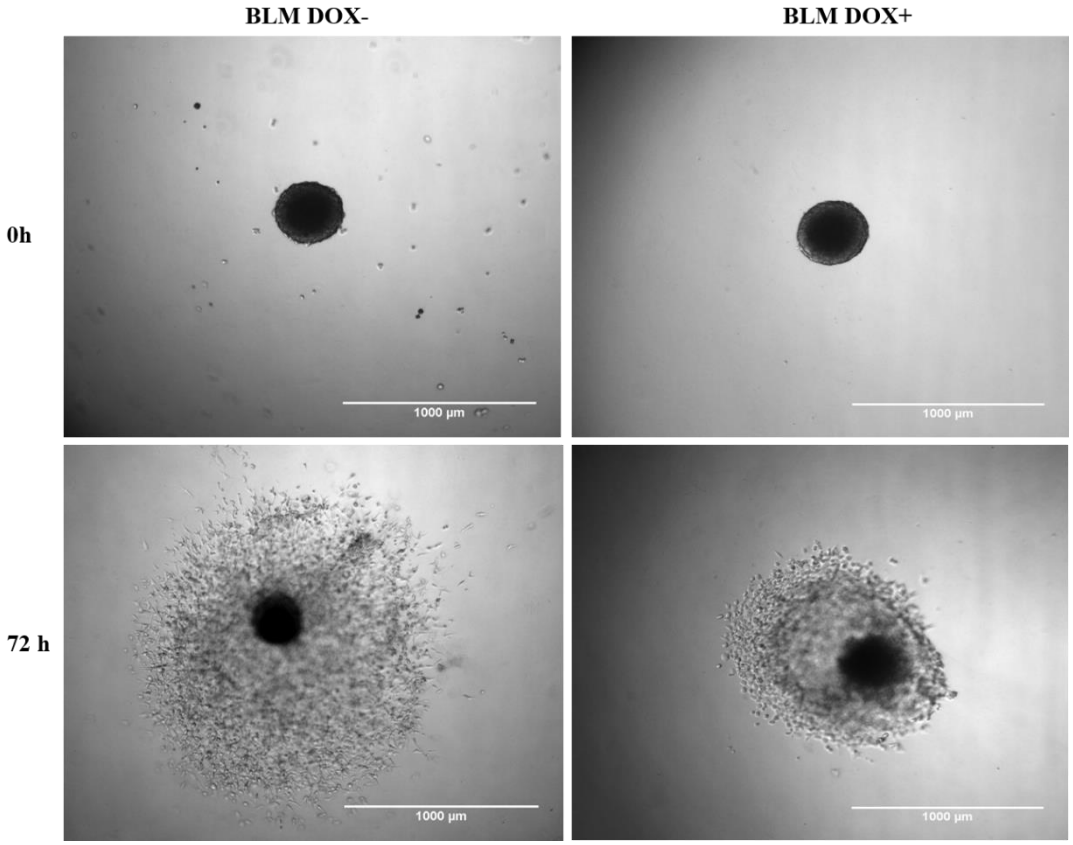

Fig. 33: Spheroid invasion of BLM cells without or with caRhoA. Representative images are shown. Cells were imaged at 0h and 72 h for upper row and lower row, respectively, using Nikon-Eclipse TE2000-S, 4x obj. Left, control cells, right cells expressing caRhoA. Scale bars 1000 µm.

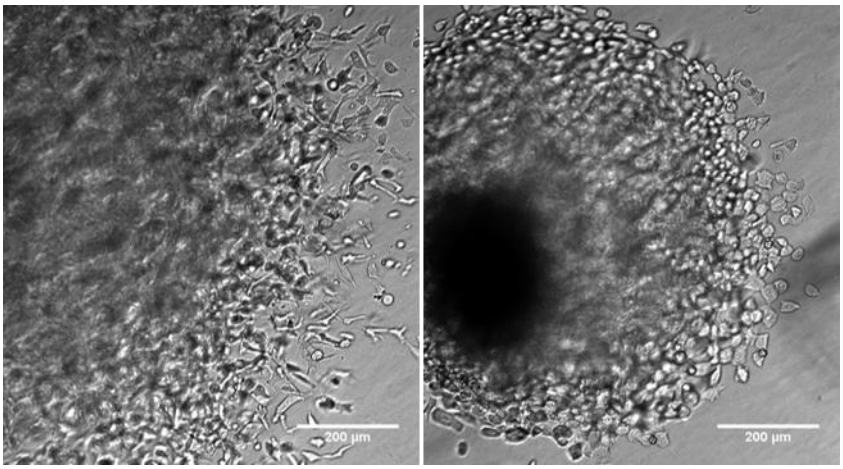

Fig. 34: Spheroid invasion of BLM cells without or with caRhoA expression- detailed view. Representative images are shown. Cells were imaged at 72 h using Nikon-Eclipse TE2000-S, HMC, 10x obj. Left, control cells, right cells with induced expression of caRhoA. Scale bars 200 µm.

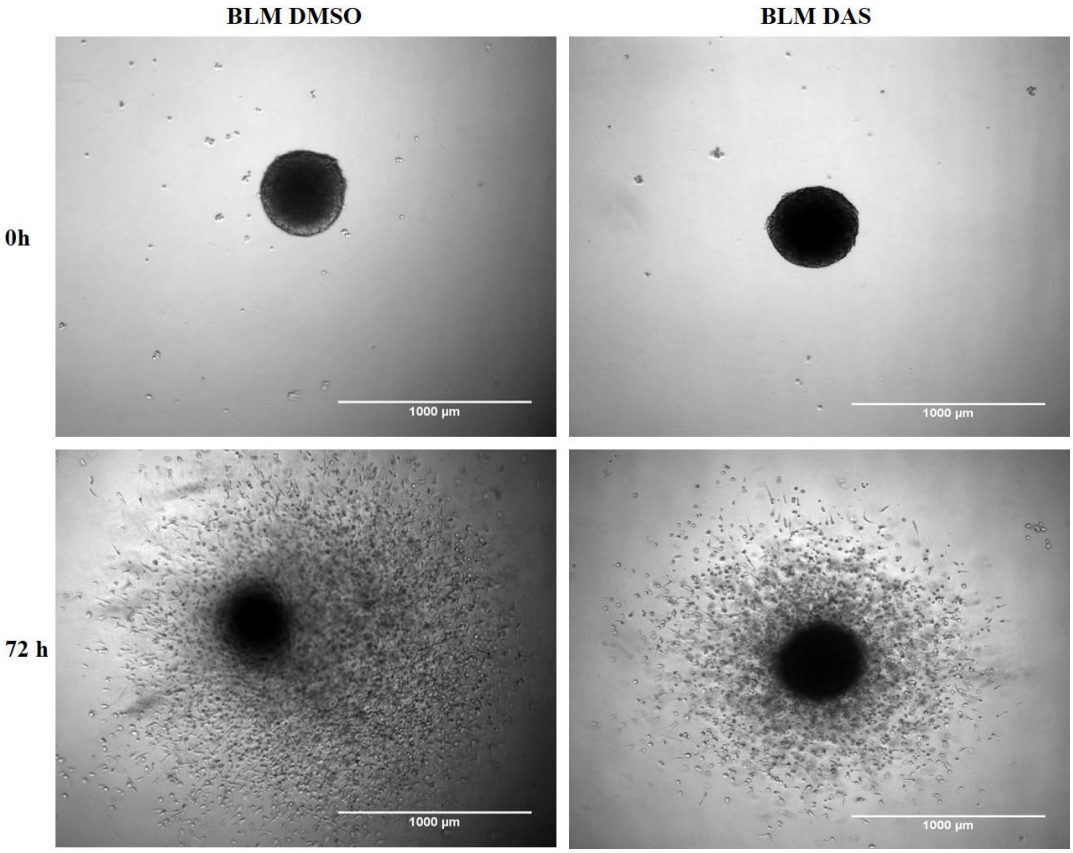

Fig. 35: Spheroid invasion of BLM cells without or with DAS. Representative images are shown. Cells were imaged at 0h and 72 h for upper row and lower row, respectively, using Nikon-Eclipse TE2000-S, 4x obj. Left, control cells, right cells treated with dasatinib. Scale bars 1000 µm.

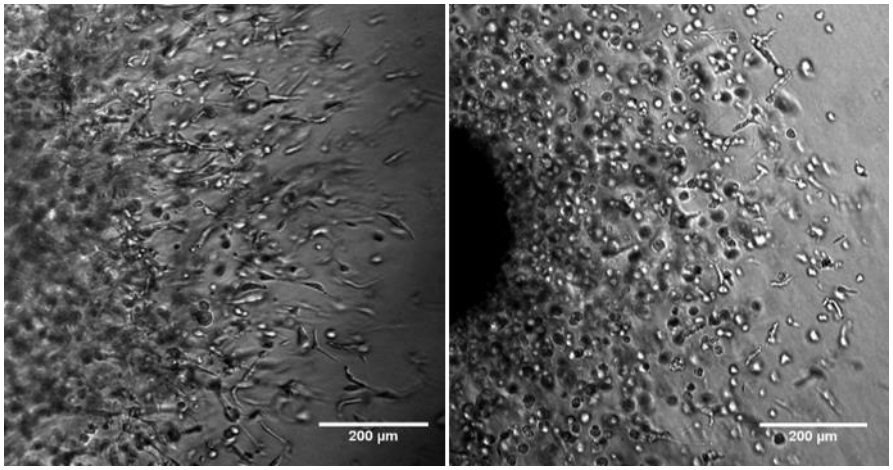

Fig. 36: Spheroid invasion of BLM cells without or with DAS-detailed view. Representative images are shown. Cells were imaged at 72 h using Nikon-Eclipse TE2000-S, HMC, 10x obj. Left, control cells, right cells treated with dasatinib. Scale bars 200 µm.

5.3.4. AMT based on manipulation of Rho/ROCK pathway

Apart from MAT experiments, we also focused on establishing AMT systems. A common approach to induce AMT is the use of ROCK inhibitors, such as Y-27632 or H-1152 (Gadea et al., 2008; Navarro-Lérida et al., 2015; Vaskovicova et al., 2015). However, while the application of these inhibitors does result in morphological changes such as elongation of cells or the formation of cell protrusions (Fig. 37), migration of cells is limited due to overall loss of contractility (Rath and Olson, 2012). Moreover, to complement our caRhoA system, we aimed to establish an inducible AMT system.

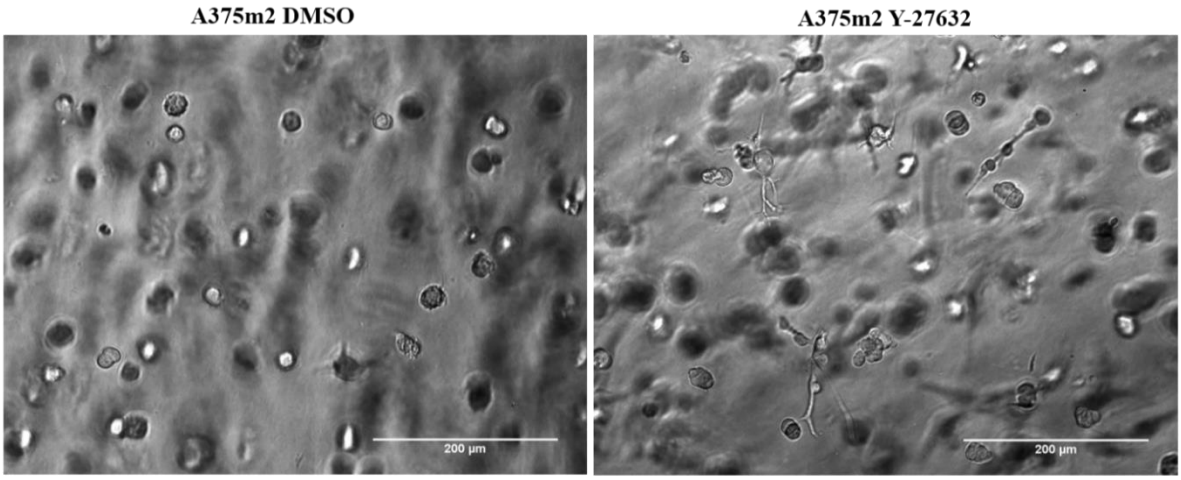

Fig. 37: Morphology of A375m2 cells without or with ROCK inhibitor Y-27632
Representative photos are shown. Cells were imaged after 48 h. Left, control cells. Right, cells treated with Y-27632 inhibitor Cell were imaged using 20x obj, HMC, Nikon-Eclipse TE2000-S.

Clostridium botulinum C3 exotransferase is a bacterial protein toxin known to inactivate Rho GTPases by ADP-ribosylation (Just et al., 2010) (Fig. 8). For this reason, a construct with C3 exotransferase was commercially synthesized (Invitrogen) and cloned into the pLVX-Tight-Puro, which enables doxycycline regulated expression (for vector map see Attachment).

Initially, an A375m2-TOB cell line was established (see chapter 4.1.8.2). Further, transfection of these cells with the C3 exotransferase construct was performed. Cells were cultivated in the presence of puromycin to select for positive clones. Despite the successful cloning, we were not able to prepare stable cell lines from these cells, due to impaired proliferation of cells with basal un-induced expression of C3 exotransferase. Moreover, after induction the cells exhibited abrogated phenotypes not compatible with cell migration (Fig. 38)

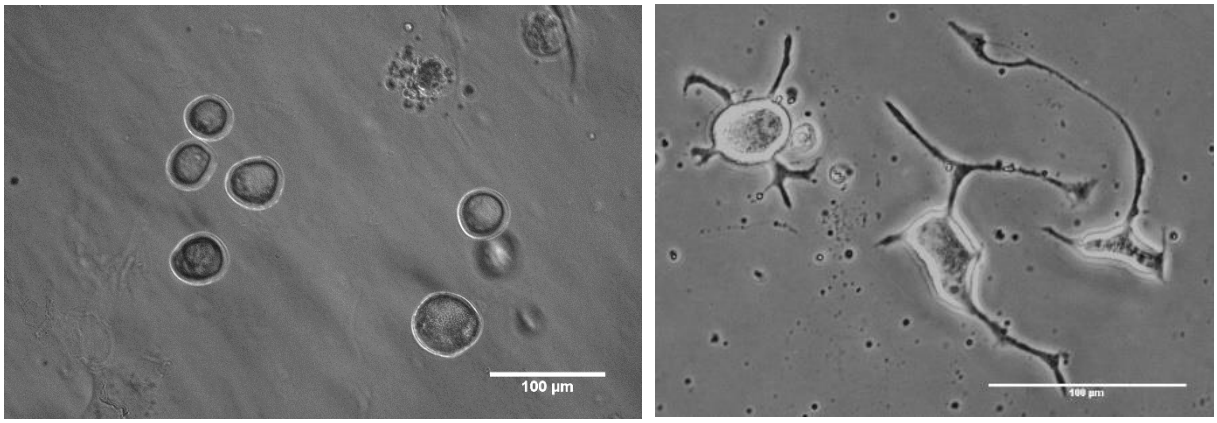

Fig. 38: Morphology of A375m2 cells expressing C3 exotransferase

Cells were images Nikon-Eclipse TE2000-S, HMC, 20x obj. Left, cells in 3D collagen after 48 h. Right, cells in 2D. Scale bars 100 µm.

5.4. Testing novel signaling pathways based on RNA-seq data

Meanwhile testing melanoma cell lines, RNA sequencing (RNA-seq) from HT1080 cells before and after MAT, induced by caRhoA expression and by dasatinib treatment, was performed. To obtain sufficient amounts of RNA, we seeded $1x10^6$ cells per 1 ml of 1 mg/ml collagen.

Both preparation of cDNA libraries from isolated RNA and data analysis was performed by Mgr. Vladimír Čermák, Ph.D. (details of the procedure are thus not part of this thesis).

Comparing datasets from cells with caRhoA induced expression and dasatinib treatment enabled us to identify signaling pathways possibly involved in MAT. Interestingly, the transcriptomic changes common to both caRhoA- and dasatinib-induced MAT include upregulation of Jak/Stat signaling pathways and NFκB signaling pathway targets (Fig. 39). Both of these pathways are involved in the inflammatory response (Ben-Neriah and Karin, 2011).

The most notably upregulated genes are known to be regulated by interferon α and γ signaling, which is mediated by Stat1 and Stat2 transcription factors (see Table 6 and Fig. 39). The induced gene expression profile corresponds to genes known to play role in the innate immunity response.

Stat1 is itself over 3x upregulated in HT1080 cells with caRhoA expression, and over 1.6x fold upregulated in cells after dasatinib treatment, when compared to control cells. Stat2 expression is upregulated 2x and 1.8x in case of caRhoA expression and dasatinib treatment, respectively.

Other significantly induced genes are CEMIP, and interleukin 6, 11 and 24, which are all regulated by the NFκB pathway (Aggarwal et al., 2004; Kuscu et al., 2012; Matsusaka et al., 1993).

The fold changes for chosen genes are summarized in Table 6.

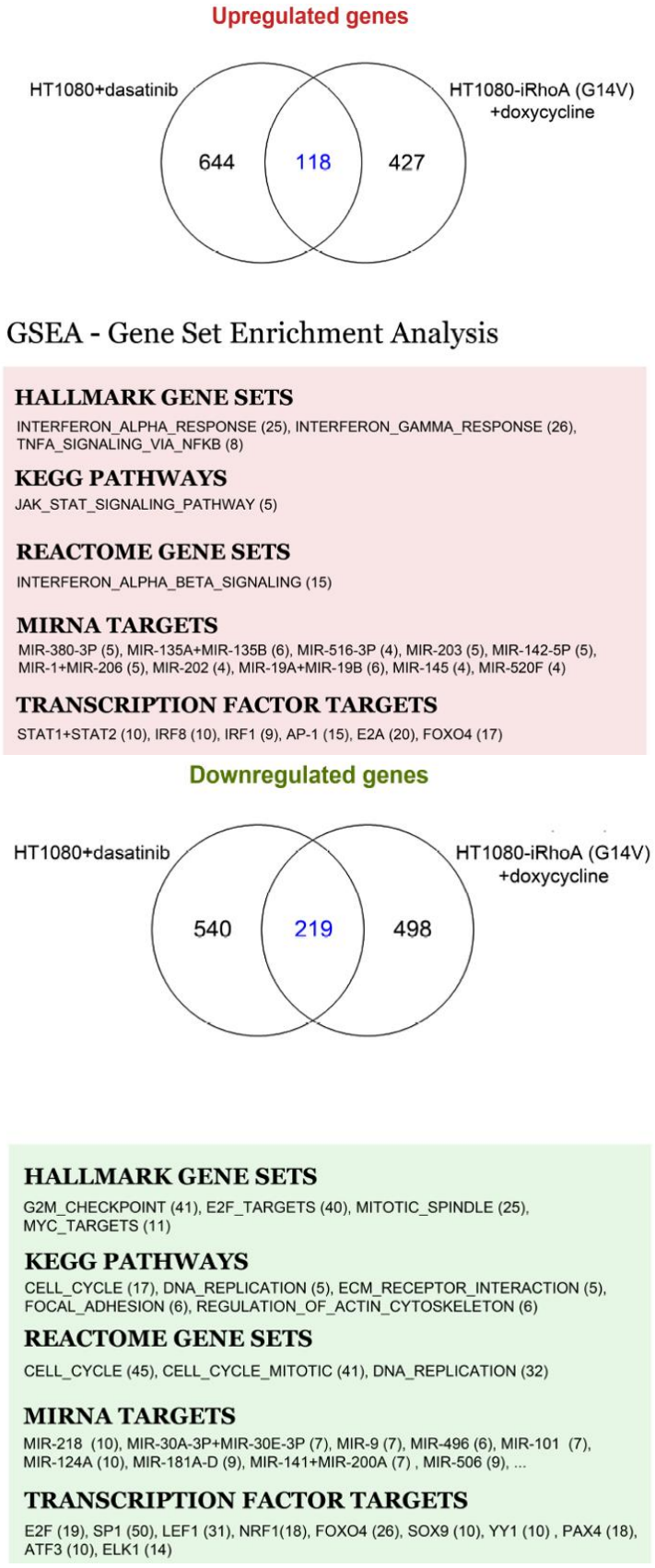

Fig. 39: Summary of up- and down-regulated genes in HT1080 cells after MAT. Image created by Mgr. Vladimír Čermák, Ph.D. Used with permission.

Gene	Fold upregulation caRhoA	Dasatinib
STAT1	3.19	1.65
STAT2	2.08	1.85
CEMIP	3.51	45.43
IL6	10.67	6.46
IL11	1.95	6.67
IL24	2.72	9.36
C1R	2.75	2.84
C1S	4.18	3.79
C3	5.95	1.96
IFI35	1.86	2.65
IFI44L	9.06	3.09
IFI6	4.73	2.89
IFIH1	3.84	1.70
IFIT1	9.94	3.05
IFIT2	4.81	2.37
IFIT3	3.85	2.59
IFITM1	3.73	3.42
IFITM3	1.94	2.51
MX1	4.57	2.08
MX2	6.57	1.99
OAS1	4.31	3.38
OAS2	5.12	2.38
RSAD2	13.00	3.36
SAA1	8.05	6.51
SAA2	7.94	3.95
USP18	5.28	2.14

Stat transcription factors
NFκB pathway associated genes
Interferon-response genes

Table 6: Summary of upregulated genes in HT1080 cells after MAT. Fold upregulation after expression of inducible caRhoA or treatment with dasatinib is shown.

Detailed annotation is available in chapter 11.1 part of the Attachment.

To test whether the Jak/Stat and NFκB pathways in fact regulate cancer cell morphology and/or invasion, we treated our melanoma cell lines with corresponding inhibitors. To inhibit Jak/Stat signaling, we utilized Ruxolitinib, which is a selective Jak1/2 inhibitor that displays 3.3 nM, 2.8 nM, 428 nM and 19 nM IC50 values for inhibition of Jak1, Jak2, Jak3, and Tyk2 respectively (Quintas-Cardama et al., 2010). The inhibition of Jak kinases results in impaired activation of Stat transcription factors.

To test the potential involvement of NFκB signaling, PS-1145 was used (Li and Prakash, 2005). This inhibitor targets the canonical NFκB pathway by inhibition of IKKβ within the nanomolar concentrations (IC50 = 88-100 nM) (Hideshima et al., 2002). IKKβ together with IKKα and IKKγ forms a protein complex that is necessary for phosphorylation and inactivation of IκB, a negative regulator of NFκB pathway.

5.4.1. The effect of Ruxolitinib on melanoma cell morphology

To test the effect of Jak/Stat pathway inhibition on melanoma cells, we analyzed the morphology of cells with and without 10 μM Ruxolitinib. Cells were embedded in 1mg/ml collagen as described in chapter 5.3.1 and imaged after 48 hours. When compared to control cells, treated with DMSO only, A375m2 cells in the presence of Ruxolitinib exhibited partial AMT (Fig. 40). The proportion of elongated mesenchymal cells was 4x higher than in control cells. The effect of Ruxolitinib was also tested on WM3629 cells. In agreement to results from A375m2 cells, and accordingly to data from RNA-seq, the inhibition of Jak1/2 in these cells impaired amoeboid morphology. WM3629 cells, which employ both invasion modes, enhanced formation of long protrusions and reduced the number of round cells in the presence of Ruxolitinib (Fig. 43). Morphology analysis is summarized in Fig. 41 and Fig. 42.

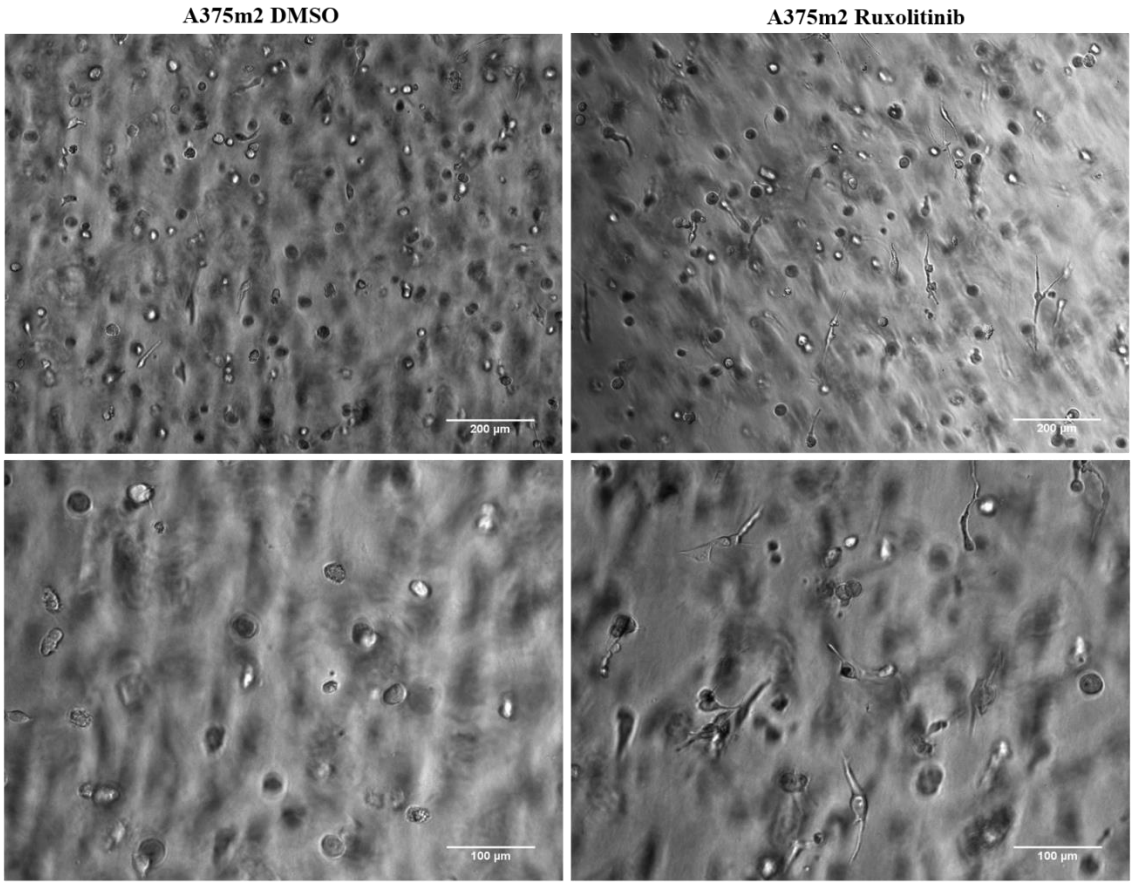

Fig. 40: Morphology of A375m2 cells after Ruxolitinib treatment

Representative images are shown. Cells were imaged after 48 hours using Nikon-Eclipse TE2000-S, HMC with 10x obj or 20 x obj shown in upper and lower row, respectively. Scale bar in upper row 200 µm, lower row 100 µm.

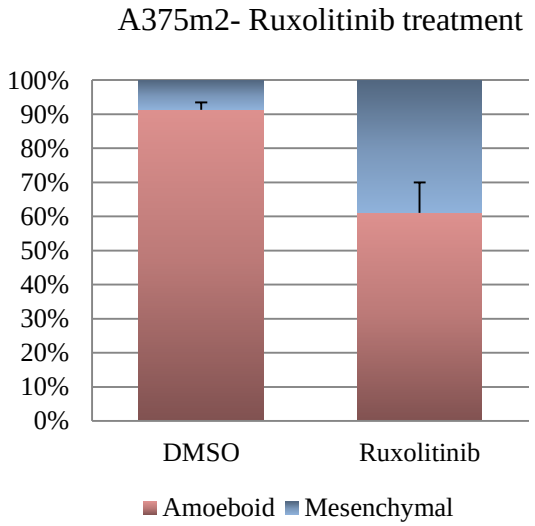

Fig. 41: Quantification of morphology of A375m2 cells without or with Ruxolitinib. The results of three independent experiments are shown. Error bars represent standard deviations.

.

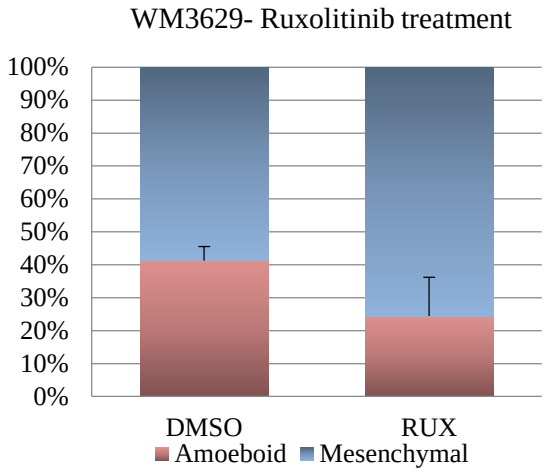

Fig. 42: Quantification of morphology of WM3629 cells without or with Ruxolitinib. The results of three independent experiments are shown. Error bars represent standard deviations.

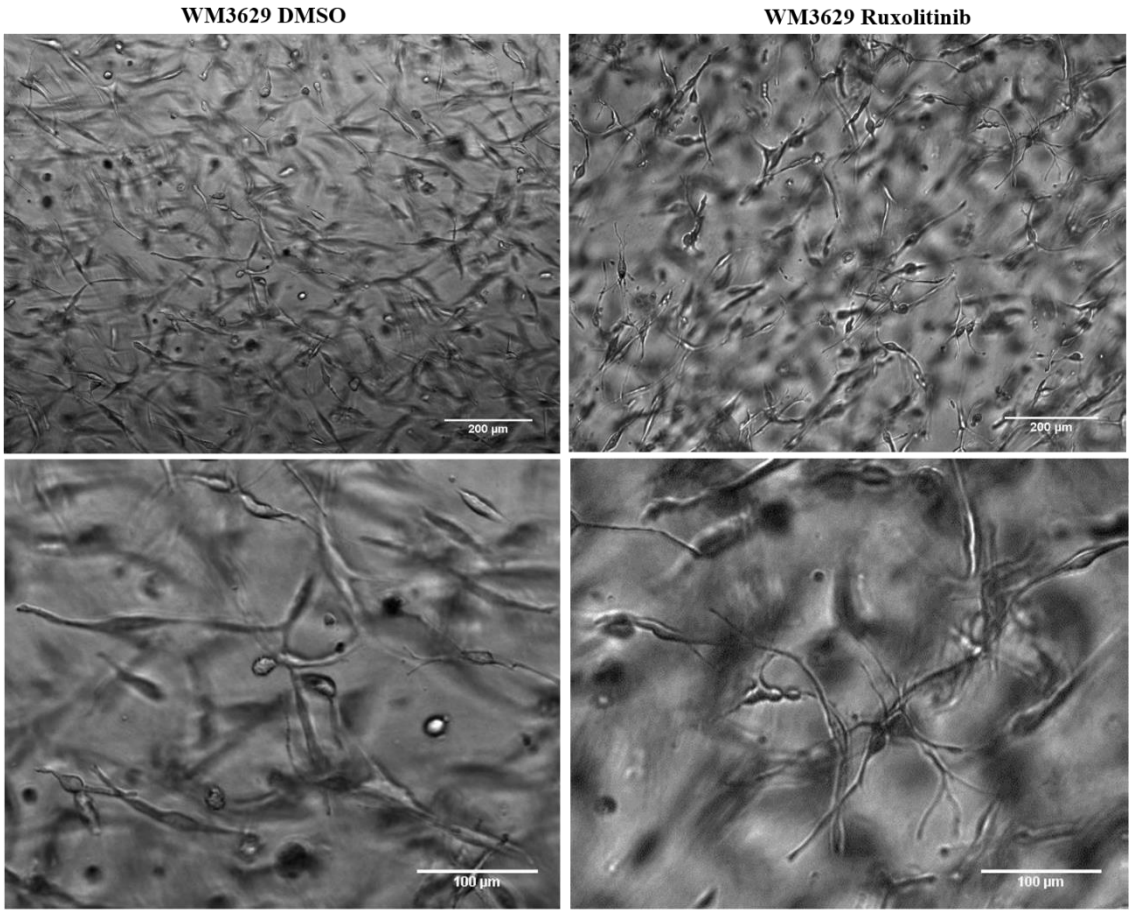

Fig. 43 Morphology of WM3629 cells after Ruxolitinib treatment. Representative images are shown. Cells were imaged after 48 hours using Nikon-Eclipse TE2000-S, HMC, 10x obj. Upper row, full field, scale bar 200 µm. Lower row, detailed view, scale bar 100 µm.

5.4.2. The effect of PS-1145 on melanoma cell morphology

To experimentally test the role of NFκB signaling in amoeboid morphology of melanoma cells, we conducted morphology analysis of A375m2 and WM3629 cells treated with 10 μM PS-1145. The experimental set-up was the same as described previously (see 5.3.1). In A375m2 cells, treatment with PS-1145 lead to AMT in approx. 25 % cells, while, surprisingly, in WM3629 cells, PS-1145 treatment resulted in profound MAT (Fig. 44 and Fig. 45). Since we were not able to find any simple explanation for MAT induced by PS-1145 treatment in WM3629 cells, we initially had to rule out apoptosis. Cells were observed for over 72 hours, which confirmed their viability was not affected. Moreover, by live cell imaging of these cells we obtained evidence that PS-1145 treatment results in an invasive, amoeboid phenotype (Fig. 48).

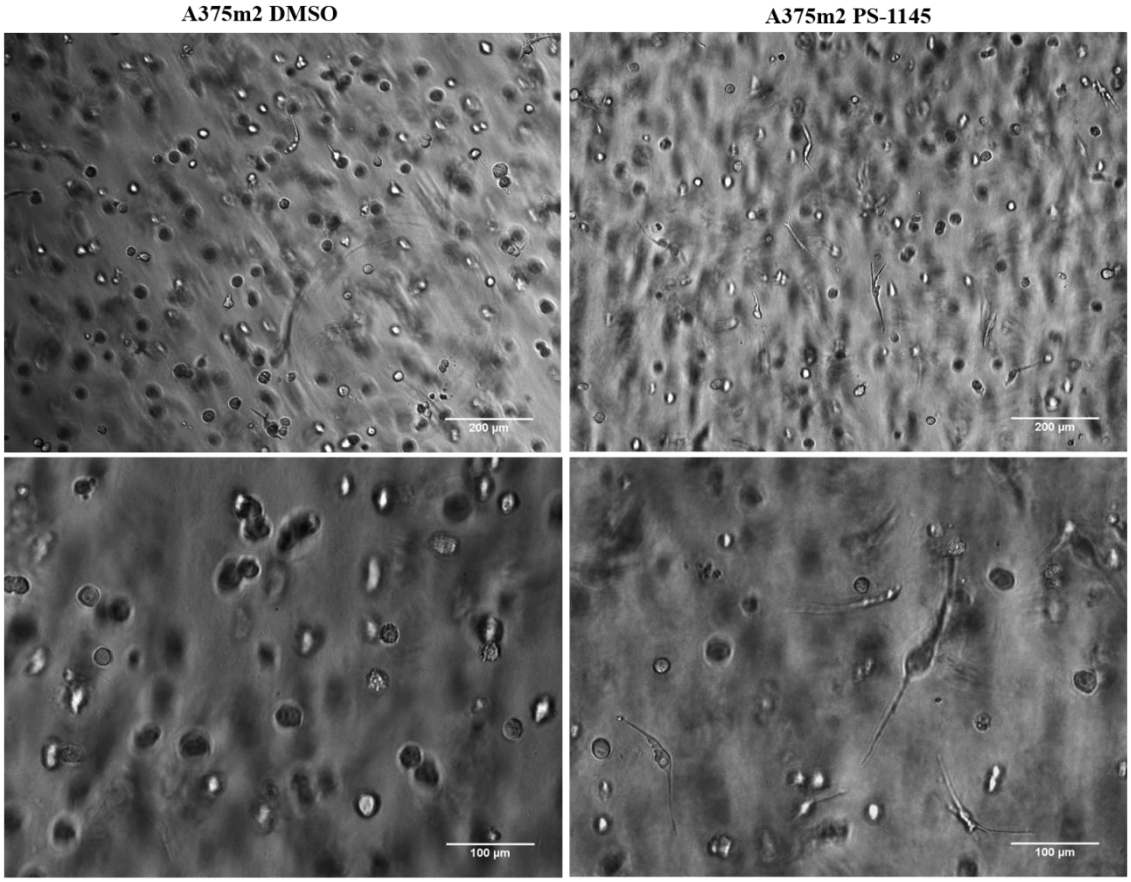

Fig. 44: Morphology of A375m2 cells after PS-1145 treatment. Representative images are shown. Cells were imaged after 48 hours using Nikon-Eclipse TE2000-S, HMC with 10x obj or 20 x obj shown in upper and lower row, respectively. Scale bar in upper row 200 μm, lower row 100 μm.

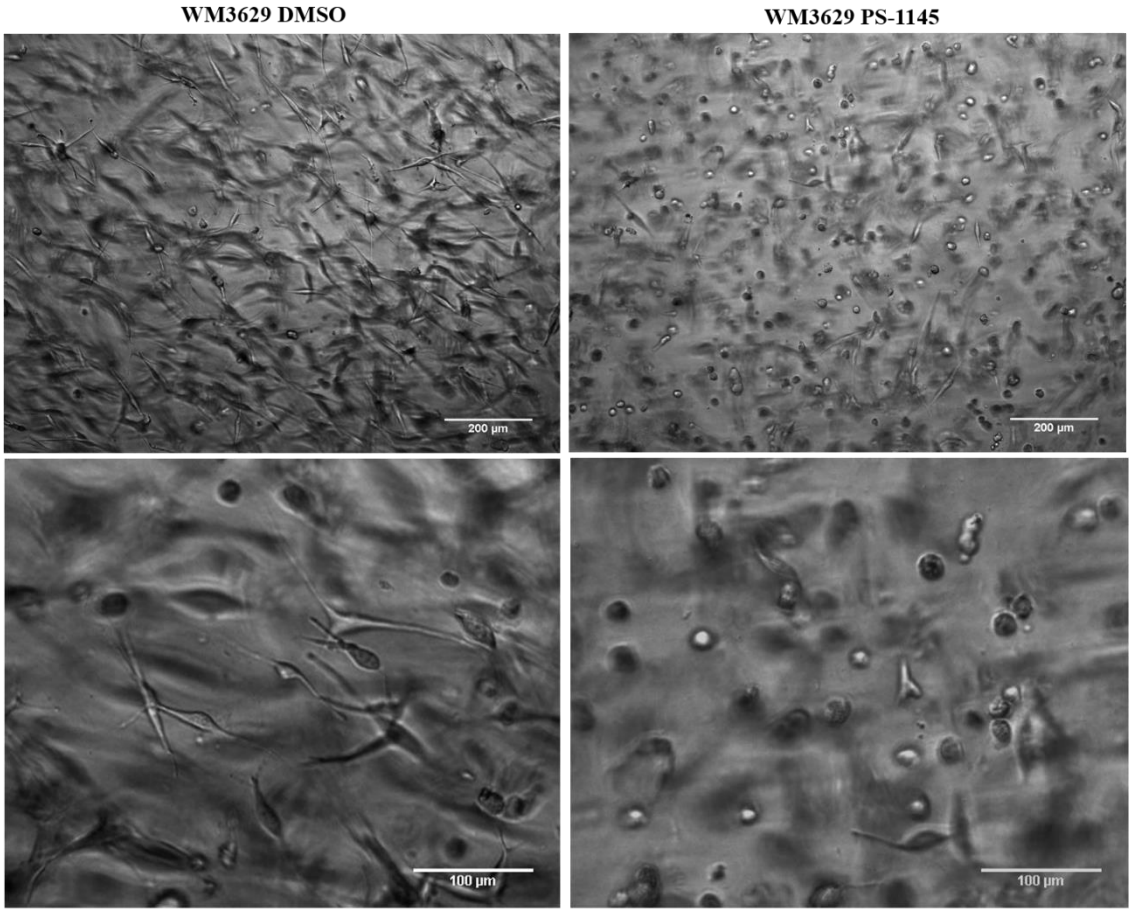

Fig. 45 Morphology of WM3629 cells after PS-1145 treatment. Representative images are shown. Cells were imaged after 48 hours using Nikon-Eclipse TE2000-S, HMC, 10x obj. Upper row, full field, scale bar 200 µm. Lower row, detailed view, scale bar 100 µm.

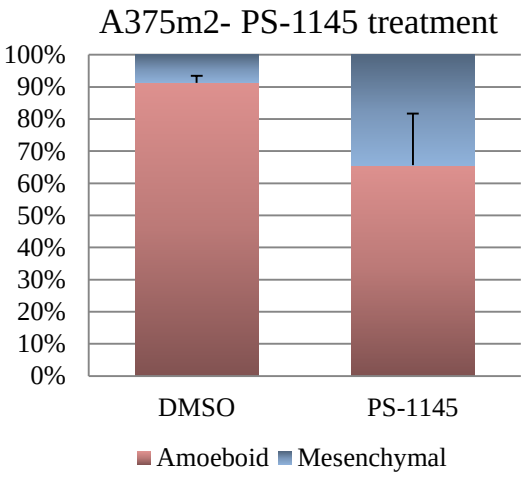

Fig. 46: Quantification of morphology of A375m2 cells without or with PS-1145. The results of three independent experiments are shown. Error bars represent standard deviations.

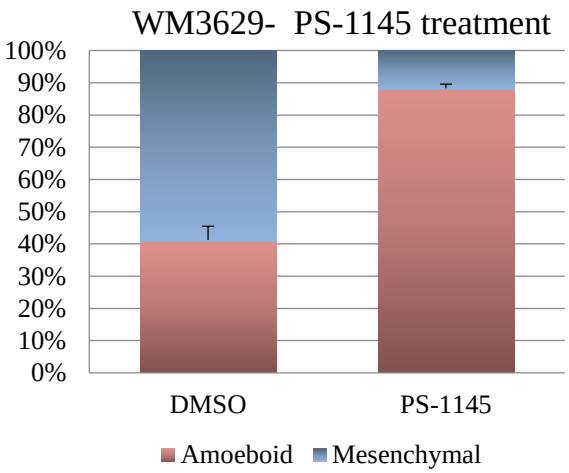

Fig. 47: Quantification of morphology of WM3629 cells without or with PS-1145. The results of three independent experiments are shown. Error bars represent standard deviations.

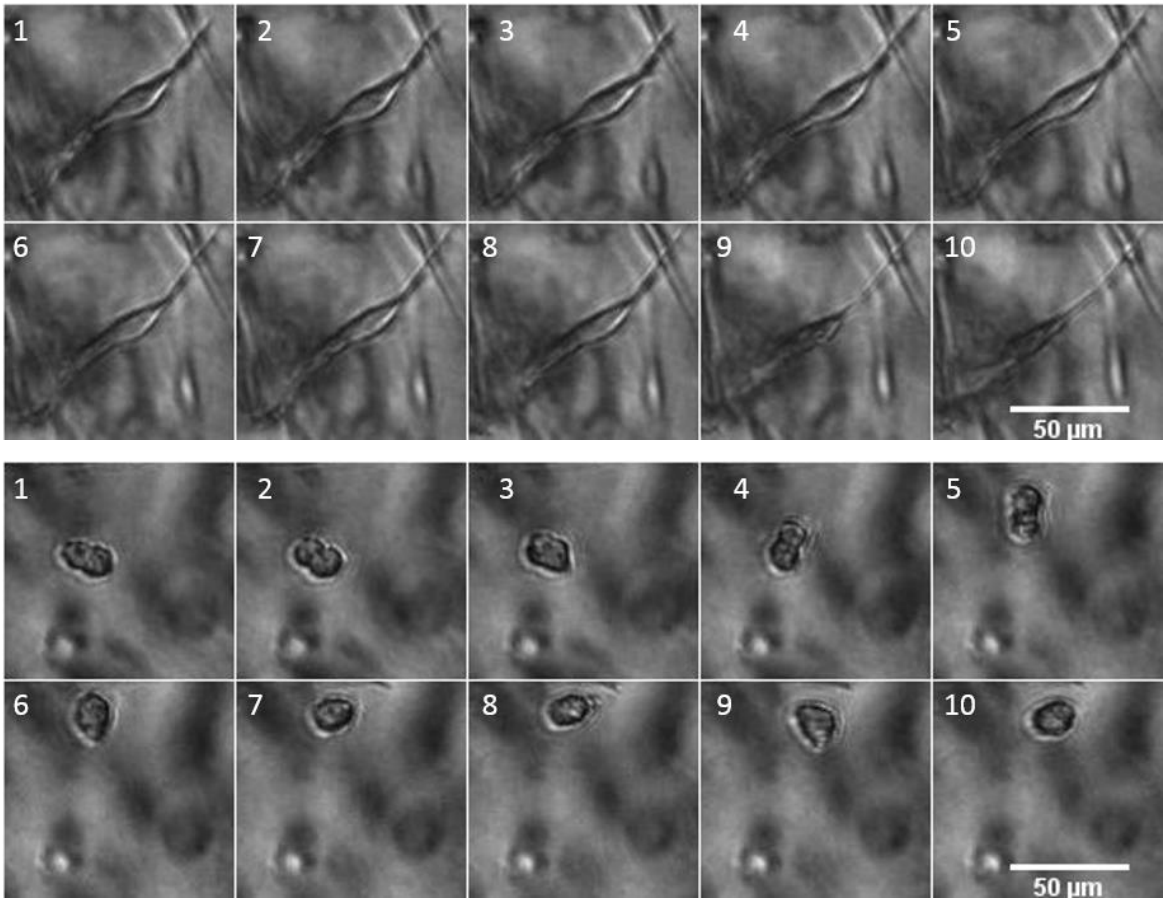

Fig. 48: Image sequences of WM3629 mesenchymal and amoeboid invasion derived from live-cell imaging videos. Upper sequence shows mesenchymal invasion of control WM3629 cell, lower sequence amoeboid invasion of WM3629 cells after PS-1145 treatment. Time interval between individual photos is 20 minutes. Images were obtained using JULI Fl+Br. Scale bar represents 50 µm.

5.4.3. Cloning proteins involved in Jak/Stat and NFκB pathways

To depict the role of the Jak/Stat and NFκB pathways in amoeboid cancer cell invasion in detail, chosen proteins involved in these signaling pathways were cloned for further studies in melanoma cell lines.

Initially, vectors were modified to be suitable for cloning of prepared constructs. The most common alteration was the deletion of certain restriction sites. This was done by either exchanging segments among vectors or by restriction digestion and sequential treatment by Klenow enzyme, followed by re-circularization by ligation. The vectors were then purified and cut with corresponding enzymes. The insert sequences were prepared by amplification of a chosen sequence from cDNA by a set of primers (for primer sequences see 11.3 in Attachment). The PCR product was purified and incubated with restriction enzymes to achieve DNA blunt ends or overhangs, which were used for cloning into vectors. The ligation reaction was used for transformation of bacteria and individual colonies were analyzed by restriction digestion of isolated DNA or by colony PCR.

In silico cloning, planning of analytical restriction digestions, and generation of vector maps was performed using WebDSV and Restriction Comparator (Mgr. Vladimír Čermák, Ph.D., unpublished; available at www.molbitools.com).

5.4.3.1. Cloning of Stat transcription factors

EGFP-Stat1 and EGFP-Stat3 fusion proteins were cloned in order to monitor intracellular localization and hence the activity of Stat1 and Stat3 proteins. Dominant negative (JAK non-phosphorylable) variants were also prepared as they are useful tools for dissecting the roles of these factors in the regulation of biological processes under study. For cloning of Stat1 and Stat3 and their dominant negative variants, pcDNA3-dSMS-gEGFPg was used. This vector is a modified pcDNA3 vector with EGFP sequence surrounded by a glycine-rich linker encoding sequences. It consists of a CMV promoter for the expression of protein of interest, a multiple cloning site before and after EGFP for EGFP N- and C- terminal fusions and SV40 promoter driving the expression of neomycin resistance. Due to this setting, it is suitable for the preparation of stable cell lines. In comparison with unmodified pcDNA3 it does not contain a SmaI site after the SV40 promoter and MluI and SpeI sites preceding the CMV promoter.

Further, in case of Stat1 cloning, it was necessary to delete XbaI and XhoI sites in the multiple cloning site region between CMV promoter and EGFP in order to retain XbaI as a unique site for future cloning of Stat1 point mutated variants (Stat1 sequence contains a XbaI site). The vector pcDNA3-dSMS-gEGFPg was cut by XbaI and XhoI enzymes. After purification, the vector was treated with Klenow enzyme to fill in the overhangs. Ligation of the blunt ends was performed. Successful deletion of XbaI-XhoI was determined by XbaI/DraI restriction enzymes. All tested clones showed pattern corresponding to the pcDNA3-dSMS-dXba/XhoI-gEGFPg vector.

Stat1 and Stat3 sequences were amplified from cDNA of HT1080 cells. Both reverse primers contain a MluI restriction site, which was used for cloning into the vector. The 5´ end was ligated as a blunt end. As such, Stat1 amplicon was cut with MluI and ligated into pcDNA3-dSMS-dXba/XhoI-gEGFPg cut with SmaI and MluI. Stat3 amplicon was cut with MluI and ligated into pcDNA3-dSMS-gEGFPg cut with SmaI and MluI.

To verify positive clones, products of Stat1 cloning were cut with Sac1. One of the positive clones was sequenced using a set of 4 primers (see Attachment for sequences of primers). Analysis of sequencing results did not reveal any mutations when compared to reference sequence and thus we proceeded with cell transfection (see Fig. 49).

In case of Stat3, the isolated cloning products were cut with PstI and NdeI. One of the positive clones was verified by sequencing.

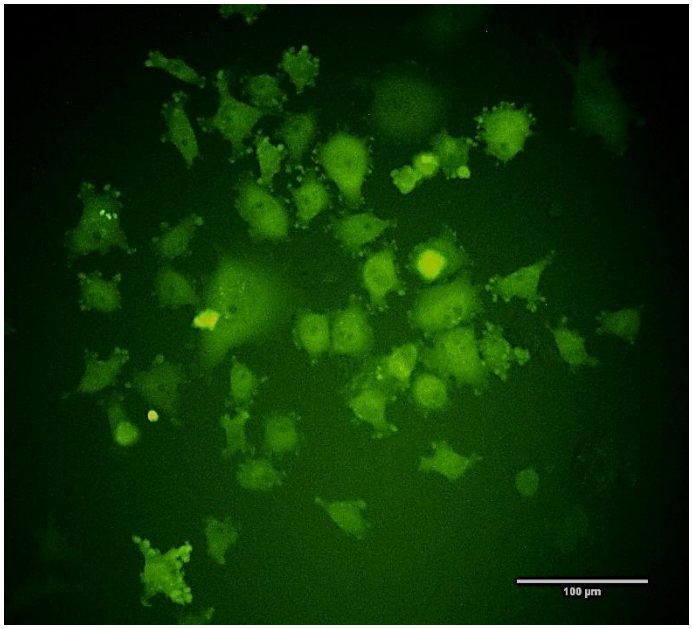

Fig. 49: Establishing BLM- EGFP-Stat1 stable cell line. BLM cells expressing EGFP-Stat1 were selected by cultivation with G418. EGFP-positive cells were imaged using Nikon-Eclipse TE2000-S, 20x obj.

5.4.3.2. Cloning of cytokine cDNAs

Our RNA sequencing results of MAT-related changes in HT1080 cells along with published data suggest a possible involvement of multiple autocrine/paracrine loops in the regulation of amoeboid invasion of cancer cells. Hence, we decided to prepare a panel of expression constructs for the enforced autocrine production of selected cytokines, potentially involved in MAT, in cancer cell lines. For this purpose the pIRESPuro3 vector was chosen. This vector enables expression of both gene of interest and puromycin resistance from one promoter due to an internal IRES site. It is suitable for stable cell line preparation, but also fast selection as the response of cells to puromycin occurs within 24 hours, which can greatly enhance the percentage of positive cells to be analyzed after transfection.

Initially, the segment between SspI and NdeI was exchanged for the corresponding region from pcDNA3-dSMS-gEGFPg, which does not contain MluI and SpeI sites preceding the CMV promoter. To verify the exchange, the vector was cut with MluI/PstI/XhoI. The pIRESPuro3-dMluI was used for ligation with TNF insert. The primers used for amplification of sTNF contain restriction sites suitable for cloning of other inserts as well, which enabled the exchange of sTNF for other cytokines to the same site.

The TNF sequence was amplified from cDNA obtained from primary human macrophages using specific primers. To express an active (not membrane-bound) version of TNF, a signal peptide-coding sequence was added to the 5'-end of the cDNA (corresponding to the mature active TNF) by two additional PCR reactions with primers encoding the signal peptide. The amplicon from the first PCR reaction with primers specific for TNF was used as a template for the second PCR reaction, which was conducted using a forward primer with overhangs coding the 3' end of the signal peptide (SigP1). This amplicon was then used for the third reaction, during which a third forward primer was used to add the 5′ segment of the signal peptide (SigP2). The three reactions are summarized in Fig. 50.

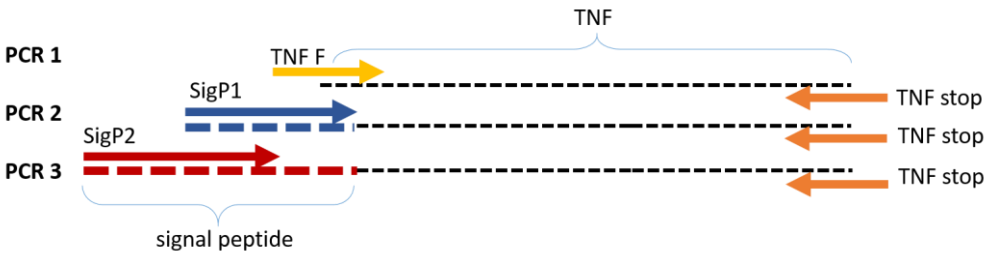

Fig. 50: Schematic overview of cloning secreted active TNF.

Three PCR reactions were performed in order to amplify TNF and add a signal peptide to its 5′ end.

The final amplicon, TNF with signal peptide for direct secretion of active form (further sTNF) was cut with BglII and ligated into pIRESPuro3-dMluI cut with EcoRV/BamHI. Sequencing identified a correct sequence.

The cloning of the sTNF was further used for preparing secreted IL-1β. The sequence coding IL-1β was amplified from macrophage DNA. It was cut with NheI/EcoRI and ligated into pIRESPuro3-dMluI-sTNF cut with corresponding enzymes. This lead to the exchange of IL-1β for TNF while maintaining the signal peptide sequence. IL-1β was added in ratio 10:1 to the vector to ensure it was in large abundance compared to original insert sTNF. Ligation products were cut with HindIII/BglII to distinguish positive clones.

In addition, cytokines IL-6 and IFN-ε were amplified from cDNA and exchanged for sTNF in the pIRESPuro3-dMluI-sTNF vector. IL-6 was amplified from fibroblast cDNA, unlike IFN-ε, which was amplified from cDNA of macrophages. The cloning procedure was identical for both cytokines. After amplification and purification, they were cut with BamHI/EcoRI and used for ligation with pIRESPuro3-dMluI-sTNF cut with the same enzymes, as described above.

Positive clones were identified by colony PCR. The expected amplicon sizes were 797 bp for IL-6 and 801 bp for IFN-ε. Positive clones were verified by PstI/BamHI in case of both IL-6 and IFN-ε. Analysis of sequencing results did not reveal any mutations.

Table 7 summarizes cloning results. For full sequences, primer sequences and plasmid maps, see Attachment.

Insert	Vector	Enzymes	Template cDNA
Stat1	pcDNA3-dSMS-dXba/XhoI-gEGFPg	MluI/SmaI	HT1080
Stat3	pcDNA3-dSMS-gEGFPg	MluI/SmaI	HT1080
sTNF	pIRESPuro3-dMluI	EcoRV/BamHI	macrophages
sIL1-β	pIRESPuro3-dMluI-sTNF	NheI/EcoRI	macrophages
IL-6	pIRESPuro3-dMluI-sTNF	BamHI/EcoRI	fibroblasts
IFN-ε	pIRESPuro3-dMluI-sTNF	BamHI/EcoRI	macrophages

Table 7: Summary of cloning results

6. Statistical analysis

Statistical analysis was performed for all morphology and spheroid invasion experiments.

For morphology assays, three independent experiments were analyzed for each condition. For each repeat, over 300 cells were analyzed. Since the results are proportional data with repetitions, the Cochran-Mantel-Haenszel test was used to assess statistical significance of differences. All results of morphology assays show extremely high level of significance (P-value $<<<$ 0.05).

For invasion assays, three independent experiments were also conducted. For each experiment, 4 or 5 spheroids for each condition were analyzed. To test for significance of differences, two-way ANOVA was performed.

Invasion of BLM cells without or with dasatinib treatment showed statistical significance (P-value $<$ 0.5). Invasion of BLM cells without or with caRhoA expression also proved to be statistically significant (P-value $<<<$ 0.05).

7. Discussion

While the role of Rho GTPases as master regulators of the cytoskeleton has been established, it still remains unclear which signaling pathways are decisive for either amoeboid or mesenchymal migration. Questions such as- *what is the in vivo trigger for the individual invasion modes, what deciphers whether the cancer cell will be efficient in invading the extracellular matrix* or *why some invasive/metastatic populations are rather amoeboid than mesenchymal or vice versa* – still have not been clearly elucidated.

This work aimed to contribute to resolving the questions above by establishing reliable AMT and MAT systems. Both AMT and MAT are processes that are inertly coupled to cell invasion and thus impose the necessity to be studied in 3D environments. Morphological changes in cells plated on 2D surfaces can predict AMT and MAT but cannot truly confirm the invasive phenotype. As such, all our experiments were done in 3D environments, e.g. conditions at least partially mimicking the *in vivo* state.

We chose melanoma as a model system for several reasons. Melanomas are highly invasive and metastatic cancers that can naturally employ various invasion modes (Cooper et al., 2015). Moreover, the studied melanoma cells lines are a profound model system used by other research groups in the field, which enables the synthesis of our data with previously published datasets.

There are many drawbacks we have had to face during our experiments. One of them is the inherent diversity of individual cells lines. Therefore, HT1080 sarcoma cells, which were used for RNA sequencing provided us with valuable data, however, the data should be critically analyzed in different context to avoid false judgements. We have challenged this by the use of three melanoma cell lines (A375m2, BLM and WM3629).

Further, we had to deal with the substantial effect of the extracellular matrix composition (discussed in chapter 3.5). To test whether our prepared collagen matrices have the potential to induce morphological changes associated with MAT/AMT, we performed control experiments with human macrophages according to Van Goethem et al, 2010. Although we were able to reproduce the results with human macrophages, the environment of dense collagen did not cause transition to the mesenchymal phenotype in case of tested melanoma cell lines. It is of interest that in an earlier study various leukocytes and certain subsets of macrophages were tested for their behavior in dense and porous collagen and none, apart from M2 macrophages, were able to switch to the mesenchymal mode in rigid collagen

(Cougoule et al., 2012). This points out a specific ability of M2 macrophages which allows them to adjust to various environments. It would be desirable to define this intrinsic characteristic as it may be key for the plasticity of invasion modes.

In order to define the most suitable conditions for analysis of cancer cell morphology, we tested various 3D matrices. Based on empirical observations we determined rat tail collagen at final concentration of 1 mg/ml as the most suitable, as in these conditions cells exhibited clearly defined morphologies. Moreover, we determined rat tail collagen at final concentration of 0.5 mg/ml as most appropriate for live-cell imaging of cancer cell invasion, since the lower concentration results in larger pores within the collagen matrix, which do not constrain amoeboid invasion (Wolf et al., 2013). Live-cell imaging enabled us to confirm that the observed morphological changes of cells corresponded to fully motile amoeboid and mesenchymal phenotypes. Further, imaging cells for prolonged times confirmed that the observed cell blebbing was a result of amoeboid invasion and not apoptosis, which is also accompanied by cell rounding and membrane blebs (Paul et al., 2010).

We were able to prepare systems of MAT based on both genetic (caRhoA) and chemical-induced changes (Src inhibition). Although there is no novelty in inducing MAT by caRhoA (Sahai and Marshall, 2003), we ameliorated the approach by preparing an inducible system, which allowed us to control RhoA expression in time and thus observe MAT in real time. Dasatinib as a tool for MAT has also been used earlier (Ahn et al., 2012). We confirmed that dasatinib treatment results in a motile and invasive amoeboid phenotype, although it does significantly decrease invasion from spheroids. This can be due to the collagen concentration used (1mg/ml), which is limiting for amoeboid migration. Therefore, the experiments should be repeated in conditions of lower collagen concentration to fully evaluate the effect of dasatinib on cell invasion.

Remarkably, we observed differences in cell invasion from spheroids after induction of caRhoA and dasatinib treatment. While both conditions resulted in amoeboid cells capable of bleb-driven invasion, dasatinib treatment resulted in individually invading cells that reached distances almost as control cells. On the other hand, cells with induced caRhoA expression invaded rather as a cell sheet with individual cells detaching at the front, although these cells scarcely invaded far from the migrating mass (Fig. 33). From this view, the invasion resembled collective invasion. This suggests that although caRhoA and dasatinib both result in amoeboid phenotype, they differ in the subtype. This may be caused by the involvement of various

isoforms of Rho GTPases as recently proposed by Cooper et. al. that distinghuish between various amoeboid phenotypes, which each exhibits distinct requirements for the certain isoforms of Rho GTPases (Cooper et al., 2015).

In spite of being a promising tool for inducing AMT, we were not able to prepare stable cell lines expressing doxycycline inducible C3 exotransferase due to affected cell proliferation. It is well known that the level of RhoA is carefully balanced during cell proliferation. Constitutively active RhoA results in retardation of the cell cycle (Morin et al., 2009). In fact, we did notice slightly slower proliferation of our cells lines after induction of caRhoA and obvious signs of cell cycle arrest in RNA sequencing data. On the other hand, lack of RhoA activity entirely impairs cytokinesis, as RhoA is important for cell division (Drechsel et al., 1997). Moreover, cells expressing the C3 exotransferase exhibited abrogated phenotypes corresponding to the inhibition of Rho/ROCK pathway. The most common defect observed was a large cell body with low adhesion to the surface (Fig. 38), which can be attributed to the lack of stress fibers for which RhoA is crucial (Chrzanowska-Wodnicka and Burridge, 1996). Most cells also formed long protrusions, which corresponds to earlier described defect in tail retraction (Worthylake et al., 2001). Other methods for studying the effects of RhoA inactivation by C3 exotransferase are possible, such as addition of purified C3 exotransferase directly to the medium (Wiegers et al., 1991). This was shown to be reversible after changing the medium, which was not feasible in our system due to problematic washout of doxycycline.

The last part of this project was dedicated to preliminary testing of hypotheses derived from the results of RNA sequencing analysis of differentially expressed genes from HT1080 cells before and after MAT induced by both approaches, e.g. dasatinib and caRhoA expression. The largest changes of gene expression after MAT involved genes responsive to activation of NFκB pathway and to Jak/Stat signaling, in particular Stat1 regulated genes. Therefore, we tested the effect of PS-1145 and Ruxolitinib, which are inhibitors of the NFκB and Jak/Stat signaling pathways, respectively.

Ruxolitinib treatment resulted in AMT in A375m2 and WM3629 melanoma cells, which is in agreement with our transcriptomic data that show a substantial increase in Stat1 and Stat2 after the transition to the amoeboid phenotype. So far, we are not able to distinguish among the contribution of the individual isoforms as Ruxolitinib inhibits both Jak1 and Jak2. Nevertheless, our results contribute to current knowledge of Jak/Stat signaling in amoeboid

cells by demonstrating that inhibition of Jak/Stat signaling abrogates amoeboid invasion and significantly increases the number of cells with mesenchymal phenotype.

Notably, earlier studies of proteomic changes in amoeboid and mesenchymal cells conducted have identified Stat signaling to be of importance. However, these results are not consistent in whether Stat1/2 signaling promotes amoeboid or mesenchymal invasion. Proteomic analysis of protein expression in the amoeboid A3 cell line and K2 mesenchymal cell line identified Stat1 to be upregulated almost 3-fold in the more invasive amoeboid A3 cell line (Rösel et al., 2008). On the other hand, proteomic data obtained by comparing A375m2 cells without or with ROCK inhibitors determined Stat1 expression to be upregulated 3x after AMT (Vaskovicova et al., 2015), suggesting its pro-mesenchymal role, opposingly to data from A375m2 presented in this thesis. Moreover, this study identified Stat3 expression to be downregulated after AMT, which corresponds to the findings of Sanz-Moreno et al. that Stat3 activity promotes the amoeboid phenotype (Sanz-Moreno et al., 2011). So far, we do not have an explanation for these contradictory results. We can assume that cells activate either Stat1/2 or Stat3 in an exclusive manner based on the given conditions. In fact, the crosstalk between Stat1/2 and Stat3 has been well documented (Regis et al., 2008).

Altogether, there is multiple evidence for the role of Stat signaling as an important signaling pathway in cancer cell migration. So far, no study has directly compared the role of the individual Stat transcription factors in cell migration. Thus, we can only conclude that Jak/Stat signaling is involved in cancer cell plasticity. The disunited results call for further evaluation.

Further, we tested the effect of NFκB signaling on invasion phenotypes by the use of PS-1145, an inhibitor of IKK. In the canonical NFκB pathway, IKK underlies activation of NFκB by phosphorylating and inactivating its negative regulator IκB. Since NFκB signaling is upregulated after MAT according to our transcriptomic data, we assumed that the treatment by PS-1145 would result in AMT. In A375m2 cells, the treatment by PS-1145 did in fact lead to enhancement of mesenchymal cells, however, WM3629 cells responded in a completely opposite manner. In these cells, PS-1145 treatment resulted in MAT. Moreover, we confirmed that the observed cell rounding and blebbing was due to the gain of the amoeboid phenotype and not apoptosis by monitoring cell behavior by live cell imaging.

The contradictory results of PS-1145 treatment of A375m2 and WM3629 cell lines were not yet assessed. Possibly, the distinct response can be attributed to the different genetic

background of these two cell lines. A375m2 cells are known to possess the activating B-Raf mutation, e.g. glutamine at position 600 instead of valine. On the other hand, WM3629 carry an activating N-Ras mutation and down-regulating B-Raf mutation. It has been documented, that cells with N-Ras mutations tend to signal through C-Raf instead of B-Raf. Notably, C-Raf and B-Raf exert distinct signaling by different capabilities to activate MAPK signaling (Karreth et al., 2009). In addition C-Raf but not B-Raf, inhibits ROCK2, an isoform of ROCK kinase (Piazzolla et al., 2005). Whether the distinct response of A375m2 and WM3629 cells to PS-1145 is due to differences in C-Raf and B-Raf signaling remains to be experimentally tested.

Of interest is that all inhibitors used in this study are of clinical importance. Dasatinib is used for chronic myeloid leukemia and is currently being tested for its therapeutic effect in solid cancer. It has also been proposed a potential target for melanoma treatment (Eustace et al., 2008) and has passed to phase II in clinical trials (Kluger et al., 2011). Ruxolitib is an approved drug for patients with polycythemia vera and is in phase trials for leukemia treatment (Eghtedar et al., 2012; Vannucchi et al., 2015). Although PS-1145 itself is not clinically used, other NFκB inhibitors are approved for treatment of disease such as multiple myeloid leukemia (Lub et al., 2015). Altogether, these inhibitors are primarily used to inhibit cancer cell proliferation. However, our data propose that the inhibitors, when used individually, do not block cell invasion, and as such do not prevent metastasis formation. What is more, dasatinib and PS-1145 caused MAT and thus may promote escape mechanisms of metastatic cells. Overall, our findings concerning the effect of dasatinib, PS-1145 and Ruxolitinib are of potential clinical interest.

Given that amoeboid migration is associated with an increase in pluripotency genes (Borrull et al., 2012; Taddei et al., 2014), and inflammation was recently shown to promote dedifferentiation (Chin and Wang, 2014; Jinushi, 2014; Shigdar et al., 2014), there is a possible connection between the amoeboid phenotype and the gain of a less differentiated state. We have recently discussed this in context of cancer cell invasion plasticity and proposed that, in fact, some form of dedifferentiation might be responsible for the loss of cell-cell and cell-ECM contact observed in amoeboid cells (Gandalovičová et al., 2016).

Cancer stem cells (CSCs) have been identified as more aggressive and often resistant sub-population of cancer cells and are associated with a less differentiated phenotype. Whether

induction of the amoeboid invasion modes is associated with gain of CSC-like features is of current interest. Of note, Stat3 has been shown to be involved in both autocrine and paracrine signaling loops involved in promoting CSC phenotypes in cancer cells (Kim et al., 2013; Yang et al., 2013). Accordingly, IL-6 was identified as a factor capable of transforming cancer cells into cancer cells with stem-like features (Iliopoulos et al., 2011). Moreover, it was shown to be upregulated in lung CSCs and was shown to promote tumorigenic potential (Yi et al., 2012). In addition, IL-1β links the NFκB pathway to cancer cell stem-like features (Li et al., 2012).

Based on our results presented in this thesis and published literature, we propose that amoeboid invasion is driven by transcriptomic changes both regulating and regulated by positive feedback loops involving autocrine and paracrine signaling through production of cytokines. Consequently, inflammatory pathways are activated and drive the expression of pro-inflammatory signals providing positive feedback to the system. 30 years ago, it was first suggested that cancer resembles a "never healing wound" (Dvorak, 1986). In context of today's knowledge, we can speculate that activation of the inflammatory-like pathways not only promotes cancer cell plasticity, but in particular, contributes to a stable feedback loop driving amoeboid invasion.

We assume an important role of IL-1β secretion. IL-1β is a key activator of the NFκB and, simultaneously, is activated by this pathway providing a strong autocrine signaling loop (Hiscott et al., 1993). IL-1β also directly binds to the IL-6 promoter and drives its expression (Isshiki et al., 1990), which then activates the Jak/Stat signaling. Notably, mutual regulatory networks between NFκB and Jak/Stat signaling exist. For example, in macrophages, TNF signaling activates an autocrine loop based on IFN-β signaling, which results in expression of Stat-1 regulated genes (Yarilina et al., 2008). Moreover, IKK-ε can modulate the balance between IFN type I and type II responses by directly phosphorylating and thus, disrupting, the formation of Stat1 homodimers that execute the type II IFN response (Ng et al., 2011).

RhoA stands out as a central effector of the system, which is activated by these pathways and in addition, can contribute to the maintenance of upstream signaling by promoting Stat3 signaling via ROCK (Sanz-Moreno et al., 2011) and by activating NFκB (Perona et al., 1997), which drives the expression of cytokines such as IL-6, IL-24. The cytokines can then activate Jak/Stat signaling that is able to re-inforce the NFκB signaling pathway. Notably, both NFκB

signaling associated cytokines, IL-1β and TNF, were shown to modulate cytokine expression in the tumor microenvironment (Katanov et al., 2015). The IL-6-Jak1-Stat3 signaling was also shown to modulate tumor microenvironment by producing cytokines, which lead to enhanced ECM remodeling mediated by cancer associated fibroblasts. Moreover, the production of cytokines directly promoted the amoeboid phenotype in a positive feedback manner (Sanz-Moreno et al., 2011).

Of note, inflammatory signaling and cell stress is known to induce amoeboid invasion of microglia, which are non-cancer cells resident in the brain. When inactive, they form multiple protrusions and resemble the mesenchymal phenotype. However, when activated, microglia gain the amoeboid phenotype (Colton and Wilcock, 2010; Saijo and Glass, 2011). This suggests that the amoeboid phenotype gained by both microglia during activation and cancer cells during invasion involves inflammatory signaling and is sustained by transcriptomic activation of cytokine expression. In fact, this would not be the only example of cancer cells taking advantage of otherwise physiological responses. Cancer cells can activate the EMT program, which is otherwise restricted to developmental processes or other physiological processes such as wound healing (Nieto, 2013). Thus, it seems that cancer cells during EMT and MAT utilize and manipulate otherwise physiological signaling to their benefit.

The fact that the same signaling pathways regulate amoeboid phenotype *in vivo* and *in vitro* is of particular interest. In our system, we manipulated the pathway by directly upregulating RhoA, which is a strong trigger of the amoeboid phenotype. In result, the cytokine feedback loop is established. Intriguingly, various triggers of this signaling pathway relevant to cancer cell plasticity exist *in vivo*. Although the most obvious trigger in case of microglia is paracrine cytokine signaling, hypoxia or cell stress are also activating signals (Kim et al., 2003; Woodroofe et al., 1991). Particularly hypoxia and mechanical stress are factors often encountered by cancer cells and thus are possible triggers of amoeboid invasion *in vivo*, leading to sustained amoeboid phenotype by activation of the cytokine feedback loop as in the case of induced caRhoA expression.

Although multiple evidence supporting this theory exists, it so far remains a mere speculation, which will have to be tested experimentally.

8. Future prospects

The findings summarized in this thesis have provoked many new directions in our research. Due to the complexity of the signaling pathways revealed to play role in amoeboid and mesenchymal migration, we will need to conduct many further experiments. Some possible approaches are listed below.

To precisely investigate the role of the Jak/Stat and NFκB pathways, it will be necessary to dissect the signaling pathways down to the level of individual proteins. This can be achieved by systematic up-regulation or downregulation of the individual proteins. For this reason, we have already started cloning other cytokines known to activate these pathways (interferon -α, -β and -γ, IL24, IL11) (Dranoff, 2004), as well as negative regulators of these pathways, e.g. SOCS1 and SOCS3 in case of the Jak/Stat pathway (Croker et al., 2003; Nakagawa et al., 2016) and GILZ and RRAD for the NFκB pathway (Ayroldi et al., 2001; Liu et al., 2015). Moreover, point mutated non-phosphorylable versions of Stat1 and Stat3 will be prepared. Another suitable approach to achieve downregulation of proteins of interest is the transfection of cells with particular siRNAs. Eventually, for promising targets, it will be possible to establish knock-out cell lines by CRISPR technology.

Our results have proved the role of the NFκB pathway in amoeboid and mesenchymal migration. However, to explain the so far contradictory results, further analysis is necessary. Comparing gene expression changes of A375m2 and WM3629 cells treated with PS-1145 in different time scales by real-time PCR will be a valuable tool for monitoring the dynamics of the pathway during the response. Moreover, the use of sorafenib, which inhibits Raf proteins, especially C-Raf over B-Raf, can help elucidate whether the pro-amoeboid response of PS-1145 treated WM3629 cells can be attributed to C-Raf, which has been shown to be predominant in cells with N-Ras mutations (Dumaz et al., 2006; Smalley et al., 2009). Importantly, these results should be repeated on A2058 and SK-MEL-3 cells, which carry the V600E B-Raf mutation and on WM3670 that have a G469E mutation. From this point of view, it will be interesting to include in further work cell lines that naturally include both amoeboid and mesenchymal populations and thus enable to induce both MAT and AMT within one cell line. By comparing gene expression from the induced amoeboid and mesenchymal cells, it will be possible to overcome problems stemming from the genetic background of cell lines.

In addition, an important tool for studying the plasticity of AMT and MAT will be high resolution imaging of cells expressing fluorescently tagged proteins of interest and

immunohistochemistry staining. While endogenous expression of fluorescently labeled proteins in cells offers the possibility of live cell imaging, immunohistochemistry requires penetration of the cell membrane and is done on fixed cells. Nevertheless, both methods are accompanied by considerable challenges. In case of preparation of fixed samples, there is risk of damaging the collagen matrix while fixing and washing steps, which can lead to disruption of cell contacts with the collagen and/or washing out cells from their original location, since adhesion, particularly of amoeboid cells, to the fibers is not as strong as adhesion to 2D surfaces. For live cell imaging, photo-toxicity and low light penetration due to diffraction by the collagen represent the largest problems. Only advanced imaging techniques can bypass these complications (Welf et al., 2016).

9. Summary

The first part of this thesis focused on optimization of 3D collagen conditions for purposes of morphology analysis and live cell imaging.

The second part focused on manipulation of Rho GTPases as a tool for AMT/MAT studies. Stable cell lines of melanoma BLM and WM3629 cancer cells expressing doxycycline inducible caRhoA by were prepared, which enabled us to confirm that caRhoA expression is a potent inducer of MAT, as previously demonstrated in HT1080 sarcoma cells. By using dasatinib, a c-Src/Abl inhibitor, we were also able to induce MAT. We further challenged the previously published observation that dasatinib treatment halts cell invasion by showing that dasatinib treated cells are able to invade 3D collagen. By live cell imaging we observed the modes of cancer cell invasion.

The last part was devoted to verifying hypotheses derived from RNA-seq results. We demonstrated that the use of Ruxolitinib and PS-1145 affects melanoma cell invasion. Further, vectors with Stat1 and Stat3 transcription factors were successfully prepared. In addition, the Stat1 construct was already utilized for stable cell line preparation of BLM cells. Other successfully cloned constructs include NFκB activating cytokines sTNF and sIL1-beta, and Stat3-activating IL-6. Finally, IFN-ε, which activates the Stat1 pathway and possibly functions as an autocrine factors in our system, was also cloned.

The emerging picture is that the both mesenchymal and amoeboid phenotypes are the result of transcriptomic reprogramming, which occurs in context-dependent manner and results in the individual invasion modes. The Jak/Stat and NFκB signaling pathways stand out as potential decisive factors for the choice of invasion modes, converging on RhoA, which apart from executing the associated cytoskeletal re-arrangements, also indirectly activates the upstream Jak/Stat and NFκB pathways and thus contributes to formation of a positive feedback loop of cytokine signaling important for sustained amoeboid invasion.

10.Literature

Aggarwal, S., Takada, Y., Mhashilkar, A.M., Sieger, K., Chada, S., and Aggarwal, B.B. (2004). Melanoma differentiation-associated gene-7/IL-24 gene enhances NF-kappa B activation and suppresses apoptosis induced by TNF. J. Immunol. *173*, 4368–4376.

Ahn, J., Sanz-Moreno, V., and Marshall, C.J. (2012). The metastasis gene NEDD9 product acts through integrin 3 and Src to promote mesenchymal motility and inhibit amoeboid motility. J. Cell Sci. *125*, 1814–1826.

Aktories, K., Wilde, C., and Vogelsgesang, M. (2004). Rho-modifying C3-like ADP-ribosyltransferases. Rev. Physiol. Biochem. Pharmacol. *152*, 1–22.

Alan, J.K., and Lundquist, E.A. (2013). Mutationally activated Rho GTPases in cancer. Small GTPases *4*, 159–163.

Albiges-Rizo, C., Destaing, O., Fourcade, B., Planus, E., and Block, M.R. (2009). Actin machinery and mechanosensitivity in invadopodia, podosomes and focal adhesions. J. Cell Sci. *122*, 3037–3049.

Alfano, D., Ragno, P., Stoppelli, M.P., and Ridley, A.J. (2012). RhoB regulates uPAR signalling. J. Cell Sci. *125*, 2369–2380.

Amano, M., Ito, M., Kimura, K., Fukata, Y., Chihara, K., Nakano, T., Matsuura, Y., and Kaibuchi, K. (1996). Phosphorylation and Activation of Myosin by Rho-associated Kinase (Rho-kinase). J. Biol. Chem. *271*, 20246–20249.

Amano, M., Nakayama, M., and Kaibuchi, K. (2010). Rho-kinase/ROCK: A key regulator of the cytoskeleton and cell polarity. Cytoskeleton (Hoboken). *67*, 545–554.

Artym, V. V, Zhang, Y., Seillier-Moiseiwitsch, F., Yamada, K.M., and Mueller, S.C. (2006). Dynamic interactions of cortactin and membrane type 1 matrix metalloproteinase at invadopodia: defining the stages of invadopodia formation and function. Cancer Res. *66*, 3034–3043.

Audebert, S., Navarro, C., and Nourry, C. (2004). Mammalian Scribble forms a tight complex with the βPIX exchange factor. Curr. Biol. *14*, 987–995.

Ayroldi, E., Migliorati, G., Bruscoli, S., Marchetti, C., Zollo, O., Cannarile, L., D'Adamio, F., and Riccardi, C. (2001). Modulation of T-cell activation by the glucocorticoid-induced leucine zipper factor via inhibition of nuclear factor kappaB. Blood *98*, 743–753.

Bassermann, F., Jahn, T., Miething, C., Seipel, P., Bai, R.Y., Coutinho, S., Tybulewicz, V.L., Peschel, C., and Duyster, J. (2002). Association of Bcr-Abl with the proto-oncogene Vav is implicated in activation of the Rac-1 pathway. J. Biol. Chem. *277*, 12437–12445.

Ben-Neriah, Y., and Karin, M. (2011). Inflammation meets cancer, with NF-κB as the matchmaker. Nat. Immunol. *12*, 715–723.

Blanchoin, L., Boujemaa-Paterski, R., Sykes, C., and Plastino, J. (2014). Actin Dynamics, Architecture, and Mechanics in Cell Motility. Physiol. Rev. *94*, 235–263.

Bond, M., Chase, a J., Baker, a H., and Newby, a C. (2001). Inhibition of transcription factor NF-kappaB reduces matrix metalloproteinase-1, -3 and -9 production by vascular smooth muscle cells. Cardiovasc. Res. *50*, 556–565.

Bornstein, M.B. (1958). Reconstituted rattail collagen used as substrate for tissue cultures on coverslips in Maximow slides and roller tubes. Lab. Invest. *7*, 134–137.

Borrull, A., Ghislin, S., Deshayes, F., Lauriol, J., Alcaide-Loridan, C., and Middendorp, S. (2012). Nanog and Oct4 overexpression increases motility and transmigration of melanoma cells. J. Cancer Res. Clin. Oncol. *138*, 1145–1154.

Boussif, O., Lezoualc'h, F., Zanta, M.A., Mergny, M.D., Scherman, D., Demeneix, B., and Behr, J.P. (1995). A versatile vector for gene and oligonucleotide transfer into cells in culture and in vivo: polyethylenimine. Proc. Natl. Acad. Sci. U. S. A. *92*, 7297–7301.

Brábek, J., Mierke, C.T., Rösel, D., Veselý, P., and Fabry, B. (2010). The role of the tissue microenvironment in the regulation of cancer cell motility and invasion. Cell Commun. Signal. *8*, 22.

Bravo-Cordero, J.J., Oser, M., Chen, X., Eddy, R., Hodgson, L., and Condeelis, J. (2011). A novel spatiotemporal RhoC activation pathway locally regulates cofilin activity at invadopodia. Curr. Biol. *21*, 635–644.

Bravo-Cordero, J.J., Sharma, V.P., Roh-Johnson, M., Chen, X., Eddy, R., Condeelis, J., and Hodgson, L. (2013). Spatial regulation of RhoC activity defines protrusion formation in migrating cells. J. Cell Sci. *126*, 3356–3369.

Bronsert, P., Enderle-Ammour, K., Bader, M., Timme, S., Kuehs, M., Csanadi, A., Kayser, G., Kohler, I., Bausch, D., Hoeppner, J., et al. (2014). Cancer cell invasion and EMT marker expression: a three-dimensional study of the human cancer–host interface. J. Pathol. *234*, 410–422.

Buettner, R., Mesa, T., Vultur, A., Lee, F., and Jove, R. (2008). Inhibition of Src family kinases with dasatinib blocks migration and invasion of human melanoma cells. Mol. Cancer Res. *6*, 1766–1774.

Byrne, K.M., Monsefi, N., Dawson, J.C., Degasperi, A., Bukowski-Wills, J.-C., Volinsky, N., Dobrzyński, M., Birtwistle, M.R., Tsyganov, M.A., Kiyatkin, A., et al. (2016). Bistability in the Rac1, PAK, and RhoA Signaling Network Drives Actin Cytoskeleton Dynamics and Cell Motility Switches. Cell Syst. *2*, 38–48.

Cantelli, G., Orgaz, J.L., Rodriguez-Hernandez, I., Karagiannis, P., Maiques, O., Matias-Guiu, X., Nestle, F.O., Marti, R.M., Karagiannis, S.N., and Sanz-Moreno, V. (2015). TGF-β-Induced Transcription Sustains Amoeboid Melanoma Migration and Dissemination. Curr. Biol. *25*, 2899–2914.

Cliche, S., Amiot, J., Avezard, C., and Gariepy, C. (2003). Extraction and characterization of collagen with or without telopeptides from chicken skin. Poult. Sci. *82* , 503–509.

Colton, C. a, and Wilcock, D.M. (2010). Assessing activation states in microglia. CNS Neurol. Disord. Drug Targets *9*, 174–191.

Coniglio, S.J., Zavarella, S., and Symons, M.H. (2008). Pak1 and Pak2 mediate tumor cell invasion through distinct signaling mechanisms. Mol. Cell. Biol. *28*, 4162–4172.

Cooper, S., Sadok, A., Bousgouni, V., and Bakal, C. (2015). Apolar and polar transitions drive the conversion between amoeboid and mesenchymal shapes in melanoma cells. Mol. Biol. Cell .

Cougoule, C., Van Goethem, E., Le Cabec, V., Lafouresse, F., Dupre, L., Mehraj, V., Mege, J.-L., Lastrucci, C., and Maridonneau-Parini, I. (2012). Blood leukocytes and macrophages of various phenotypes have distinct abilities to form podosomes and to migrate in 3D environments. Eur. J. Cell Biol. *91*, 938–949.

Courtemanche, N., Gifford, S.M., Simpson, M.A., Pollard, T.D., and Koleske, A.J. (2015). Abl2/Abl-related gene stabilizes actin filaments, stimulates actin branching by actin-related protein 2/3 complex, and promotes actin filament severing by cofilin. J. Biol. Chem. *290*, 4038–4046.

Coussens, L.M., and Werb, Z. (2002). Inflammation and cancer. Nature *420*, 860–867.

Croker, B. a, Krebs, D.L., Zhang, J.-G., Wormald, S., Willson, T. a, Stanley, E.G., Robb, L., Greenhalgh, C.J., Förster, I., Clausen, B.E., et al. (2003). SOCS3 negatively regulates IL-6 signaling in vivo. Nat. Immunol. *4*, 540–545.

Davidson, P.M., Denais, C., Bakshi, M.C., and Lammerding, J. (2014). Nuclear deformability constitutes a rate-limiting step during cell migration in 3-D environments. Cell. Mol. Bioeng. *7*, 293–306.

Demou, Z.N., Awad, M., McKee, T., Perentes, J.Y., Wang, X., Munn, L.L., Jain, R.K., and Boucher, Y. (2005). Lack of telopeptides in fibrillar collagen I promotes the invasion of a metastatic breast tumor cell line. Cancer Res. *65*, 5674–5682.

Diekmann, D., Nobes, C.D., Burbelo, P.D., Abo, A., and Hall, A. (1995). Rac GTPase interacts with GAPs and target proteins through multiple effector sites. EMBO J. *14*, 5297–5305.

Dolcet, X., Llobet, D., Pallares, J., and Matias-Guiu, X. (2005). NF-kB in development and progression of human cancer. Virchows Arch. *446*, 475–482.

Dovas, A., and Couchman, J.R. (2005). RhoGDI: multiple functions in the regulation of Rho family GTPase activities. Biochem. J. *390*, 1–9.

Doyle, A.D., Wang, F.W., Matsumoto, K., and Yamada, K.M. (2009). One-dimensional topography underlies three-dimensional fibrillar cell migration. J. Cell Biol. *184*, 481–490.

Dranoff, G. (2004). Cytokines in cancer pathogenesis and cancer therapy. Nat Rev Cancer *4*, 11–22.

Drechsel, D.N., Hyman, A.A., Hall, A., and Glotzer, M. (1997). A requirement for Rho and Cdc42 during cytokinesis in Xenopus embryos. Curr. Biol. *7*, 12–23.

Dumaz, N., Hayward, R., Martin, J., Ogilvie, L., Hedley, D., Curtin, J.A., Bastian, B.C., Springer, C., and Marais, R. (2006). In melanoma, RAS mutations are accompanied by switching signaling from BRAF to CRAF and disrupted cyclic AMP signaling. Cancer Res. *66*, 9483–9491.

Dvorak, H.F. (1986). Tumors: wounds that do not heal. Similarities between tumor stroma generation and wound healing. N. Engl. J. Med. *315*, 1650–1659.

Eden, S., Rohatgi, R., Podtelejnikov, A. V, Mann, M., and Kirschner, M.W. (2002). Mechanism of regulation of WAVE1-induced actin nucleation by Rac1 and Nck. Nature *418*, 790–793.

Eghtedar, A., Verstovsek, S., Estrov, Z., Burger, J., Cortes, J., Bivins, C., Faderl, S., Ferrajoli, A., Borthakur, G., George, S., et al. (2012). Phase 2 study of the JAK kinase inhibitor ruxolitinib in patients with refractory leukemias, including postmyeloproliferative neoplasm acute myeloid leukemia. Blood *119*, 4614–4618.

Etienne-Manneville, S. (2004). Cdc42-the centre of polarity. J. Cell Sci. *117*, 1291–1300.

Etienne-Manneville, S., and Hall, A. (2003). Cdc42 regulates GSK-3β and adenomatous polyposis coli to control cell polarity. Nature *421*, 753–756.

Etienne-Manneville, S., Manneville, J., Nicholls, S., Ferenczi, M.A., and Hall, A. (2005). Cdc42 and Par6–PKCζ regulate the spatially localized association of Dlg1 and APC to control cell polarization. J. Cell Biol. *170*, 895–901.

Eustace, A.J., Crown, J., Clynes, M., and O'Donovan, N. (2008). Preclinical evaluation of dasatinib, a potent Src kinase inhibitor, in melanoma cell lines. J. Transl. Med. *6*, 53.

Fan, Y., Mao, R., and Yang, J. (2013). NF-kB and STAT3 signaling pathways collaboratively link inflammation to cancer. Protein Cell *4*, 176–185.

Fleming, I.N., Gray, A., and Downes, C.P. (2000). Regulation of the Rac1-specific exchange factor Tiam1 involves both phosphoinositide 3-kinase-dependent and -independent components. Biochem. J. *351*, 173.

Friedl, P. (2004). Prespecification and plasticity: shifting mechanisms of cell migration. Curr. Opin. Cell Biol. *16*, 14–23.

Friedl, P., and Alexander, S. (2011). Cancer invasion and the microenvironment: plasticity and reciprocity. Cell *147*, 992–1009.

Friedl, P., and Wolf, K. (2008). Tube travel: the role of proteases in individual and collective cancer cell invasion. Cancer Res. *68*, 7247–7249.

Friedl, P., and Wolf, K. (2009). Proteolytic interstitial cell migration: a five-step process. Cancer Metastasis Rev. *28*, 129–135.

Friedl, P., and Wolf, K. (2010). Plasticity of cell migration: a multiscale tuning model. J. Cell Biol. *188*, 11–19.

Friedl, P., Noble, P.B., Shields, E.D., and Zanker, K.S. (1994). Locomotor phenotypes of unstimulated CD45RAhigh and CD45ROhigh CD4+ and CD8+ lymphocytes in three-dimensional collagen lattices. Immunology *82*, 617–624.

Fujimoto, D. (1968). Isolation of collagens of high hydroxyproline, hydroxylsine and carbohydrate content from muscle layer of Ascaris lumbricoides and pig kidney. Biochim. Biophys. Acta *168*, 537–543.

Gadea, G., Sanz-Moreno, V., Self, A., Godi, A., and Marshall, C.J. (2008). DOCK10-mediated Cdc42 activation is necessary for amoeboid invasion of melanoma cells. Curr. Biol. *18*, 1456–1465.

Gandalovičová, A., Vomastek, T., Rosel, D., and Brábek, J. (2016). Cell polarity signaling in the plasticity of cancer cell invasiveness. Oncotarget; Adv. Online Publ.

Gao, L., Bai, L., and Nan, Q. zhen (2013). Activation of Rho GTPase Cdc42 promotes adhesion and invasion in colorectal cancer cells. Med. Sci. Monit. Basic Res. *19*, 201–207.

Garcia-Gareta, E. (2014). Collagen gels and the "Bornstein legacy": from a substrate for tissue culture to cell culture systems and biomaterials for tissue regeneration. Exp. Dermatol. *23*, 473–474.

Geiger, T.R., and Peeper, D.S. (2009). Metastasis mechanisms. Biochim. Biophys. Acta *1796*, 293–308.

Geraldo, S., Simon, A., Elkhatib, N., Louvard, D., Fetler, L., and Vignjevic, D.M. (2012). Do cancer cells have distinct adhesions in 3D collagen matrices and in vivo? Eur. J. Cell Biol. *91*, 930–937.

Gimona, M., Buccione, R., Courtneidge, S.A., and Linder, S. (2008). Assembly and biological role of podosomes and invadopodia. Curr. Opin. Cell Biol. *20*, 235–241.

Van Goethem, E., Poincloux, R., Gauffre, F., Maridonneau-Parini, I., and Le Cabec, V. (2010). Matrix architecture dictates three-dimensional migration modes of human macrophages: differential involvement of proteases and podosome-like structures. J. Immunol. *184*, 1049–1061.

Gu, Z., Liu, F., Tonkova, E. a, Lee, S.Y., Tschumperlin, D.J., and Brenner, M.B. (2014). Soft matrix is a natural stimulator for cellular invasiveness. Mol. Biol. Cell *25*, 457–469.

Guilluy, C., Garcia-Mata, R., and Burridge, K. (2011). Rho protein crosstalk: another social network? Trends Cell Biol. *21*, 718–726.

Hagerty, L., Weitzel, D.H., Chambers, J., Fortner, C.N., Brush, M.H., Loiselle, D., Hosoya, H., and Haystead, T.A. (2007). ROCK1 phosphorylates and activates zipper-interacting protein kinase. J. Biol. Chem. *282*, 4884–4893.

Halaoui, R., and McCaffrey, L. (2014). Rewiring cell polarity signaling in cancer. Oncogene 1–12.

Hanahan, D., and Weinberg, R.A. (2011). Hallmarks of Cancer : The Next Generation. Cell *144*, 646–674.

Harada, T., Swift, J., Irianto, J., Shin, J.W., Spinler, K.R., Athirasala, A., Diegmiller, R., Dingal, P.C.D.P., Ivanovska, I.L., and Discher, D.E. (2014). Nuclear lamin stiffness is a barrier to 3D migration, but softness can limit survival. J. Cell Biol. *204*, 669–682.

Hideshima, T., Chauhan, D., Richardson, P., Mitsiades, C., Mitsiades, N., Hayashi, T., Munshi, N., Dang, L., Castro, A., Palombella, V., et al. (2002). NF-kappa B as a therapeutic target in multiple myeloma. J. Biol. Chem. *277*, 16639–16647.

Hiscott, J., Marois, J., Garoufalis, J., D'Addario, M., Roulston, A., Kwan, I., Pepin, N., Lacoste, J., Nguyen, H., and Bensi, G. (1993). Characterization of a functional NF-kappa B site in the human interleukin 1 beta promoter: evidence for a positive autoregulatory loop. Mol. Cell. Biol. *13* , 6231–6240.

Holstein, S. a, and Hohl, R.J. (2012). Is there a future for prenyltransferase inhibitors in cancer therapy? Curr. Opin. Pharmacol. *12*, 704–709.

Huang, B., Lu, M., Jolly, M.K., Tsarfaty, I., Onuchic, J., and Ben-Jacob, E. (2014). The three-way switch operation of Rac1/RhoA GTPase-based circuit controlling amoeboid-hybrid-mesenchymal transition. Sci. Rep. *4*, 6449.

Huttenlocher, A., and Horwitz, A.R. (2011). Integrins in cell migration. Cold Spring Harb. Perspect. Biol. *3*, a005074.

Charras, G., and Paluch, E. (2008). Blebs lead the way: how to migrate without lamellipodia. Nat. Rev. Mol. Cell Biol. *9*, 730–736.

Charras, G.T., Hu, C.-K., Coughlin, M., and Mitchison, T.J. (2006). Reassembly of contractile actin cortex in cell blebs. J. Cell Biol. *175* , 477–490.

Chin, A.R., and Wang, S.E. (2014). Cytokines driving breast cancer stemness. Mol. Cell. Endocrinol. *382*, 598–602.

Cho, H.J., Baek, K.E., and Yoo, J. (2010). RhoGDI2 as a therapeutic target in cancer. Expert Opin. Ther. Targets *14*, 67–75.

Chrzanowska-Wodnicka, M., and Burridge, K. (1996). Rho-stimulated contractility drives the formation of stress fibers and focal adhesions. J. Cell Biol. *133*, 1403–1415.

Ihara, K., Muraguchi, S., Kato, M., Shimizu, T., Shirakawa, M., Kuroda, S., Kaibuchi, K., and Hakoshima, T. (1998). Crystal Structure of Human RhoA in a Dominantly Active Form Complexed with a GTP Analogue. J. Biol. Chem. *273* , 9656–9666.

Iliopoulos, D., Hirsch, H.A., Wang, G., and Struhl, K. (2011). Inducible formation of breast cancer stem cells and their dynamic equilibrium with non-stem cancer cells via IL6 secretion. Proc. Natl. Acad. Sci. *108* , 1397–1402.

Isshiki, H., Akira, S., Tanabe, O., Nakajima, T., Shimamoto, T., Hirano, T., and Kishimoto, T. (1990). Constitutive and interleukin-1 (IL-1)-inducible factors interact with the IL-1-responsive element in the IL-6 gene. Mol. Cell. Biol. *10* , 2757–2764.

Jinushi, M. (2014). Role of cancer stem cell-associated inflammation in creating pro-inflammatory tumorigenic microenvironments. Oncoimmunology *3*, e28862.

Just, I., Huelsenbeck, S.C., and Genth, H. (2010). Clostridium Botulinum C3 Exoenzyme: Rho-Inactivating Tool in Cell Biology and a Neurotrophic Agent~!2009-08-26~!2009-09-08~!2010-03-09~! Open Toxinology J. *3*, 19–23.

Karreth, F.A., DeNicola, G.M., Winter, S.P., and Tuveson, D.A. (2009). C-Raf Inhibits MAPK Activation and Transformation by B-RafV600E. Mol. Cell *36*, 477–486.

Katanov, C., Lerrer, S., Liubomirski, Y., Leider-Trejo, L., Meshel, T., Bar, J., Feniger-Barish, R., Kamer, I., Soria-Artzi, G., Kahani, H., et al. (2015). Regulation of the inflammatory profile of stromal cells in human breast cancer: prominent roles for TNF-α and the NF-κB pathway. Stem Cell Res. Ther. *6*, 1–17.

Khalil, A.A., and Friedl, P. (2010). Determinants of leader cells in collective cell migration. Integr. Biol. (Camb). *2*, 568–574.

Kim, T.K., and Eberwine, J.H. (2010). Mammalian cell transfection: the present and the future. Anal. Bioanal. Chem. *397*, 3173–3178.

Kim, N.-G., Lee, H., Son, E., Kwon, O.-Y., Park, J.-Y., Park, J.-H., Jae Cho, G., Sung Choi, W., and Suk, K. (2003). Hypoxic induction of caspase-11/caspase-1/interleukin-1β in brain microglia. Mol. Brain Res. *114*, 107–114.

Kim, S.-Y., Kang, J.W., Song, X., Kim, B.K., Yoo, Y.D., Kwon, Y.T., and Lee, Y.J. (2013). Role of the IL-6-JAK1-STAT3-Oct-4 pathway in the conversion of non-stem cancer cells into cancer stem-like cells. Cell. Signal. *25*, 961–969.

Kimura, K., Ito, M., Amano, M., Chihara, K., Fukata, Y., Nakafuku, M., Yamamori, B., Feng, J., Nakano, T., Okawa, K., et al. (1996). Regulation of Myosin Phosphatase by Rho and Rho-Associated Kinase (Rho-Kinase). Sci. *273* , 245–248.

Kitzing, T.M., Wang, Y., Pertz, O., Copeland, J.W., and Grosse, R. (2010). Formin-like 2 drives amoeboid invasive cell motility downstream of RhoC. Oncogene *29*, 2441–2448.

Kleinman, H.K., and Martin, G.R. (2005). Matrigel: Basement membrane matrix with biological activity. Semin. Cancer Biol. *15*, 378–386.

Ten Klooster, J.P., Evers, E.E., Janssen, L., Machesky, L.M., Michiels, F., Hordijk, P., and Collard, J.G. (2006). Interaction between Tiam1 and the Arp2/3 complex links activation of Rac to actin polymerization. Biochem. J. *397*, 39–45.

Kluger, H.M., Dudek, A.Z., McCann, C., Ritacco, J., Southard, N., Jilaveanu, L.B., Molinaro, A., and Sznol, M. (2011). A phase 2 trial of dasatinib in advanced melanoma. Cancer *117*, 2202–2208.

Kobayashi, T., Hattori, S., and Shinkai, H. (2003). Matrix metalloproteinases-2 and -9 are secreted from human fibroblasts. Acta Derm. Venereol. *83*, 105–107.

Kosla, J., Paňková, D., Plachý, J., Tolde, O., Bicanová, K., Dvořák, M., Rösel, D., and Brábek, J. (2013). Metastasis of aggressive amoeboid sarcoma cells is dependent on Rho/ROCK/MLC signaling. Cell Commun. Signal. *11*, 51.

Kramer, N., Walzl, A., Unger, C., Rosner, M., Krupitza, G., Hengstschläger, M., and Dolznig, H. (2013). In vitro cell migration and invasion assays. Mutat. Res. *752*, 10–24.

Krause, M., and Wolf, K. (2015). Cancer cell migration in 3d tissue: Negotiating space by proteolysis and nuclear deformability. Cell Adhes. Migr. *9*, 357–366.

Kraynov, V.S., Chamberlain, C., Bokoch, G.M., Schwartz, M., Slabaugh, S., and Hahn, K.M. (2000). Localized Rac activation dynamics visualized in living cells. Science *290*, 333–337.

Kusama, T., Mukai, M., Endo, H., Ishikawa, O., Tatsuta, M., Nakamura, H., and Inoue, M. (2006). Inactivation of Rho GTPases by p190 RhoGAP reduces human pancreatic cancer cell invasion and metastasis. Cancer Sci. *97*, 848–853.

Kuscu, C., Evensen, N., Kim, D., Hu, Y.-J., Zucker, S., and Cao, J. (2012). Transcriptional and epigenetic regulation of KIAA1199 gene expression in human breast cancer. PLoS One *7*, e44661.

Kutys, M.L., and Yamada, K.M. (2014). An extracellular-matrix-specific GEF–GAP interaction regulates Rho GTPase crosstalk for 3D collagen migration. Nat. Cell Biol. *16*.

Lämmermann, T., and Sixt, M. (2009). Mechanical modes of "amoeboid" cell migration. Curr. Opin. Cell Biol. *21*, 636–644.

Lämmermann, T., Bader, B.L., Monkley, S.J., Worbs, T., Wedlich-Söldner, R., Hirsch, K., Keller, M., Förster, R., Critchley, D.R., Fässler, R., et al. (2008). Rapid leukocyte migration by integrin-independent flowing and squeezing. Nature *453*, 51–55.

Lamouille, S., Xu, J., and Derynck, R. (2014). Molecular mechanisms of epithelial-mesenchymal transition. Nat. Rev. Mol. Cell Biol. *15*, 178–196.

Lanza, A.M., Kim, D.S., and Alper, H.S. (2013). Evaluating the influence of selection markers on obtaining selected pools and stable cell lines in human cells. Biotechnol. J. *8*, 811–821.

Lazebnik, Y. (2010). What are the hallmarks of cancer? Nat. Rev. Cancer *10*, 232–233.

Lazer, G., and Katzav, S. (2011). Guanine nucleotide exchange factors for RhoGTPases: good therapeutic targets for cancer therapy? Cell. Signal. *23*, 969–979.

Li, Y., and Prakash, S.R. (2005). Synthesis of C-14-labeled novel IKK inhibitor: 2-[14C]-N-(6-chloro-9H-pyrido [3,4-b]indol-8-yl)-3-pyridinecarboxamide. J. Label. Compd. Radiopharm. *48*, 323–330.

Li, A., Dawson, J.C., Forero-Vargas, M., Spence, H.J., Yu, X., König, I., Anderson, K., and Machesky, L.M. (2010). The Actin-Bundling Protein Fascin Stabilizes Actin in Invadopodia and Potentiates Protrusive Invasion. Curr. Biol. *20*, 339–345.

Li, Y., Wang, L., Pappan, L., Galliher-Beckley, A., and Shi, J. (2012). IL-1β promotes stemness and invasiveness of colon cancer cells through Zeb1 activation. Mol. Cancer *11*, 1–13.

Li, Z., Hannigan, M., Mo, Z., Liu, B., Lu, W., Wu, Y., Smrcka, A. V, Wu, G., Li, L., Liu, M., et al. (2003). Directional sensing requires G beta gamma-mediated PAK1 and PIX alpha-dependent activation of Cdc42. Cell *114*, 215–227.

Linder, S., Wiesner, C., and Himmel, M. (2011). Degrading devices: invadosomes in proteolytic cell invasion. Annu. Rev. Cell Dev. Biol. *27*, 185–211.

Liu, J., Zhang, C., Wu, R., Lin, M., Liang, Y., Liu, J., Wang, X., Yang, B., and Feng, Z. (2015). RRAD inhibits the Warburg effect through negative regulation of the NF-kappaB signaling. Oncotarget *6*, 14982–14992.

Lombardo, L.J., Lee, F.Y., Chen, P., Norris, D., Barrish, J.C., Behnia, K., Castaneda, S., Cornelius, L.A.M., Das, J., Doweyko, A.M., et al. (2004). Discovery of N-(2-chloro-6-methyl- phenyl)-2-(6-(4-(2-hydroxyethyl)- piperazin-1-yl)-2-methylpyrimidin-4- ylamino)thiazole-5-carboxamide (BMS-354825), a dual Src/Abl kinase inhibitor with potent antitumor activity in preclinical assays. J. Med. Chem. *47*, 6658–6661.

Lorentzen, A., Bamber, J., Sadok, A., Elson-Schwab, I., and Marshall, C.J. (2011). An ezrin-rich, rigid uropod-like structure directs movement of amoeboid blebbing cells. J. Cell Sci. *124*, 1256–1267.

Lub, S., Maes, K., Menu, E., Bruyne, E. De, Vanderkerken, K., and Valckenborgh, E. Van (2015). Novel strategies to target the ubiquitin proteasome system in multiple myeloma. Oncotarget *7*.

Macara, I.G., and McCaffrey, L. (2013). Cell polarity in morphogenesis and metastasis. Philos. Trans. R. Soc. Lond. B. Biol. Sci. *368*, 20130012.

Margheri, F., Luciani, C., Taddei, M.L., Giannoni, E., Laurenzana, A., Biagioni, A., Chillà, A., Chiarugi, P., Fibbi, G., and Del Rosso, M. (2014). The receptor for urokinase-plasminogen activator

(uPAR) controls plasticity of cancer cell movement in mesenchymal and amoeboid migration style. Oncotarget *5*, 1538–1553.

Matsusaka, T., Fujikawa, K., Nishio, Y., Mukaida, N., Matsushima, K., Kishimoto, T., and Akira, S. (1993). Transcription factors NF-IL6 and NF-kappa B synergistically activate transcription of the inflammatory cytokines, interleukin 6 and interleukin 8. Proc. Natl. Acad. Sci. *90*, 10193–10197.

McCaffrey, L.M., and Macara, I.G. (2011). Epithelial organization, cell polarity and tumorigenesis. Trends Cell Biol. *21*, 727–735.

McGregor, A.L., Hsia, C.-R., and Lammerding, J. (2016). Squish and squeeze—the nucleus as a physical barrier during migration in confined environments. Curr. Opin. Cell Biol. *40*, 32–40.

Mitchison, T.J., and Cramer, L.P. (1996). Actin-based cell motility and cell locomotion. Cell *84*, 371–379.

Molnar, G., Dagher, M.C., Geiszt, M., Settleman, J., and Ligeti, E. (2001). Role of prenylation in the interaction of Rho-family small GTPases with GTPase activating proteins. Biochemistry *40*, 10542–10549.

Monypenny, J., Zicha, D., Higashida, C., Oceguera-Yanez, F., Narumiya, S., and Watanabe, N. (2009). Cdc42 and Rac Family GTPases Regulate Mode and Speed but Not Direction of Primary Fibroblast Migration during Platelet-Derived Growth Factor-Dependent Chemotaxis. Mol. Cell. Biol. *29* , 2730–2747.

Morin, P., Flors, C., and Olson, M.F. (2009). Constitutively active RhoA inhibits proliferation by retarding G1 to S phase cell cycle progression and impairing cytokinesis. Eur. J. Cell Biol. *88*, 495–507.

Mouw, J.K., Ou, G., and Weaver, V.M. (2014). Extracellular matrix assembly: a multiscale deconstruction. Nat Rev Mol Cell Biol *15*, 771–785.

Murakami, M., Hibi, M., Nakagawa, N., Nakagawa, T., Yasukawa, K., Yamanishi, K., Taga, T., and Kishimoto, T. (1993). IL-6-induced homodimerization of gp130 and associated activation of a tyrosine kinase. Science (80-.). *260*, 1808–1810.

Murali, A., and Rajalingam, K. (2014). Small Rho GTPases in the control of cell shape and mobility. Cell. Mol. Life Sci. *71*, 1703–1721.

Nabeshima, K., Inoue, T., Shimao, Y., Kataoka, H., and Koono, M. (1999). Cohort migration of carcinoma cells: differentiated colorectal carcinoma cells move as coherent cell clusters or sheets. Histol. Histopathol. *14*, 1183–1197.

Nabeshima, K., Inoue, T., Shimao, Y., Okada, Y., Itoh, Y., Seiki, M., and Koono, M. (2000). Front-cell-specific expression of membrane-type 1 matrix metalloproteinase and gelatinase A during cohort migration of colon carcinoma cells induced by hepatocyte growth factor/scatter factor. Cancer Res. *60*, 3364–3369.

Nagano, M., Hoshino, D., Koshikawa, N., Akizawa, T., and Seiki, M. (2012). Turnover of focal adhesions and cancer cell migration. Int. J. Cell Biol. *2012*, 310616.

Nakagawa, R., Naka, T., Tsutsui, H., Fujimoto, M., Kimura, A., Abe, T., Seki, E., Sato, S., Takeuchi, O., Takeda, K., et al. (2016). SOCS-1 Participates in Negative Regulation of LPS Responses. Immunity *17*, 677–687.

Nakayama, M., Goto, T.M., Sugimoto, M., Nishimura, T., Shinagawa, T., Ohno, S., Amano, M., and Kaibuchi, K. (2008). Rho-kinase phosphorylates PAR-3 and disrupts PAR complex formation. Dev. Cell *14*, 205–215.

Napolitano, A.P., Dean, D.M., Man, A.J., Youssef, J., Ho, D.N., Rago, A.P., Lech, M.P., and Morgan, J.R. (2007). Scaffold-free three-dimensional cell culture utilizing micromolded nonadhesive hydrogels. Biotechniques *43*, 494–500.

Navarro-Lérida, I., Pellinen, T., Sanchez, S.A., Guadamillas, M.C., Wang, Y., Mirtti, T., Calvo, E., and Del Pozo, M.A. (2015). Rac1 Nucleocytoplasmic Shuttling Drives Nuclear Shape Changes and Tumor Invasion. Dev. Cell *32*, 318–334.

Nelson, W.J. (2009). Remodeling epithelial cell organization: transitions between front-rear and apical-basal polarity. Cold Spring Harb. Perspect. Biol. *1*, 1–19.

Ng, S.-L., Friedman, B.A., Schmid, S., Gertz, J., Myers, R.M., Tenoever, B.R., and Maniatis, T. (2011). IkappaB kinase epsilon (IKK(epsilon)) regulates the balance between type I and type II interferon responses. Proc. Natl. Acad. Sci. U. S. A. *108*, 21170–21175.

Nieto, M.A. (2013). Epithelial plasticity: a common theme in embryonic and cancer cells. Science *342*, 1234850.

Nobes, C., and Hall, A. (1999). Rho GTPases control polarity, protrusion, and adhesion during cell movement. J. Cell Biol. *144*, 1235–1244.

Ohta, Y., Hartwig, J.H., and Stossel, T.P. (2006). FilGAP, a Rho- and ROCK-regulated GAP for Rac binds filamin A to control actin remodelling. Nat. Cell Biol. *8*, 803–814.

Orgaz, J.L., Pandya, P., Dalmeida, R., Karagiannis, P., Sanchez-Laorden, B., Viros, A., Albrengues, J., Nestle, F.O., Ridley, A.J., and Gaggioli, C. (2014a). Diverse matrix metalloproteinase functions regulate cancer amoeboid migration. Nat. Commun. *5*.

Orgaz, J.L., Herraiz, C., and Sanz-Moreno, V. (2014b). Rho GTPases modulate malignant transformation of tumor cells. Small GTPases *5*, 1–15.

Paňková, D., Jobe, N., Kratochvílová, M., Buccione, R., Brábek, J., and Rösel, D. (2012). NG2-mediated Rho activation promotes amoeboid invasiveness of cancer cells. Eur. J. Cell Biol. *91*, 969–977.

Parri, M., and Chiarugi, P. (2010). Rac and Rho GTPases in cancer cell motility control. 1–14.

Parsons, J.T., Horwitz, A.R., and Schwartz, M.A. (2010). Cell adhesion: integrating cytoskeletal dynamics and cellular tension. Nat. Rev. Mol. Cell Biol. *11*, 633–643.

Paul, C., Simon, S., Gibert, B., Virot, S., Manero, F., and Arrigo, A.-P. (2010). Dynamic processes that reflect anti-apoptotic strategies set up by HspB1 (Hsp27). Exp. Cell Res. *316*, 1535–1552.

Peacock, J.G., Miller, A.L., Bradley, W.D., Rodriguez, O.C., Webb, D.J., and Koleske, A.J. (2007). The Abl-related gene tyrosine kinase acts through p190RhoGAP to inhibit actomyosin contractility and regulate focal adhesion dynamics upon adhesion to fibronectin. Mol. Biol. Cell *18*, 3860–3872.

Pegtel, D.M., Ellenbroek, S.I.J., Mertens, A.E.E., van der Kammen, R. a, de Rooij, J., and Collard, J.G. (2007). The Par-Tiam1 complex controls persistent migration by stabilizing microtubule-dependent front-rear polarity. Curr. Biol. *17*, 1623–1634.

Perona, R., Montaner, S., Saniger, L., Sánchez-Pérez, I., Bravo, R., and Lacal, J.C. (1997). Activation of the nuclear factor-kappaB by Rho, CDC42, and Rac-1 proteins. Genes Dev. *11* , 463–475.

Pertz, O., Hodgson, L., Klemke, R.L., and Hahn, K.M. (2006). Spatiotemporal dynamics of RhoA activity in migrating cells. Nature *440*, 1069–1072.

Piazzolla, D., Meissl, K., Kucerova, L., Rubiolo, C., and Baccarini, M. (2005). Raf-1 sets the threshold of Fas sensitivity by modulating Rok-α signaling. J. Cell Biol. *171* , 1013–1022.

Pinner, S., and Sahai, E. (2008). Imaging amoeboid cancer cell motility in vivo. J. Microsc. *231*, 441–445.

Platanias, L.C. (2005). Mechanisms of type-I- and type-II-interferon-mediated signalling. Nat Rev Immunol *5*, 375–386.

Poincloux, R., Lizárraga, F., and Chavrier, P. (2009). Matrix invasion by tumour cells: a focus on MT1-MMP trafficking to invadopodia. J. Cell Sci. *122*, 3015–3024.

Quintas-Cardama, A., Vaddi, K., Liu, P., Manshouri, T., Li, J., Scherle, P.A., Caulder, E., Wen, X., Li, Y., Waeltz, P., et al. (2010). Preclinical characterization of the selective JAK1/2 inhibitor INCB018424: therapeutic implications for the treatment of myeloproliferative neoplasms. Blood *115*, 3109–3117.

Rath, N., and Olson, M.F. (2012). Rho-associated kinases in tumorigenesis: re-considering ROCK inhibition for cancer therapy. EMBO Rep. *13*, 900–908.

Regis, G., Pensa, S., Boselli, D., Novelli, F., and Poli, V. (2008). Ups and downs: The STAT1:STAT3 seesaw of Interferon and gp130 receptor signalling. Semin. Cell Dev. Biol. *19*, 351–359.

Ridley, A.J. (2013). RhoA, RhoB and RhoC have different roles in cancer cell migration. J. Microsc. *251*, 242–249.

Rohatgi, R., Ma, L., Miki, H., Lopez, M., Kirchhausen, T., Takenawa, T., and Kirschner, M.W. (1999). The interaction between N-WASP and the Arp2/3 complex links Cdc42-dependent signals to actin assembly. Cell *97*, 221–231.

Rösel, D., Brábek, J., Tolde, O., Mierke, C.T., Zitterbart, D.P., Raupach, C., Bicanová, K., Kollmannsberger, P., Panková, D., Vesely, P., et al. (2008). Up-regulation of Rho/ROCK signaling in sarcoma cells drives invasion and increased generation of protrusive forces. Mol. Cancer Res. *6*, 1410–1420.

Rosenfeldt, H., Castellone, M.D., Randazzo, P.A., and Gutkind, J.S. (2006). Rac inhibits thrombin-induced Rho activation: evidence of a Pak-dependent GTPase crosstalk. J. Mol. Signal. *1*, 8.

Sabeh, F., Shimizu-Hirota, R., and Weiss, S.J. (2009). Protease-dependent versus-independent cancer cell invasion programs: Three-dimensional amoeboid movement revisited. J. Cell Biol. *185*, 11–19.

Sadok, A., and Marshall, C.J. (2014). Rho GTPases: Masters of cell migration. Small GTPases *5*, e29710.

Sahai, E., and Marshall, C.J. (2003). Differing modes of tumour cell invasion have distinct requirements for Rho/ROCK signalling and extracellular proteolysis. Nat. Cell Biol. *5*, 711–719.

Sahai, E., Garcia-Medina, R., Pouysségur, J., and Vial, E. (2007). Smurf1 regulates tumor cell plasticity and motility through degradation of RhoA leading to localized inhibition of contractility. J. Cell Biol. *176*, 35–42.

Saijo, K., and Glass, C.K. (2011). Microglial cell origin and phenotypes in health and disease. Nat. Rev. Immunol. *11*, 775–787.

Sanders, L.C., Matsumura, F., Bokoch, G.M., and Lanerolle, P. De (1999). Inhibition of myosin light chain kinase by p21-activated kinase. Science (80-.). *283*, 2083–2085.

Sanz-Moreno, V., Gadea, G., Ahn, J., Paterson, H., Marra, P., Pinner, S., Sahai, E., and Marshall, C.J. (2008). Rac activation and inactivation control plasticity of tumor cell movement. Cell *135*, 510–523.

Sanz-Moreno, V., Gaggioli, C., Yeo, M., Albrengues, J., Wallberg, F., Viros, A., Hooper, S., Mitter, R., Féral, C.C., Cook, M., et al. (2011). ROCK and JAK1 Signaling Cooperate to Control Actomyosin Contractility in Tumor Cells and Stroma. Cancer Cell *20*, 229–245.

Sekine, A., Fujiwara, M., and Narumiya, S. (1989). Asparagine residue in the rho gene product is the modification site for botulinum ADP-ribosyltransferase. J. Biol. Chem. *264* , 8602–8605.

Shamir, E.R., and Ewald, A.J. (2014). Three-dimensional organotypic culture: experimental models of mammalian biology and disease. Nat. Rev. Mol. Cell Biol. *15*, 647–664.

Shigdar, S., Li, Y., Bhattacharya, S., O'Connor, M., Pu, C., Lin, J., Wang, T., Xiang, D., Kong, L., Wei, M.Q., et al. (2014). Inflammation and cancer stem cells. Cancer Lett. *345*, 271–278.

Shor, A.C., Keschman, E. a., Lee, F.Y., Muro-Cacho, C., Letson, G.D., Trent, J.C., Pledger, W.J., and Jove, R. (2007). Dasatinib inhibits migration and invasion in diverse human sarcoma cell lines and induces apoptosis in bone sarcoma cells dependent on Src kinase for survival. Cancer Res. *67*, 2800–2808.

Schindler, C., and Plumlee, C. (2008). Inteferons pen the JAK-STAT pathway. Semin. Cell Dev. Biol. *19*, 311–318.

Schmidt, A., and Hall, A. (2002). Guanine nucleotide exchange factors for Rho GTPases: turning on the switch. Genes Dev. *16* , 1587–1609.

Schmidt, S., and Friedl, P. (2010). Interstitial cell migration: integrin-dependent and alternative adhesion mechanisms. Cell Tissue Res. *339*, 83–92.

Simpson, K.J., Dugan, A.S., and Mercurio, A.M. (2004). Functional Analysis of the Contribution of RhoA and RhoC GTPases to Invasive Breast Carcinoma. Cancer Res. *64* , 8694–8701.

Skorski, T., Wlodarski, P., Daheron, L., Salomoni, P., Nieborowska-Skorska, M., Majewski, M., Wasik, M., and Calabretta, B. (1998). BCR/ABL-mediated leukemogenesis requires the activity of the small GTP-binding protein Rac. Proc. Natl. Acad. Sci. U. S. A. *95*, 11858–11862.

Sleeman, J., and Steeg, P.S. (2010). Cancer metastasis as a therapeutic target. Eur. J. Cancer *46*, 1177–1180.

Smalley, K.S.M., Xiao, M., Villanueva, J., Nguyen, T.K., Keith, T., Letrero, R., Belle, P. Van, Elder, D.E., Wang, Y., Katherine, L., et al. (2009). CRAF inhibition induces apoptosis in melanoma cells with non- V600E BRAF mutations. Oncogene *28*, 85–94.

Solinas, G., Marchesi, F., Garlanda, C., Mantovani, A., and Allavena, P. (2010). Inflammation-mediated promotion of invasion and metastasis. Cancer Metastasis Rev. *29*, 243–248.

Sporn, M.B. (1996). The war on cancer. Lancet *347*, 1377–1381.

Srinivasan, S., Wang, F., Glavas, S., Ott, A., Hofmann, F., Aktories, K., Kalman, D., and Bourne, H.R. (2003). Rac and Cdc42 play distinct roles in regulating PI(3,4,5)P3 and polarity during neutrophil chemotaxis. J. Cell Biol. *160*, 375–385.

Sun, S.-C. (2011). Non-canonical NF-κB signaling pathway. Cell Res. *21*, 71–85.

Sun, J., He, H., Xiong, Y., Lu, S., Shen, J., Cheng, A., Chang, W.-C., Hou, M.-F., Lancaster, J.M., Kim, M., et al. (2011). Fascin is critical for transforming growth factor β induced invasion and filopodia formation in spindle-shaped tumor cells. J. Biol. Chem. .

Taddei, M.L., Giannoni, E., Comito, G., and Chiarugi, P. (2013). Microenvironment and tumor cell plasticity: an easy way out. Cancer Lett. *341*, 80–96.

Taddei, M.L., Giannoni, E., Morandi, A., Ippolito, L., Ramazzotti, M., Callari, M., Gandellini, P., and Chiarugi, P. (2014). Mesenchymal to amoeboid transition is associated with stem-like features of melanoma cells. Cell Commun. Signal. *12*, 24.

Terry, S.J., Elbediwy, A., Zihni, C., Harris, A.R., Bailly, M., Charras, G.T., Balda, M.S., and Matter, K. (2012). Stimulation of cortical myosin phosphorylation by p114RhoGEF drives cell migration and tumor cell invasion. PLoS One *7*, e50188.

Tester, A.M., Ruangpanit, N., Anderson, R.L., and Thompson, E.W. (1993). MMP-9 secretion and MMP-2 activation distinguish invasive and metastatic sublines of a mouse mammary carcinoma system showing epithelial-mesenchymal transition traits. Clin. Exp. Metastasis *18*, 553–560.

Thiery, J.P., Acloque, H., Huang, R.Y.J., and Nieto, M.A. (2009). Epithelial-Mesenchymal Transitions in Development and Disease. Cell *139*, 871–890.

Tcherkezian, J., and Lamarche-Vane, N. (2007). Current knowledge of the large RhoGAP family of proteins. Biol. Cell *99*, 67–86.

Tolde, O., Rösel, D., Veselý, P., Folk, P., and Brábek, J. (2010). The structure of invadopodia in a complex 3D environment. Eur. J. Cell Biol. *89*, 674–680.

Tozluoğlu, M., Tournier, A.L., Jenkins, R.P., Hooper, S., Bates, P.A., and Sahai, E. (2013). Matrix geometry determines optimal cancer cell migration strategy and modulates response to interventions. Nat. Cell Biol. *15*, 751–762.

Vannucchi, A.M., Kiladjian, J.J., Griesshammer, M., Masszi, T., Durrant, S., Passamonti, F., Harrison, C.N., Pane, F., Zachee, P., Mesa, R., et al. (2015). Ruxolitinib versus Standard Therapy for the Treatment of Polycythemia Vera. N. Engl. J. Med. *372*, 426–435.

Vaskovicova, K., Szabadosova, E., Cermak, V., Gandalovicova, A., Kasalova, L., Rosel, D., and Brabek, J. (2015). PKCalpha promotes the mesenchymal to amoeboid transition and increases cancer cell invasiveness. BMC Cancer *15*, 326.

Vega, F.M., Colomba, A., Reymond, N., Thomas, M., and Ridley, A.J. (2012). RhoB regulates cell migration through altered focal adhesion dynamics. Open Biol. *2*, 120076.

Viennois, E., Chen, F., and Merlin, D. (2012). NF-κB pathway in colitis-associated cancers. Transl. Gastrointest. Cancer *2*.

Watanabe, N., Kato, T., Fujita, A., Ishizaki, T., and Narumiya, S. (1999). Cooperation between mDia1 and ROCK in Rho-induced actin reorganization. Nat. Cell Biol. *1*, 136–143.

Welf, E.S., Driscoll, M.K., Dean, K.M., Lin, M.Z., Chu, J., Davidson, M.W., and Lin, M.Z. (2016). Quantitative Multiscale Cell Imaging in Controlled 3D Technology. Dev. Cell *36*, 462–475.

Wiegers, W., Just, I., Muller, H., Hellwig, A., Traub, P., and Aktories, K. (1991). Alteration of the cytoskeleton of mammalian cells cultured in vitro by Clostridium botulinum C2 toxin and C3 ADP-ribosyltransferase. Eur. J. Cell Biol. *54*, 237–245.

Wilkinson, S., Paterson, H.F., and Marshall, C.J. (2005). Cdc42-MRCK and Rho-ROCK signalling cooperate in myosin phosphorylation and cell invasion. Nat. Cell Biol. *7*, 255–261.

Wolf, K., Mazo, I., Leung, H., Engelke, K., von Andrian, U.H., Deryugina, E.I., Strongin, A.Y., Bröcker, E.-B., and Friedl, P. (2003). Compensation mechanism in tumor cell migration: mesenchymal-amoeboid transition after blocking of pericellular proteolysis. J. Cell Biol. *160*, 267–277.

Wolf, K., Wu, Y.I., Liu, Y., Geiger, J., Tam, E., Overall, C., Stack, M.S., and Friedl, P. (2007). Multi-step pericellular proteolysis controls the transition from individual to collective cancer cell invasion. Nat Cell Biol *9*, 893–904.

Wolf, K., te Lindert, M., Krause, M., Alexander, S., te Riet, J., Willis, A.L., Hoffman, R.M., Figdor, C.G., Weiss, S.J., and Friedl, P. (2013). Physical limits of cell migration: Control by ECM space and nuclear deformation and tuning by proteolysis and traction force. J. Cell Biol. *201*, 1069–1084.

Woodroofe, M.N., Sarna, G.S., Wadhwa, M., Hayes, G.M., Loughlin, A.J., Tinker, A., and Cuzner, M.L. (1991). Detection of interleukin-1 and interleukin-6 in adult rat brain, following mechanical injury, by in vivo microdialysis: evidence of a role for microglia in cytokine production. J. Neuroimmunol. *33*, 227–236.

Worthylake, R. a., Lemoine, S., Watson, J.M., and Burridge, K. (2001). RhoA is required for monocyte tail retraction during transendothelial migration. J. Cell Biol. *154*, 147–160.

Wyckoff, J.B., Pinner, S.E., Gschmeissner, S., Condeelis, J.S., and Sahai, E. (2006). ROCK- and myosin-dependent matrix deformation enables protease-independent tumor-cell invasion in vivo. Curr. Biol. *16*, 1515–1523.

Yang, J., Liao, D., Chen, C., Liu, Y., Chuang, T.-H., Xiang, R., Markowitz, D., Reisfeld, R.A., and Luo, Y. (2013). Tumor-Associated Macrophages Regulate Murine Breast Cancer Stem Cells Through a Novel Paracrine EGFR/Stat3/Sox-2 Signaling Pathway. Stem Cells *31*, 248–258.

Yang, L., Wang, L., and Zheng, Y. (2006). Gene Targeting of Cdc42 and Cdc42GAP Affirms the Critical Involvement of Cdc42 in Filopodia Induction, Directed Migration, and Proliferation in Primary Mouse Embryonic Fibroblasts. Mol. Biol. Cell *17*, 4675–4685.

Yarilina, A., Park-Min, K.-H., Antoniv, T., Hu, X., and Ivashkiv, L.B. (2008). TNF activates an IRF1-dependent autocrine loop leading to sustained expression of chemokines and STAT1-dependent type I interferon-response genes. Nat. Immunol. *9*, 378–387.

Yeh, J.E., Toniolo, P. a, and Frank, D. a (2013). Targeting transcription factors. Curr. Opin. Oncol. *25*, 652–658.

Yi, H., Cho, H.-J., Cho, S.-M., Jo, K., Park, J.-A., Kim, N.-H., Amidon, G.L., Kim, J.-S., and Shin, H.-C. (2012). Blockade of interleukin-6 receptor suppresses the proliferation of H460 lung cancer stem cells. Int. J. Oncol. *41*, 310–316.

Yoo, H.Y., Sung, M.K., Lee, S.H., Kim, S., Lee, H., Park, S., Kim, S.C., Lee, B., Rho, K., Lee, J.E., et al. (2014). A recurrent inactivating mutation in RHOA GTPase in angioimmunoblastic T cell lymphoma. Nat Genet *46*, 371–375.

Zijl, F. Van, Krupitza, G., and Mikulits, W. (2011). Initial steps of metastasis: cell invasion and endothelial transmigration. Mutat. Res. Mutat. *728*, 23–34.

11.Attachment

11.1. RNA-seq data

Gene	Fold upregulation		
	caRhoA	Dasatinib	Specification
STAT1	3.19	1.65	signal transducer and activator of transcription 1
STAT2	2.08	1.85	signal transducer and activator of transcription 2
CEMIP	3.51	45.43	cell migration-inducing and hyaluronan-binding protein
IL6	10.67	6.46	interleukin 6
IL11	1.95	6.67	interleukin 11
IL24	2.72	9.36	interleukin 24
C1R	2.75	2.84	complement component 1, r subcomponent
C1S	4.18	3.79	complement component 1, s subcomponent
C3a1	5.95	1.96	complement component 3a receptor 1
IFI35	1.86	2.65	interferon-induced protein 35
IFI44L	9.06	3.09	interferon-induced protein 44-like
IFI6	4.73	2.89	interferon, alpha-inducible protein 6
IFIH1	3.84	1.70	interferon induced with helicase C domain 1
IFIT1	9.94	3.05	interferon-induced protein with tetratricopeptide repeats 1
IFIT2	4.81	2.37	interferon-induced protein with tetratricopeptide repeats 2
IFIT3	3.85	2.59	interferon-induced protein with tetratricopeptide repeats 3
IFITM1	3.73	3.42	interferon induced transmembrane protein 1
IFITM3	1.94	2.51	interferon induced transmembrane protein 3
MX1	4.57	2.08	MX dynamin-like GTPase 1
MX2	6.57	1.99	MX dynamin-like GTPase 2
OAS1	4.31	3.38	2'-5'-oligoadenylate synthetase 1
OAS2	5.12	2.38	2'-5'-oligoadenylate synthetase 2
RSAD2	13.00	3.36	radical S-adenosyl methionine domain containing 2
SAA1	8.05	6.51	serum amyloid A1
SAA2	7.94	3.95	serum amyloid A2
USP18	5.28	2.14	ubiquitin specific peptidase 18

TableA. 1: Specification of chosen upregulated genes after caRhoA expression and dasatinib treatment. The fold upregulation for each treatment is depicted.

11.2. Restriction enzyme digestion- cloning results

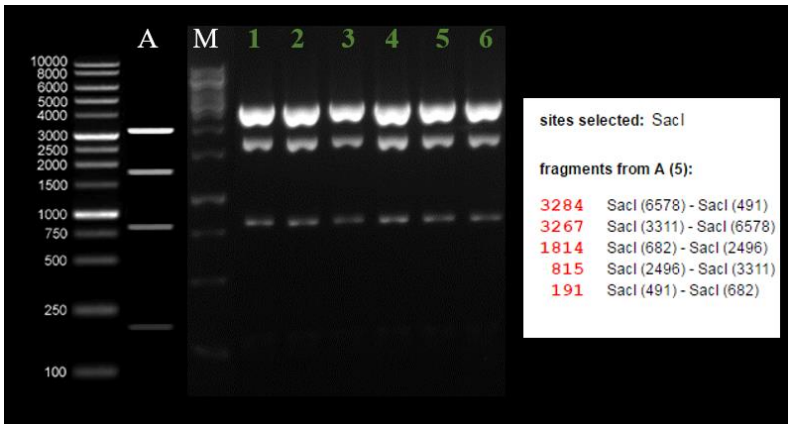

Fig.A. 1: The verification of pLVX-TightPuro-C3exo. To verify positive clones, Sac1 enzyme digestion was used. Pattern depicted under letter A predicts positive clones. Positive clones are highlighted in green.

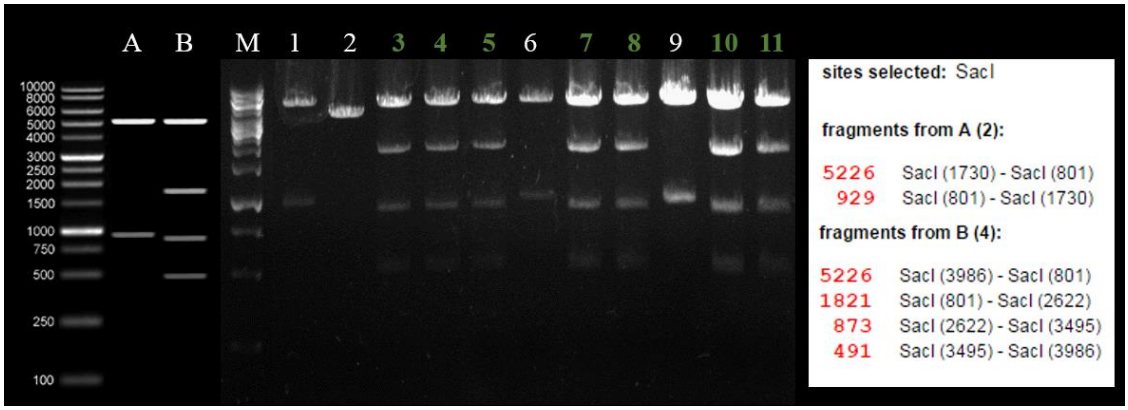

Fig.A. 2: The verification of pcDNA3-dSMS-dXba/XhoI-gEGFPg-Stat1. To verify positive clones, Sac1 enzyme digestion was used. Pattern depicted under letter A corresponds to vector. B shows 4 fragments corresponding to vector with Stat1 insert. Positive clones are highlighted in green.

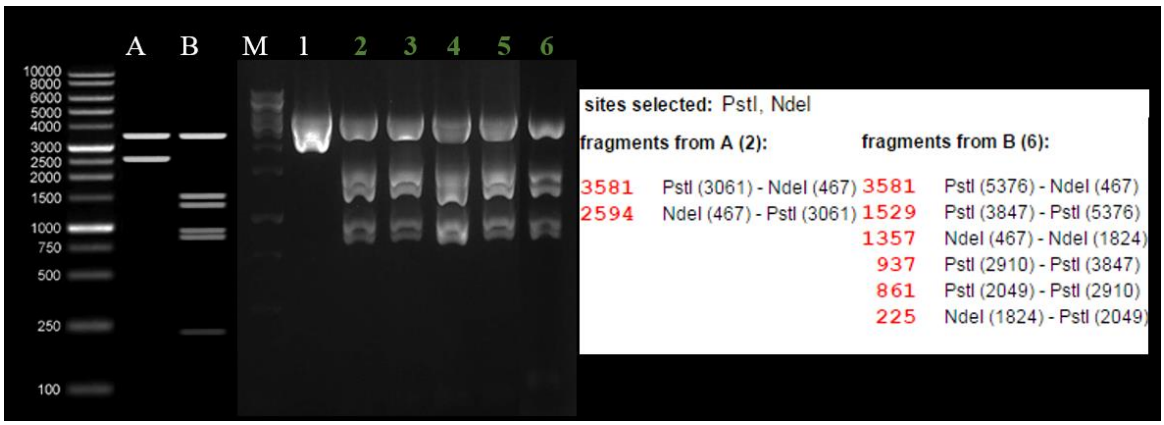

Fig.A. 3: The verification of pcDNA3-dSMS-gEGFPg-Stat3. To verify positive clones, PstI and NdeI enzymes were used. Pattern depicted under letter A corresponds to vector. B shows 4 fragments corresponding to vector with Stat1 insert. Positive clones are highlighted in green.

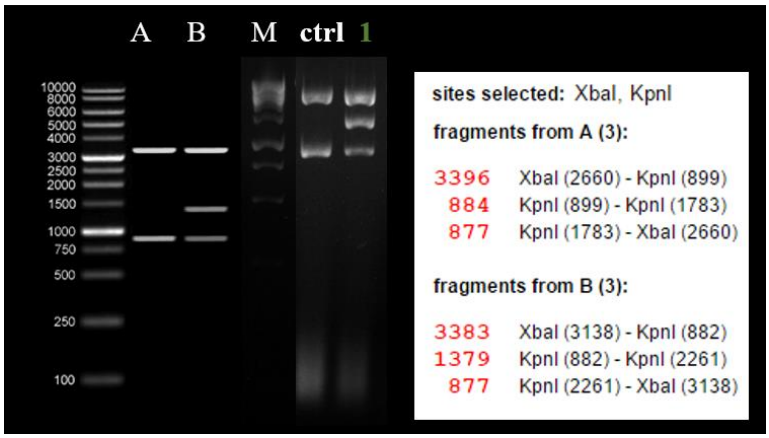

Fig.A. 4: The verification of pIRESPuro3-dMluI–sTNF. To verify positive clones, XbaI and KpnI enzymes were used. Pattern depicted under letter A corresponds to vector, used as control. B shows 3 fragments corresponding to the vector with sTNF insert.

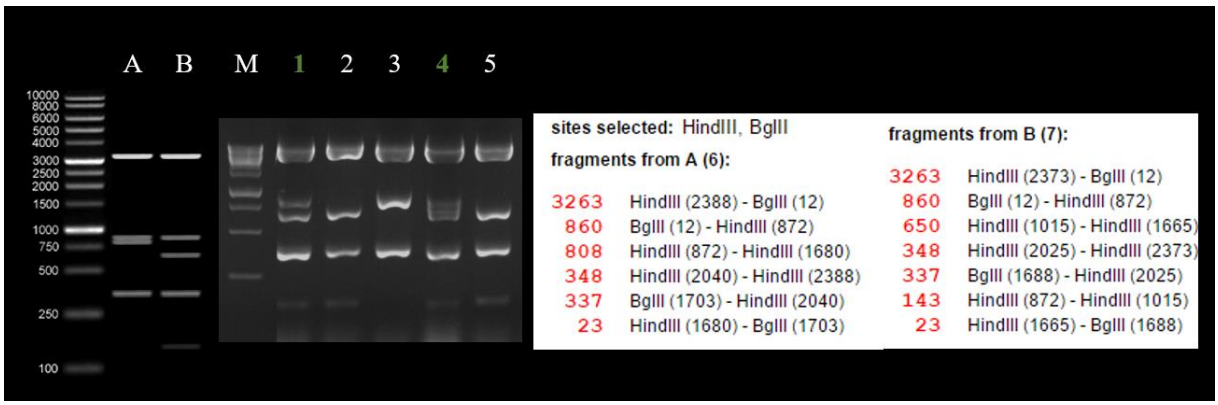

Fig.A. 6: The verification of pIRESPuro3-dMluI–sIL1β. To verify positive clones, HindlII and BglII enzymes were used. Pattern depicted under letter A corresponds to original vector. B shows fragments corresponding to the vector with sIL1β insert.

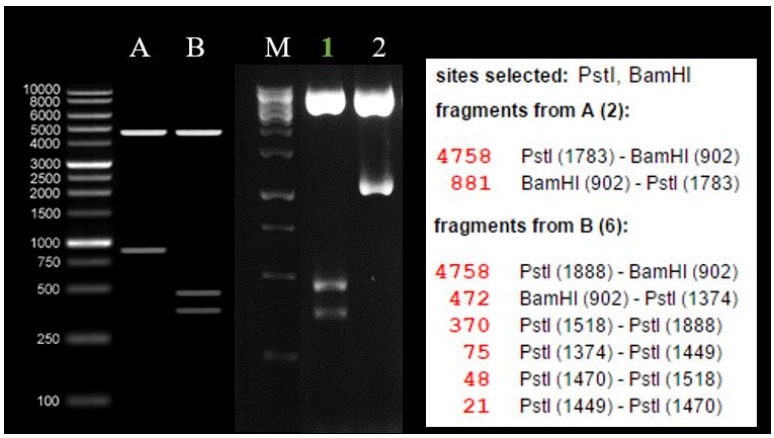

Fig.A. 5: The verification of pIRESPuro3-dMluI–IL6. To verify positive clones, PstI/BamHI were used. Pattern depicted under letter A corresponds to original vector pIRESPuro3-dMluI–sTNF. B shows expected pattern of positive clones.

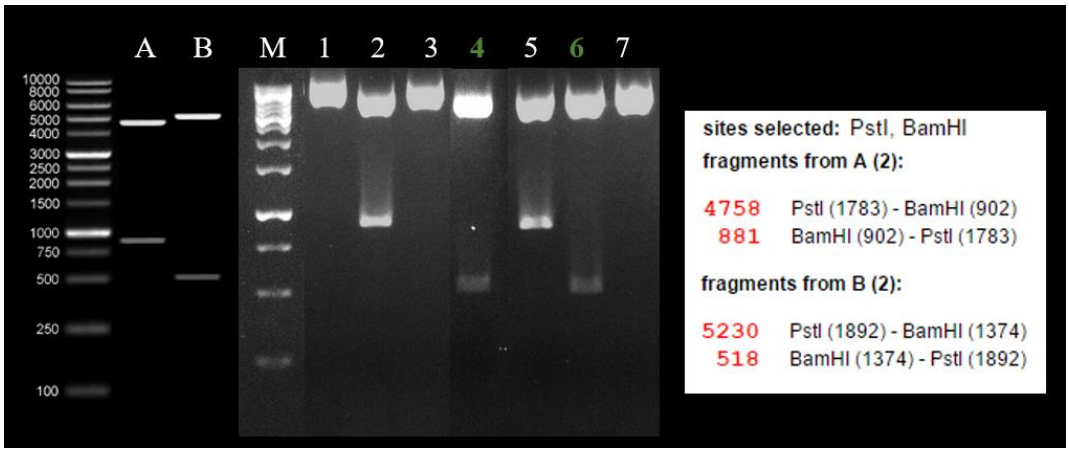

Fig.A. 7: The verification of pIRESPuro3-dMluI-IFNε. To verify positive clones, PstI and BamHI enzymes were used. Pattern depicted under letter A corresponds to original vector pIRESPuro3-dMluI –sTNF. B shows expected pattern of positive clones. Clones 4 and 6 proved to be positive.

11.3. Primers

Sequencing primers:

pcDNA3a: GAAGGCACAGTCGAGGCTGATC
tightseq5: GTAGGCGTGTACGGTGGGA
IP3seqR: AGTACTCACCCCAACAGCT
T7 long: GAAATTAATACGACTCACTATA
STAT1f: CTGAATTTCGGCACCTGCAAT
STAT1r: GCTCTTCAGTAACGATGAGAGGA
STAT3f: AGTGTGCATTGACAAAGACTCTG
STAT3r: CGTTGTTGGATTCTTCCATGTTC

	Sequencing primer	**Colony PCR**
Stat1:	pcDNA3a; tightseq5 Stat1f, Stat1r	/
Stat3:	pcDNA3a; tightseq5 Stat3f, Stat3r	/
sTNF:	IP3seqR	/
sIL-1β	IP3seqR	/
IL-6:	tightseq5	IP3seqR; T7 long
IFNE:	tightseq5	IP3seqR; T7 long

Cloning primers:

STAT1atg: CTCTGGATCCACCATGTCTCAGTGGTACGAACTTC
STAT1stop: GTGTTACGCGTTAGCTAGCTATACTGTGTTCATCATACTGT

STAT3atg: AGCTGCTAGCGCCATGGCCCAATGGAATCAGCTAC
STAT3stop: CTTTGTTCGAACGCGTTCTCAGCTCCTCACATG

sTNFf: GGTTCTGCCTTCGCTAGCGCTGTCAGATCATCTTCTCGAACC
SigP1: CTTTCTCCTGCTCCTCTTCATCTCCGGTTCTGCCTTCGCTA
SigP2: ATCCGGATCCACCATGAAGTGGGTAACCTTTCTCCTGCTCCTCTTCA
TNFstop: ACTCACAGATCTACGCGTGAATTCACAGGGCAATGATCCCAAAGTAG

sIL1βf: GACTCTGCTAGCGCTCCTGTACGATCACTGAAC
sIL1 βstop: GACACTTCGAATTCAGGAAGACACAAATTGCATGGTG

IL6atg: CAAACGGATCCGCCATGAACTCCTTCTCCACAAG
IL6stop: CTAGAGAATTCACATTTGCCGAAGAGCCCT

IFN-εf: GGGATAAGTAGCATATTTGACCTTCA
IFN-εstop: GTTAGAATTCTACCTCGGGCTTCTAAACTC

11.4. PCR products- sequences

Product Size	Sequence
Stat1 2284 bp	CAAAGGATCCACCATGTCTCAGTGGTACGAACTTCAGCAGCTTGACTCAAAATTCCTGGAGC AGGTTCACCAGCTTTATGATGACAGTTTTCCCATGGAAATCAGACAGTACCTGGCACAGTGGT TAGAAAAGCAAGACTGGGAGCACGCTGCCAATGATGTTTCATTTGCCACCATCCGTTTTCATG ACCTCCTGTCACAGCTGGATGATCAATATAGTCGCTTTTCTTTGGAGAATAACTTCTTGCTAC AGCATAACATAAGGAAAAGCAAGCGTAATCTTCAGGATAATTTTCAGGAAGACCCAATCCAG ATGTCTATGATCATTTACAGCTGTCTGAAGGAAGAAAGGAAAATTCTGGAAAACGCCCAGAG ATTTAATCAGGCTCAGTCGGGGAATATTCAGAGCACAGTGATGTTAGACAAACAGAAAGAGC TTGACAGTAAAGTCAGAAATGTGAAGGACAAGGTTATGTGTATAGAGCATGAAATCAAGAG CCTGGAAGATTTACAAGATGAATATGACTTCAAATGCAAAACCTTGCAGAACAGAGAACACG AGACCAATGGTGTGGCAAAGAGTGATCAGAAACAAGAACAGCTGTTACTCAAGAAGATGTA TTTAATGCTTGACAATAAGAGAAAGGAAGTAGTTCACAAAATAATAGAGTTGCTGAATGTCA CTGAACTTACCCAGAATGCCCTGATTAATGATGAACTAGTGGAGTGGAAGCGGAGACAGCAG AGCGCCTGTATTGGGGGGCCGCCCAATGCTTGCTTGGATCAGCTGCAGAACTGGTTCACTATA GTTGCGGAGAGTCTGCAGCAAGTTCGGCAGCAGCTTAAAAAGTTGGAGGAATTGGAACAGA AATACACCTACGAACATGACCCTATCACAAAAAACAAACAAGTGTTATGGGACCGCACCTTC AGTCTTTTCCAGCAGCTCATTCAGAGCTCGTTTGTGGTGGAAAGACAGCCCTGCATGCCAACG CACCCTCAGAGGCCGCTGGTCTTGAAGACAGGGGTCCAGTTCACTGTGAAGTTGAGACTGTT GGTGAAATTGCAAGAGCTGAATTATAATTTGAAAGTCAAAGTCTTATTTGATAAAGATGTGA ATGAGAGAAATACAGTAAAAGGATTTAGGAAGTTCAACATTTTGGGCACGCACACAAAAGT GATGAACATGGAGGAGTCCACCAATGGCAGTCTGGCGGCTGAATTTCGGCACCTGCAATTGA AAGAACAGAAAAATGCTGGCACCAGAACGAATGAGGGTCCTCTCATCGTTACTGAAGAGCTT CACTCCCTTAGTTTTGAAACCCAATTGTGCCAGCCTGGTTTGGTAATTGACCTCGAGACGACC TCTCTGCCCGTTGTGGTGATCTCCAACGTCAGCCAGCTCCCGAGCGGTTGGGCCTCCATCCTT TGGTACAACATGCTGGTGGCGGAACCCAGGAATCTGTCCTTCTTCCTGACTCCACCATGTGCA CGATGGGCTCAGCTTTCAGAAGTGCTGAGTTGGCAGTTTTCTTCTGTCACCAAAAGAGGTCTC AATGTGGACCAGCTGAACATGTTGGGAGAGAAGCTTCTTGGTCCTAACGCCAGCCCCGATGG TCTCATTCCGTGGACGAGGTTTTGTAAGGAAAATATAAATGATAAAAATTTTCCCTTCTGGCT TTGGATTGAAAGCATCCTAGAACTCATTAAAAAACACCTGCTCCCTCTCTGGAATGATGGGTG CATCATGGGCTTCATCAGCAAGGAGCGAGAGCGTGCCCTGTTGAAGGACCAGCAGCCGGGG ACCTTCCTGCTGCGGTTCAGTGAGAGCTCCCGGGAAGGGGCCATCACATTCACATGGGTGGA GCGGTCCCAGAACGGAGGCGAACCTGACTTCCATGCGGTTGAACCCTACACGAAGAAAGAA CTTTCTGCTGTTACTTTCCCTGACATCATTCGCAATTACAAAGTCATGGCTGCTGAGAATATTC CTGAGAATCCCCTGAAGTATCTGTATCCAAATATTGACAAAGACCATGCCTTTGGAAAGTATT ACTCCAGGCCAAAGGAAGCACCAGAGCCAATGGAACTTGATGGCCCTAAAGGAACTGGATA TATCAAGACTGAGTTGATTTCTGTGTCTGAAGTTCACCCTTCTAGACTTCAGACCACAGACAA CCTGCTCCCCATGTCTCCTGAGGAGTTTGACGAGGTGTCTCGGATAGTGGGCTCTGTAGAATT CGACAGTATGATGAACACAGTATAGCTAGCTAACGCGTAACAC

Stat3 **2352 bp**	AGCTGCTAGCGCCATGGCCCAATGGAATCAGCTACAGCAGCTTGACACACGGTACCTGGAGC AGCTCCATCAGCTCTACAGTGACAGCTTCCCAATGGAGCTGCGGCAGTTTCTGGCCCCTTGGA TTGAGAGTCAAGATTGGGCATATGCGGCCAGCAAAGAATCACATGCCACTTTGGTGTTTCAT AATCTCCTGGGAGAGATTGACCAGCAGTATAGCCGCTTCCTGCAAGAGTCGAATGTTCTCTAT CAGCACAATCTACGAAGAATCAAGCAGTTTCTTCAGAGCAGGTATCTTGAGAAGCCAATGGA GATTGCCCGGATTGTGGCCCGGTGCCTGTGGGAAGAATCACGCCTTCTACAGACTGCAGCCA CTGCGGCCCAGCAAGGGGGCCAGGCCAACCACCCCACAGCAGCCGTGGTGACGGAGAAGCA GCAGATGCTGGAGCAGCACCTTCAGGATGTCCGGAAGAGAGTGCAGGATCTAGAACAGAAA ATGAAAGTGGTAGAGAATCTCCAGGATGACTTTGATTTCAACTATAAAACCCTCAAGAGTCA AGGAGACATGCAAGATCTGAATGGAAACAACCAGTCAGTGACCAGGCAGAAGATGCAGCAG CTGGAACAGATGCTCACTGCGCTGGACCAGATGCGGAGAAGCATCGTGAGTGAGCTGGCGG GGCTTTTGTCAGCGATGGAGTACGTGCAGAAAACTCTCACGGACGAGGAGCTGGCTGACTGG AAGAGGCGGCAACAGATTGCCTGCATTGGAGGCCCGCCCAACATCTGCCTAGATCGGCTAGA AAACTGGATAACGTCATTAGCAGAATCTCAACTTCAGACCCGTCAACAAATTAAGAAACTGG AGGAGTTGCAGCAAAAAGTTTCCTACAAAGGGGACCCCATTGTACAGCACCGGCCGATGCTG GAGGAGAGAATCGTGGAGCTGTTTAGAAACTTAATGAAAAGTGCCTTTGTGGTGGAGCGGCA GCCCTGCATGCCCATGCATCCTGACCGGCCCCTCGTCATCAAGACCGGCGTCCAGTTCACTAC TAAAGTCAGGTTGCTGGTCAAATTCCCTGAGTTGAATTATCAGCTTAAAATTAAAGTGTGCAT TGACAAAGACTCTGGGGACGTTGCAGCTCTCAGAGGATCCCGGAAATTTAACATTCTGGGCA CAAACACAAAAGTGATGAACATGGAAGAATCCAACAACGGCAGCCTCTCTGCAGAATTCAA ACACTTGACCCTGAGGGAGCAGAGATGTGGGAATGGGGGCCGAGCCAATTGTGATGCTTCCC TGATTGTGACTGAGGAGCTGCACCTGATCACCTTTGAGACCGAGGTGTATCACCAAGGCCTC AAGATTGACCTAGAGACCCACTCCTTGCCAGTTGTGGTGATCTCCAACATCTGTCAGATGCCA AATGCCTGGGCGTCCATCCTGTGGTACAACATGCTGACCAACAATCCCAAGAATGTAAACTT TTTTACCAAGCCCCCAATTGGAACCTGGGATCAAGTGGCCGAGGTCCTGAGCTGGCAGTTCTC CTCCACCACCAAGCGAGGACTGAGCATCGAGCAGCTGACTACACTGGCAGAGAAACTCTTGG GACCTGGTGTGAATTATTCAGGGTGTCAGATCACATGGGCTAAATTTTGCAAAGAAAACATG GCTGGCAAGGGCTTCTCCTTCTGGGTCTGGCTGGACAATATCATTGACCTTGTGAAAAAGTAC ATCCTGGCCCTTTGGAACGAAGGGTACATCATGGGCTTTATCAGTAAGGAGCGGGAGCGGGC CATCTTGAGCACTAAGCCTCCAGGCACCTTCCTGCTAAGATTCAGTGAAAGCAGCAAAGAAG GAGGCGTCACTTTCACTTGGGTGGAGAAGGACATCAGCGGTAAGACCCAGATCCAGTCCGTG GAACCATACACAAAGCAGCAGCTGAACAACATGTCATTTGCTGAAATCATCATGGGCTATAA GATCATGGATGCTACCAATATCCTGGTGTCTCCACTGGTCTATCTCTATCCTGACATTCCCAA GGAGGAGGCATTCGGAAAGTATTGTCGGCCAGAGAGCCAGGAGCATCCTGAAGCTGACCCA GGTAGCGCTGCCCCATACCTGAAGACCAAGTTTATCTGTGTGACACCAACGACCTGCAGCAA TACCATTGACCTGCCGATGTCCCCCCGCACTTTAGATTCATTGATGCAGTTTGGAAATAATGG TGAAGGTGCTGAACCCTCAGCAGGAGGGCAGTTTGAGTCCCTCACCTTTGACATGGAGTTGA CCTCGGAGTGCGCTACCTCCCCCATGTGAGGAGCTGAGAACGCGTTCGAACAAAG

sTNF **569 bp**	ATCCGGATCCACCATGAAGTGGGTAACCTTTCTCCTGCTCCTCTTCATCTCCGGTTCTGCCTTC GCTAGCGCTGTCAGATCATCTTCTCGAACCCCGAGTGACAAGCCTGTAGCCCATGTTGTAGCA AACCCTCAAGCTGAGGGGCAGCTCCAGTGGCTGAACCGCCGGGCCAATGCCCTCCTGGCCAA TGGCGTGGAGCTGAGAGATAACCAGCTGGTGGTGCCATCAGAGGGCCTGTACCTCATCTACT CCCAGGTCCTCTTCAAGGGCCAAGGCTGCCCCTCCACCCATGTGCTCCTCACCCACACCATCA GCCGCATCGCCGTCTCCTACCAGACCAAGGTCAACCTCCTCTCTGCCATCAAGAGCCCCTGCC AGAGGGAGACCCCAGAGGGGGCTGAGGCCAAGCCCTGGTATGAGCCCATCTATCTGGGAGG GGTCTTCCAGCTGGAGAAGGGTGACCGACTCAGCGCTGAGATCAATCGGCCCGACTATCTCG ACTTTGCCGAGTCTGGGCAGGTCTACTTTGGGATCATTGCCCTGTGAATTCACGCGTAGATCT GTGAGT
sIL-1β **486 bp**	GACTCTGCTAGCGCTCCTGTACGATCACTGAACTGCACGCTCCGGGACTCACAGCAAAAAAG CTTGGTGATGTCTGGTCCATATGAACTGAAAGCTCTCCACCTCCAGGGACAGGATATGGAGC AACAAGTGGTGTTCTCCATGTCCTTTGTACAAGGAGAAGAAAGTAATGACAAAATACCTGTG GCCTTGGGCCTCAAGGAAAAGAATCTGTACCTGTCCTGCGTGTTGAAAGATGATAAGCCCAC TCTACAGCTGGAGAGTGTAGATCCCAAAAATTACCCAAAGAAGAAGATGGAAAAGCGATTT GTCTTCAACAAGATAGAAATCAATAACAAGCTGGAATTTGAGTCTGCCCAGTTCCCCAACTG GTACATCAGCACCTCTCAAGCAGAAAACATGCCCGTCTTCCTGGGAGGGACCAAAGGCGGCC AGGATATAACTGACTTCACCATGCAATTTGTGTCTTCCTGAATTCGAAGTGTC
IL-6 **662 bp**	CAAACGGATCCGCCATGAACTCCTTCTCCACAAGCGCCTTCGGTCCAGTTGCCTTCTCCCTGG GGCTGCTCCTGGTGTTGCCTGCTGCCTTCCCTGCCCCAGTACCCCCAGGAGAAGATTCCAAAG ATGTAGCCGCCCCACACAGACAGCCACTCACCTCTTCAGAACGAATTGACAAACAAATTCGG TACATCCTCGACGGCATCTCAGCCCTGAGAAAGGAGACATGTAACAAGAGTAACATGTGTGA AAGCAGCAAAGAGGCACTGGCAGAAAACAACCTGAACCTTCCAAAGATGGCTGAAAAAGAT GGATGCTTCCAATCTGGATTCAATGAGGAGACTTGCCTGGTGAAAATCATCACTGGTCTTTTG GAGTTTGAGGTATACCTAGAGTACCTCCAGAACAGATTTGAGAGTAGTGAGGAACAAGCCAG AGCTGTGCAGATGAGTACAAAAGTCCTGATCCAGTTCCTGCAGAAAAAGGCAAAGAATCTAG ATGCAATAACCACCCCTGACCCAACCACAAATGCCAGCCTGCTGACGAAGCTGCAGGCACAG AACCAGTGGCTGCAGGACATGACAACTCATCTCATTCTGCGCAGCTTTAAGGAGTTCCTGCA GTCCAGCCTGAGGGCTCTTCGGCAAATGTGAATTCTCTAG
IFN-ε **663 bp**	GGGATAAGTAGCATATTTGACCTTCACCATGATTATCAAGCACTTCTTTGGAACTGTGTTGGT GCTGCTGGCCTCTACCACTATCTTCTCTCTAGATTTGAAACTGATTATCTTCCAGCAAAGACA AGTGAATCAAGAAAGTTTAAAACTCTTGAATAAGTTGCAAACCTTGTCAATTCAGCAGTGTCT ACCACACAGGAAAAACTTTCTGCTTCCTCAGAAGTCTTTGAGTCCTCAGCAGTACCAAAAAG GACACACTCTGGCCATTCTCCATGAGATGCTTCAGCAGATCTTCAGCCTCTTCAGGGCAAATA TTTCTCTGGATGGTTGGGAGGAAAACCACACGGAGAAATTCCTCATTCAACTTCATCAACAG CTAGAATACCTAGAAGCACTCATGGGACTGGAAGCAGAGAAGCTAAGTGGTACTTTGGGTAG TGATAACCTTAGATTACAAGTTAAAATGTACTTCCGAAGGATCCATGATTACCTGGAAAACC AGGACTACAGCACCTGTGCCTGGGCCATTGTCCAAGTAGAAATCAGCCGATGTCTGTTCTTTG TGTTCAGTCTCACAGAAAAACTGAGCAAACAAGGAAGACCCTTGAACGACATGAAGCAAGA GCTTACTACAGAGTTTAGAAGCCCGAGGTAGATTCTAAC

11.5. Vectors:

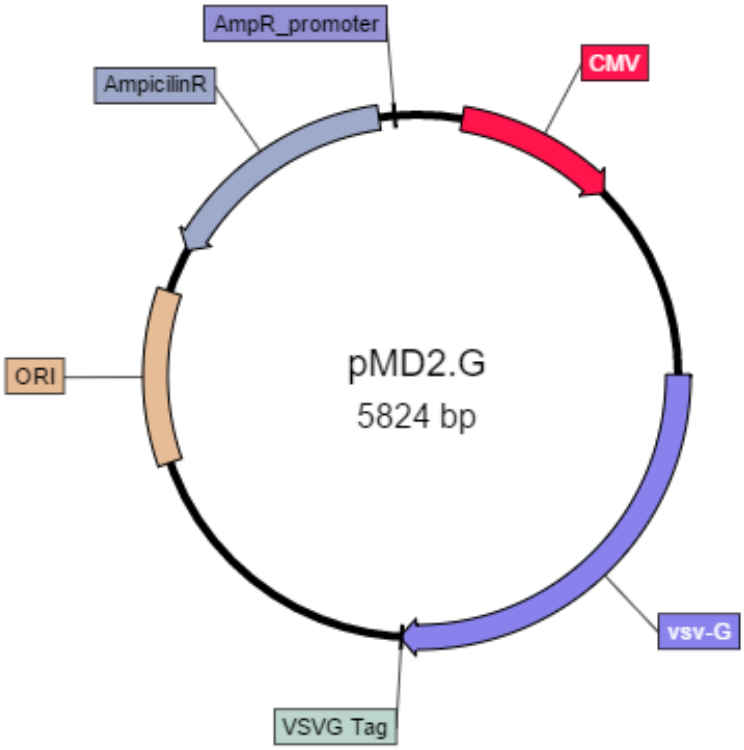
AmpR_promoter
CMV
AmpicilinR
ORI
pMD2.G
5824 bp
vsv-G
VSVG Tag

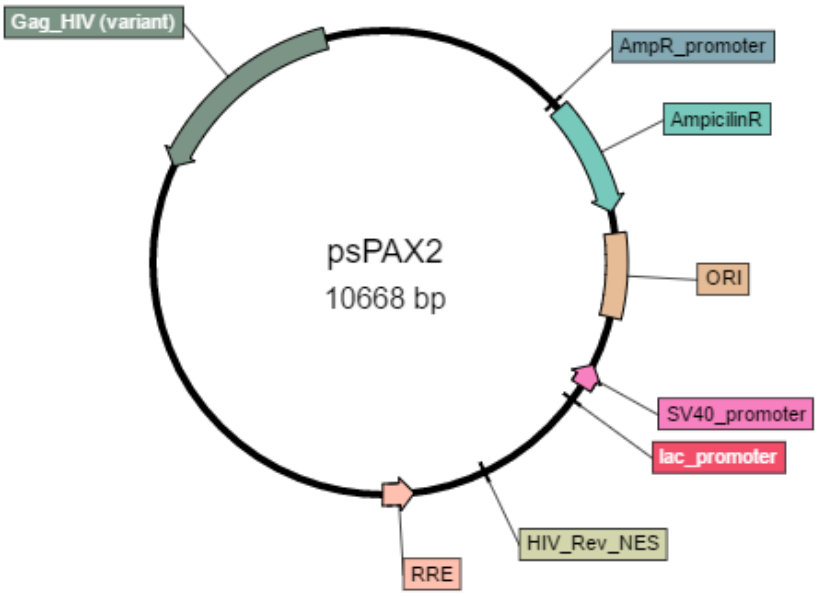
Gag_HIV (variant)
AmpR_promoter
AmpicilinR
psPAX2
10668 bp
ORI
SV40_promoter
lac_promoter
HIV_Rev_NES
RRE

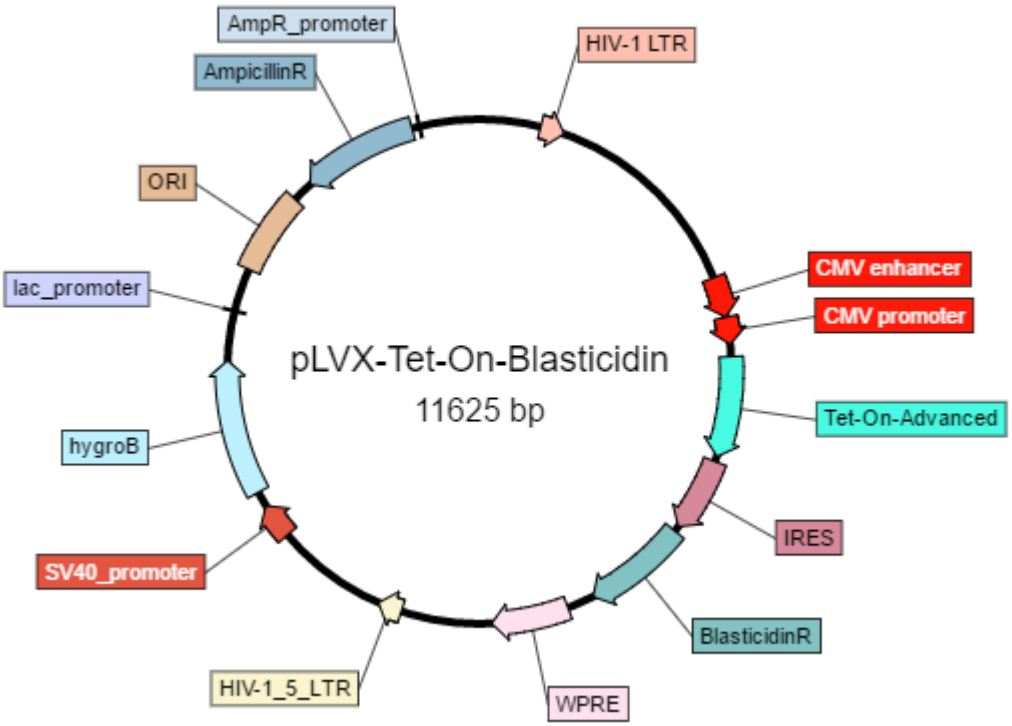
AmpR_promoter
AmpicillinR
ORI
lac_promoter
hygroB
SV40_promoter
HIV-1_5_LTR
WPRE
BlasticidinR
IRES
Tet-On-Advanced
CMV promoter
CMV enhancer
HIV-1 LTR
pLVX-Tet-On-Blasticidin
11625 bp

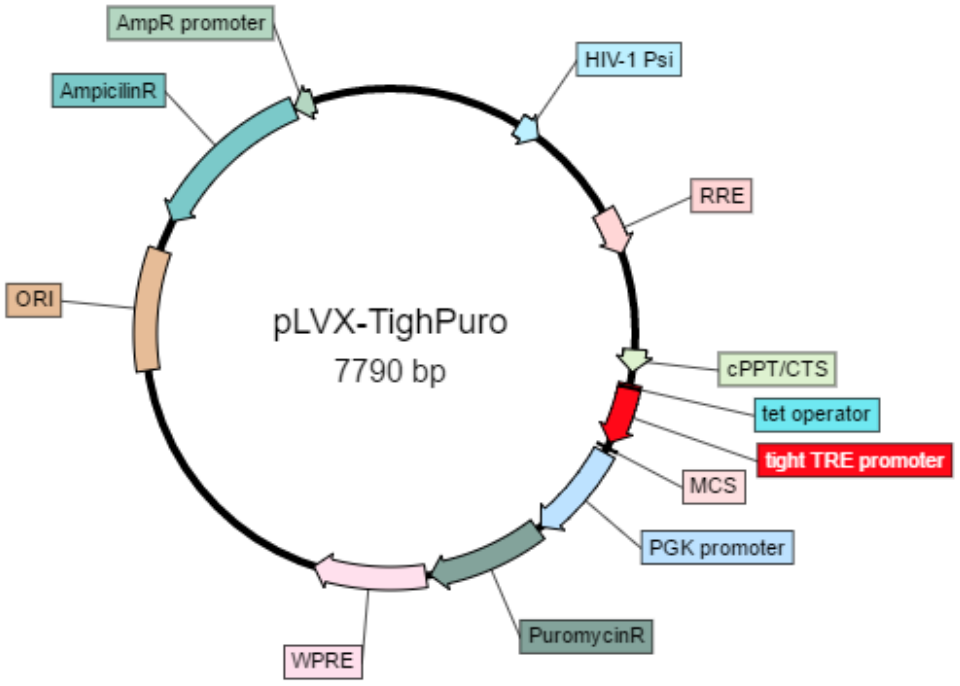
AmpR promoter
AmpicilinR
ORI
WPRE
PuromycinR
PGK promoter
MCS
tight TRE promoter
tet operator
cPPT/CTS
RRE
HIV-1 Psi
pLVX-TighPuro
7790 bp

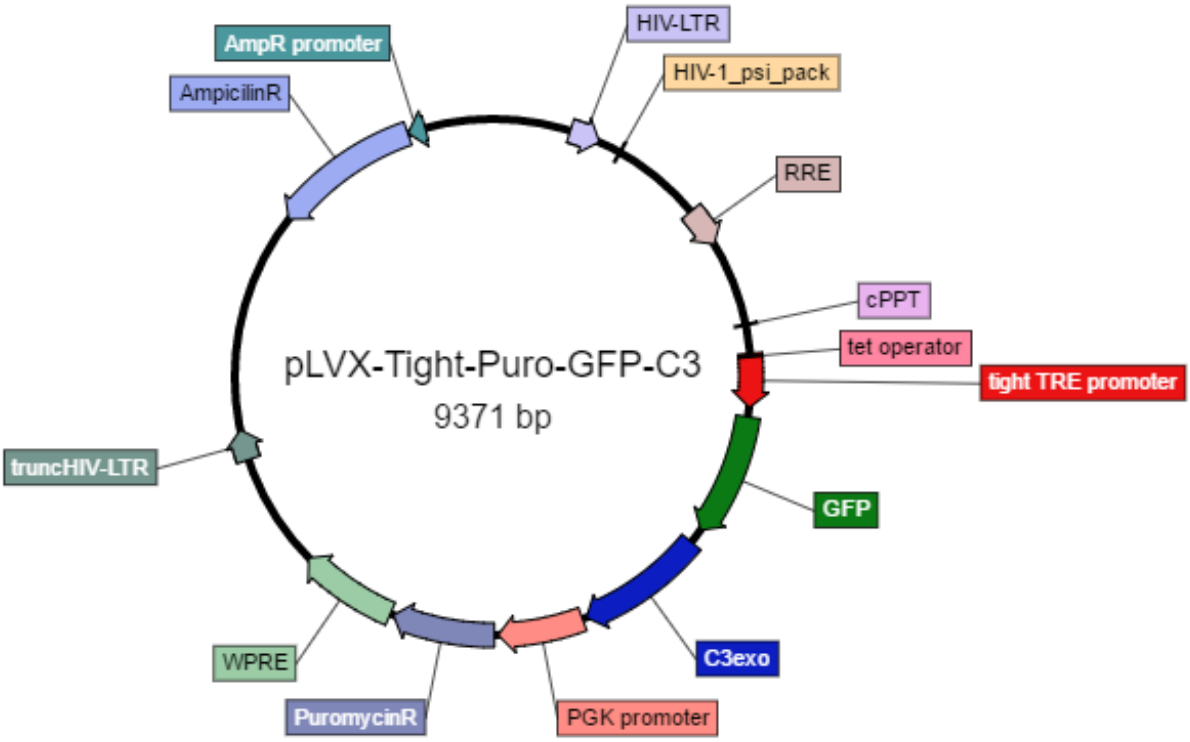
pLVX-Tight-Puro-GFP-C3
9371 bp
AmpR promoter
AmpicilinR
HIV-LTR
HIV-1_psi_pack
RRE
cPPT
tet operator
tight TRE promoter
GFP
C3exo
PGK promoter
PuromycinR
WPRE
truncHIV-LTR

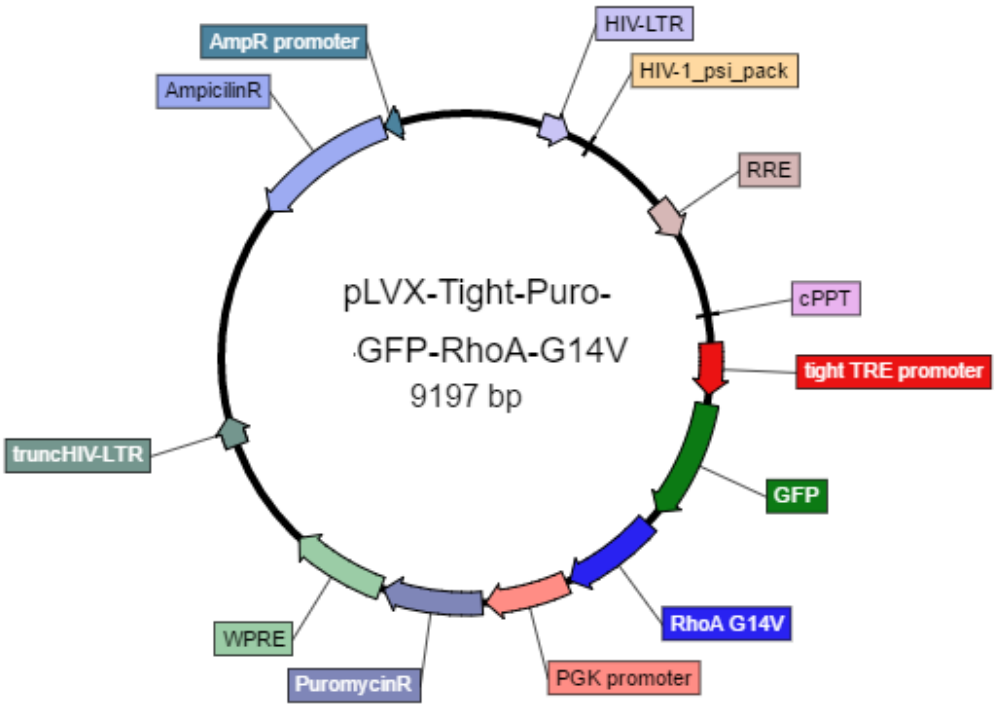
pLVX-Tight-Puro-
GFP-RhoA-G14V
9197 bp
AmpR promoter
AmpicilinR
HIV-LTR
HIV-1_psi_pack
RRE
cPPT
tight TRE promoter
GFP
RhoA G14V
PGK promoter
PuromycinR
WPRE
truncHIV-LTR

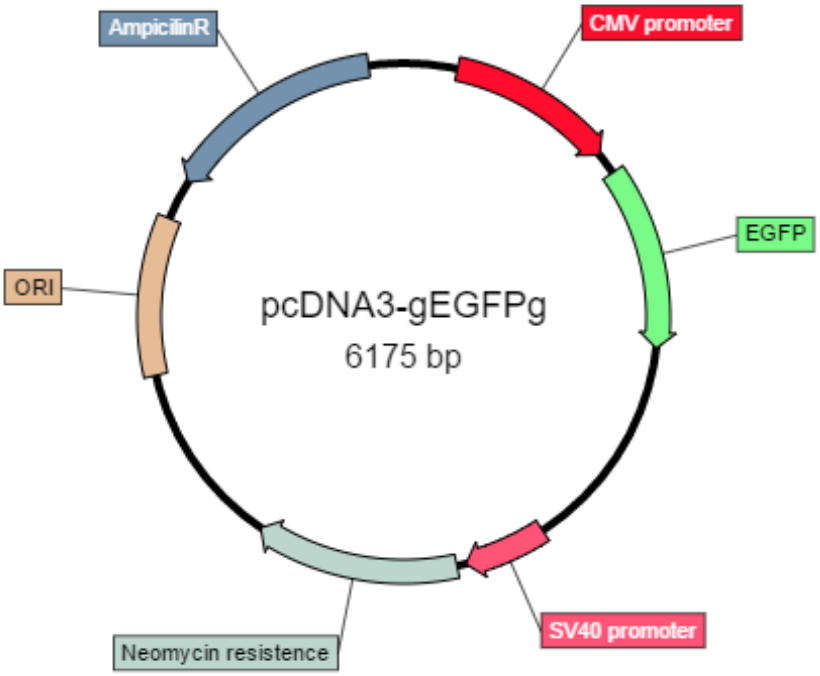
AmpicilinR
CMV promoter
EGFP
ORI
pcDNA3-gEGFPg
6175 bp
Neomycin resistence
SV40 promoter

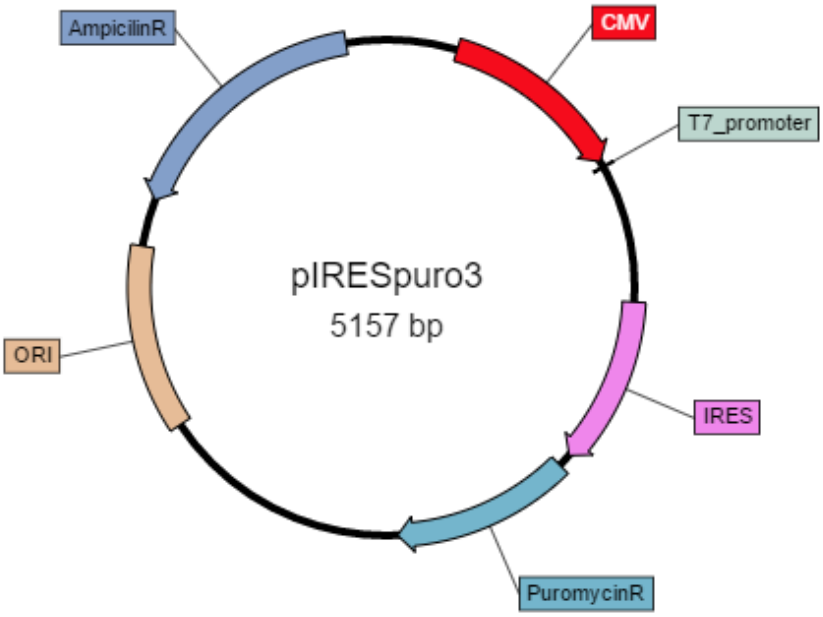
AmpicilinR
CMV
T7_promoter
ORI
pIRESpuro3
5157 bp
IRES
PuromycinR

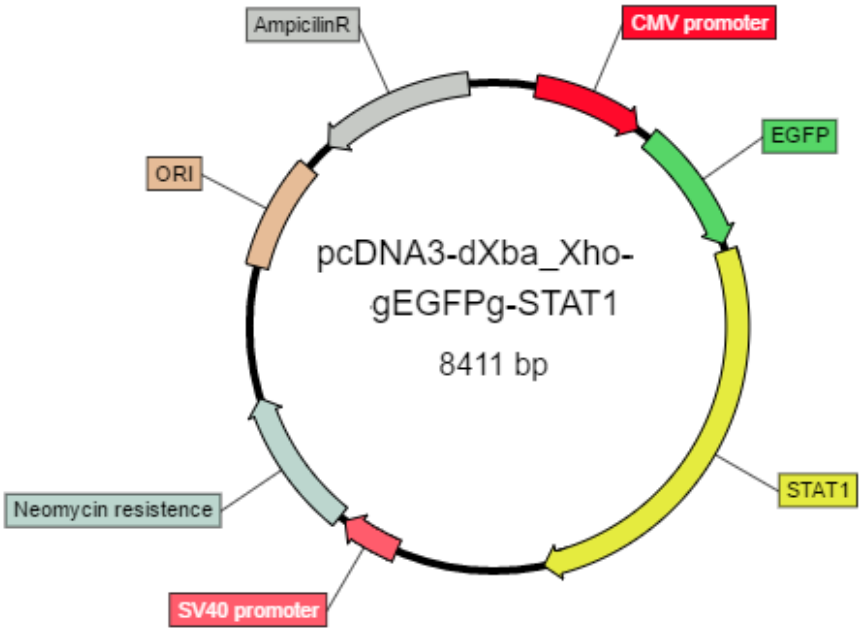
AmpicilinR
CMV promoter
EGFP
ORI
pcDNA3-dXba_Xho-
gEGFPg-STAT1
8411 bp
STAT1
Neomycin resistence
SV40 promoter

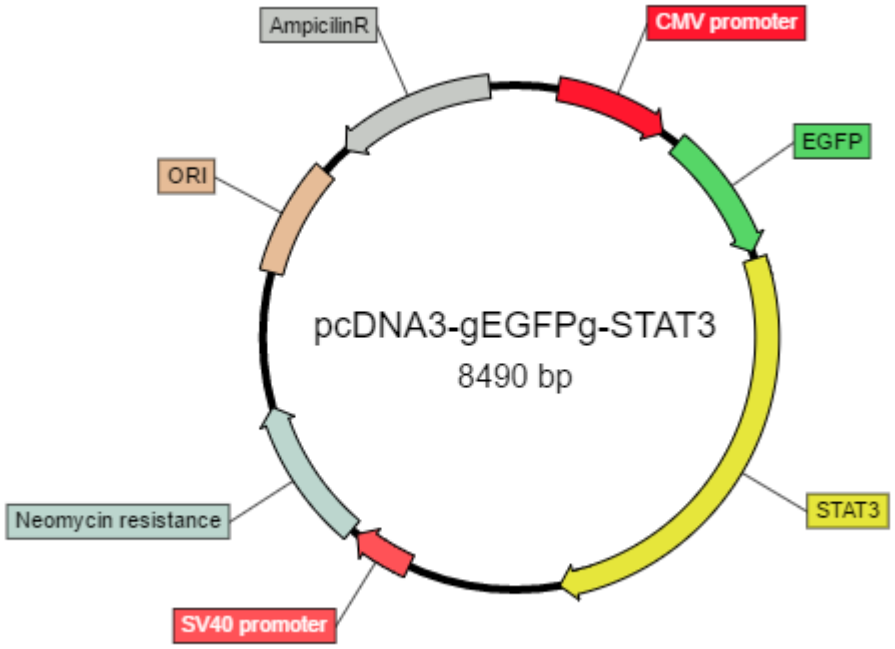
AmpicilinR
CMV promoter
EGFP
ORI
pcDNA3-gEGFPg-STAT3
8490 bp
STAT3
Neomycin resistance
SV40 promoter

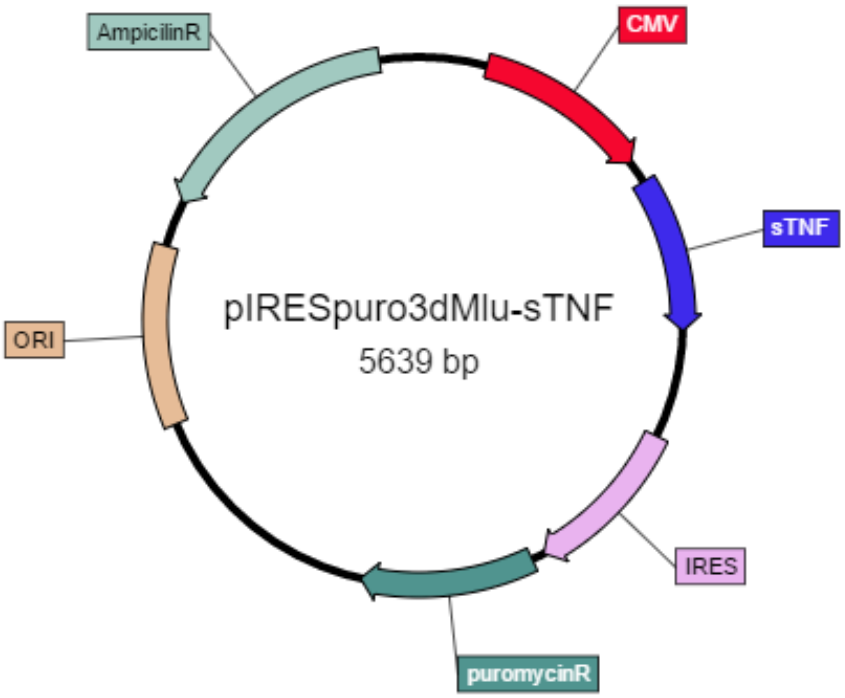
AmpicilinR
CMV
sTNF
pIRESpuro3dMlu-sTNF
5639 bp
ORI
IRES
puromycinR

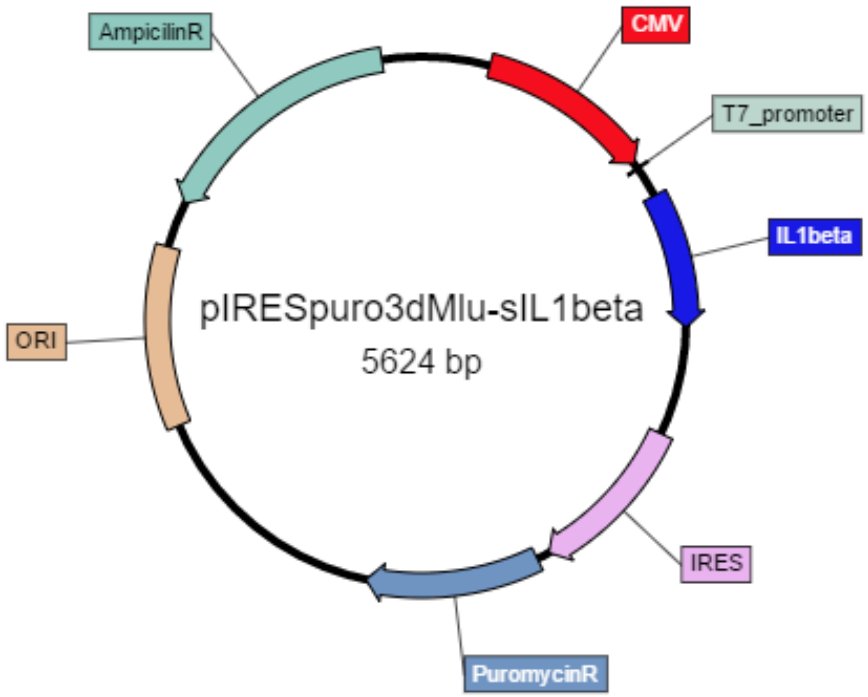
AmpicilinR
CMV
T7_promoter
IL1beta
pIRESpuro3dMlu-sIL1beta
5624 bp
ORI
IRES
PuromycinR

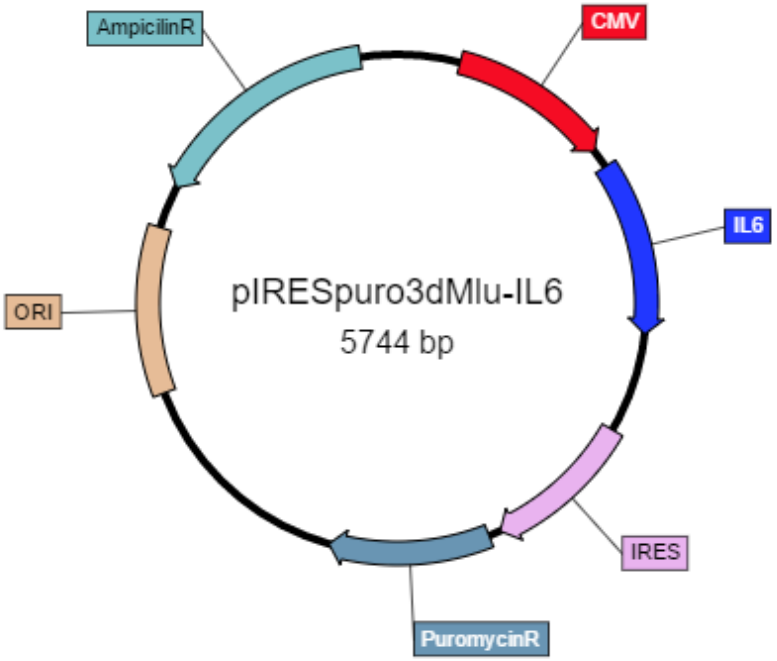
AmpicilinR
CMV
IL6
pIRESpuro3dMlu-IL6
5744 bp
ORI
IRES
PuromycinR

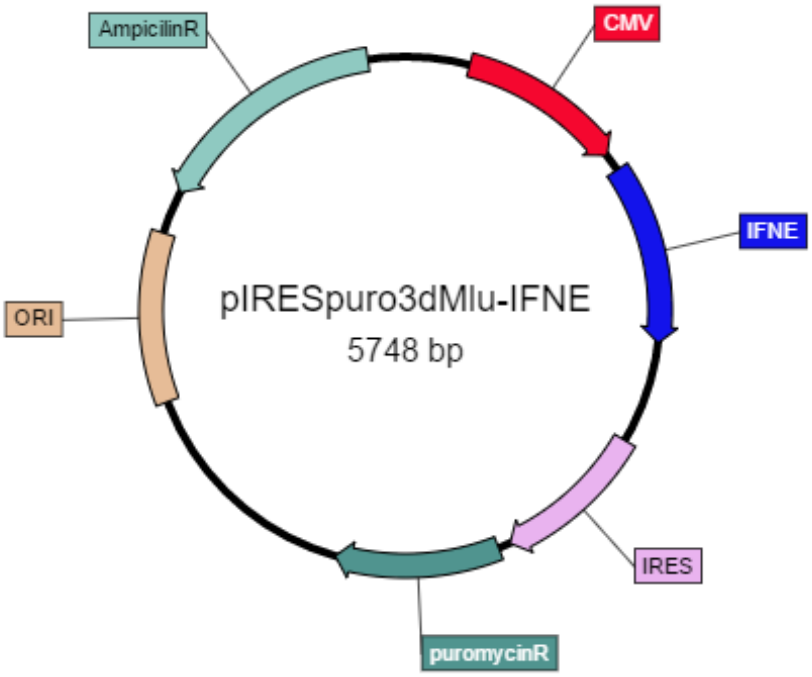
AmpicilinR
CMV
IFNE
pIRESpuro3dMlu-IFNE
5748 bp
ORI
IRES
puromycinR